Stockholm University

Master Thesis

Degree Project in Geology 60 hp

Remobilization of the Simon lens in the Renström VMS deposit, Skellefte district, Sweden

Felix Makowsky

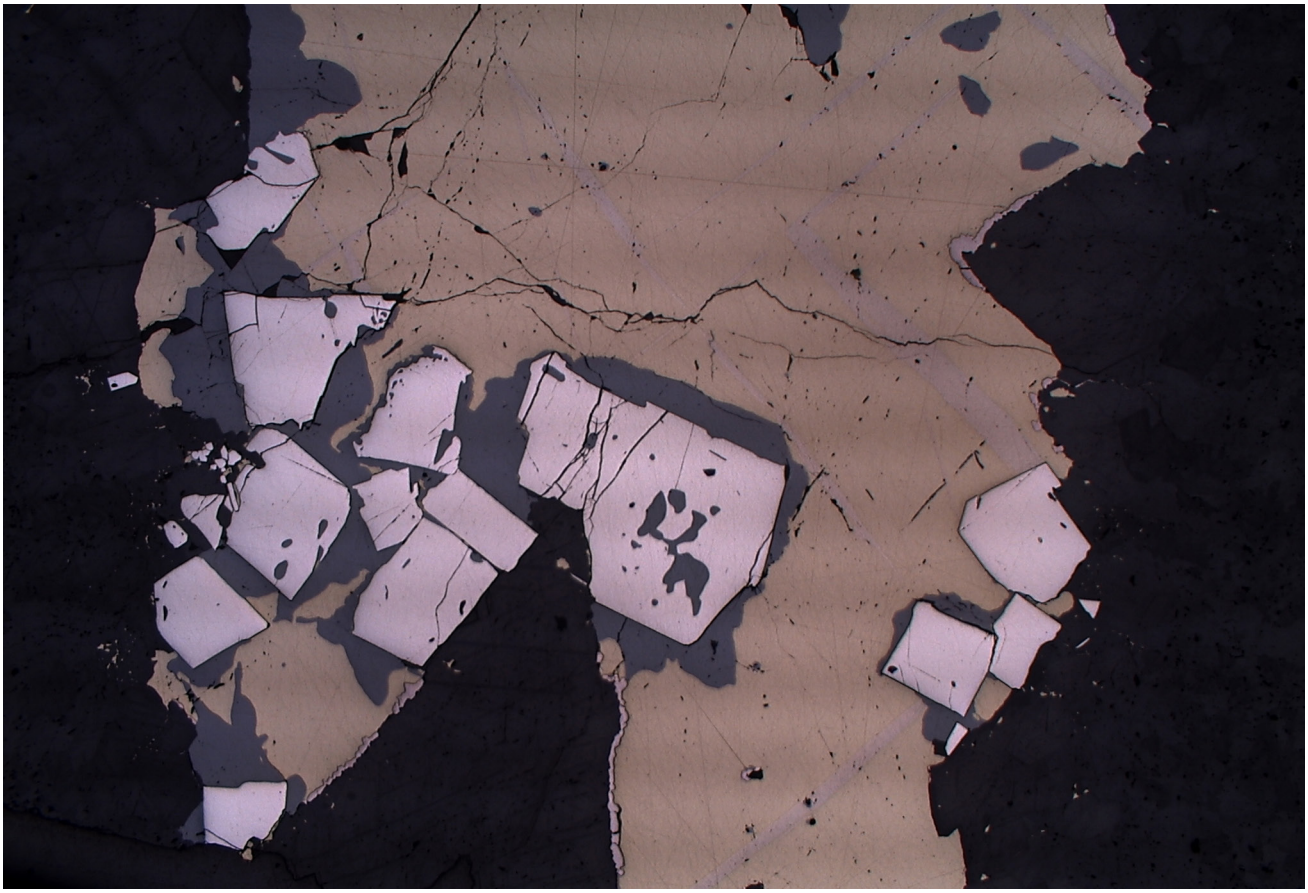

Stockholm 2015

Department of Geological Sciences
Stockholm University
SE-106 91 Stockholm
Sweden

Remobilization of the Simon lens in the Renström VMS deposit, Skellefte district, Sweden

Abstract

Unravelling layer upon layer of overprinting events that have affected an ore body is a complex matter, but it can provide important information for near-mine exploration: how minerals have formed and been reworked ultimately determines the distribution of metals in a deposit. Although the regional geological history of the Skellefte district is fairly well known, how metamorphism has affected the ore bodies requires additional attention.

In this study, visual investigation by optical- and electron scanning environmental microscopy in tandem with in-situ analysis by electron microprobe and laser ablation inductively coupled plasma mass spectrometry of a drill core have been applied to improve our understanding of how the latest regional metamorphism has affected parts of the Renström deposit. A paragenetical model has been established, and additional constrains on this model has been set by U-Pb dating of titanite, geothermometry of arsenopyrite and fluid inclusion studies in dolomite. Extra attention has been given to the distribution of Au and Ag.

The study shows that different remobilization processes have affected the ore, causing a fractionation of metals during regional metamorphism. In particular gold seems to have been redistributed from the massive sulphide assemblage to heavily deformed zones, and the retrograde breakdown of tetrahedrite-group minerals is suggested as a possible trap for gold. The distribution of silver, on the other hand, is largely determined by pre-metamorphic conditions. The geochronological age of titanite indicates peak metamorphism at 1816 ± 28 Ma, and the As content of arsenopyrite, indicating peak metamorphic temperature, was in equilibrium at 379 ± 29° C. Fluid inclusions of dolomite is in line with previous fluid inclusion studies in the area, pointing towards a seafloor hydrothermal origin of dolomite, while calcite is related to peak- and retrograde metamorphism.

Contents

Introduction

The Paleoproterozoic Skellefte district in northern Sweden host 79 VMS deposits (Bauer, et al., 2014), several of them auriferous (Mercier-Langevin & Hannington, 2011), including the world-class Boliden deposit (Bergman Weihed, et al., 1996). The district comprises an area of approximately 120 x 30 km, stretching WNW from the town of Boliden, where the first mine in the district opened in the early 1920s. Zn, Cu, Au, and Ag are the major commodities extracted from the district, reflecting the overall above-average content of precious metals in the Skellefte VMS deposits (Mercier-Langevin & Hannington, 2011). In addition to classic Zn-Cu-Pb VMS deposits (e.g. Renström: Allen & Svenson, 2004; Kristineberg: Årebäck, et al., 2005), the district hosts several more quirky VMS-related deposits of disputed origin, like the Au-Cu-As Boliden (Bergman Weihed, et al., 1996; Wagner & Jonsson, 2001) and Au-Te Åkulla deposits (Wasström, et al., 1999).

The district has undergone multiple generations of deformation, and structural geology is the main control on distribution and shape of the VMS deposits in the district (Bauer, et al., 2014). Normal faulting during an extensional phase (D1) at 1.89 – 1.87 Ga (Lundström & Persson, 1999) created pathways for hydrothermal fluids in the seafloor, enabling emplacement of sub-seafloor replacement and mound-style VMS deposits. Crustal shortening at 1.87 – 1.86 Ga (D2) caused upright folding of

the stratigraphy (Skyttä, et al., 2013) and reactivation of earlier faults (Bauer, et al., 2011), with deformation being focused in the massive sulphide bodies (e.g. Bergman Weihed, et al., 1996; Årebäck, et al., 2005). Lastly, E – W shortening at 1.82 – 1.80 Ga (D3) (Weihed, et al., 2002) led to additional fault reactivation in N – S striking high-strain zones (Bauer, et al., 2011; Skyttä, et al., 2012). Post-formational peak regional metamorphism of the district is inferred to have taken place at ~1.82 Ga (Weihed, et al., 2002), with upper greenschist- to lower amphibolite grade metamorphism affecting ore bodies in the district (Allen, et al., 1996). This regional metamorphism has changed the alteration mineralogy and caused remobilization of base- and precious metals within ore bodies. At Boliden, Au has been enriched in brecciated parts of the deposit related to post-formational deformation (Bergman Weihed, et al., 1996), while the Zn-Cu-Pb-Au-Ag Kristineberg deposit show evidence of extensive remobilization of the whole ore body, with the Einarsson lens possibly being formed by remobilization alone (Årebäck, et al., 2005).

The main aim of this study is to (1) establish the mineral paragenesis of the Simon lens in the Renström deposit, with focus on regional metamorphic remobilization. In addition to this, the study also intends to (2) map out the mineralogical distribution of base- and precious metals in relation to the paragenetic model and (3) put temporal- and temperature constrains on the model. In the light of recent research, (4) partial sulphide melting will be considered as a possible remobilization process. A drill core from the lens has been investigated with visual- (i.e. core logging and microscopy) and analytical (LA-ICP-MS and EMPA) methods, and it is proposed that metamorphic remobilization at greenschist facies has redistributed base- and precious metals to various extents, possibly through the process of partial sulphide melting. The emphasis of the study will be on the distribution of Au and Ag.

Background

VMS deposits

Volcanogenic, volcanic-associated and volcanic-hosted massive sulphide deposits, generally referred to as “VMS deposits” (Solomon, 1976; Franklin, et al., 1981), are a group of exhalative Zn-Cu±(Pb, Ag, Au) deposits that may also contain economic concentrations of Co, Sn, Se, Mn, Cd, In, Bi, Te, Ga and/or Ge (Galley, et al., 2007). VMS deposits have been formed throughout Earth’s history and can now be found in many geological terrains, ranging from Archean cratons (e.g. Kidd Creek, Abitibi greenstone belt, Ontario: Barrie, et al., 1999; Hannington, et al., 1999) to the present day mid-ocean ridges (e.g. the TAG deposit, Mid-Atlantic Ridge: Humphris, et al., 1995; Hannington, et al., 1998). Various characteristics has been applied to classify VMS deposits (e.g. main metal commodities:

Hutchington, 1973; Franklin, et al., 1981; Large, 1992); type-localities: Sawkins, 1976), but the classification scheme proposed by Barrie & Hannington (1999), further refined by Franklin et al. (2005) and Galley et al. (2007), based on host rock composition, is the one most frequently used in recent papers.

Formed through hydrothermal convection of sea water in submarine rift environments, the shape and composition of a VMS deposit is largely dependent on the geological setting in which it was formed (Sawkins, 1990; Tornos, et al., 2015). Tornos et al. (2015) describes three distinct types of VMS mineralization based on various characteristics, namely the mound-style mineralizations (e.g. TAG deposit, Mid-Atlantic Ridge: Humphris, et al., 1995; Windy Craggy, British Columbia, Canada: Peter & Scott, 1999; deposits in the Troodos Ophiolite, Cyprus: Oudin & Constantinou, 1984), stratiform deposits in anoxic settings (e.g. Atlantis II Deep, Red Sea: Miller, et al., 1966; Laurila, et al., 2014; Bathurst Mining Camp, New Brunswick, Canada: Goodfellow, et al., 2003), and sub-seafloor replacement deposits (e.g. Deep Copper Zone, Middle Valley, Juan de Fuca Ridge: Zierenberg, et al., 1998; several deposits in the Iberian Pyrite Belt: Tornos, 2006; and the Skellefte District: Allen & Svenson, 2004).

Precipitation of metals occurs when hot, hydrothermal fluids come in contact with cold seawater. The setting in which this trapping takes place determines the shape and likelihood of preservation of the deposit. Mounds, formed directly on the seafloor, are generally shaped as tens of meters thick and hundreds of meters long lenses centred on black- (>280°, Cu-Fe-rich) and/or white (<280°, Zn-Pb-rich) smokers: chimneys and spires of mainly sulphides that act as exhausts for the hydrothermal system. The sulphide mound itself often contains relict pieces aforementioned chimneys (Oudin & Constantinou, 1984). The mound is underlain by a vertical stringer zone: a network of semi-massive sulphides, quartz and brecciated host rock that serves as plumbing for the hydrothermal system (Franklin, et al., 1981; Humphris, et al., 1995). The root and centre of the deposit is generally rich in Cu-Fe, with Zn-Pb occurring in higher concentrations further out, reflecting the differences in solubility of the metals in the hydrothermal fluid. Mounds are commonly capped by a barite rich layer (Ohmoto, 1996). Mound-type mineralizations are unstable in oxic environments, due to oxidation of minerals precipitated, and can no longer sustain their size when hydrothermal convection wanes (Herzig & Hannington, 1995). This can be seen in the geologic record, where a relatively smaller amount of mound-style mineralizations are preserved, compared to their occurrence on the modern seafloor (Tornos, et al., 2015). In anoxic environments, minerals precipitated from the hydrothermal fluid will not be oxidized and re-dissolved, which enables formation of widespread stratiform deposits (Goodfellow & Peter, 1996). Brine pools, depressions filled with dense saline fluids exhaled from black- or white smokers, may form in such environments.

Stratabound sub-seafloor replacement, where hydrothermal fluids infiltrate, and replace, permeable stratigraphic units below the seafloor, have been highlighted as an important sub-class of VMS deposits in recent years (Gibson & Gamble, 2000; Doyle & Allen, 2003; Tornos, 2006). Forming in an anoxic environment, these deposits are also more likely to be preserved after formation (Doyle & Allen, 2003; Tornos, 2006).

Hydrothermal convection cells in the sea-floor are not static systems; with time, geodynamic changes may cause fluctuations in, for example, temperature, flow rate and pathways. As a sea-floor VMS mineralization evolves, early low temperature minerals in the centre of a deposit, rich in Zn-Pb, tend to be re-dissolved and replaced by later stage high temperature Cu-rich minerals, causing a migration of metal zonation (i.e. zone refining) (Lydon, 1988; Large, 1992). Such remobilization may reinforce metal association and concentrate precious metals in the outer zones of a VMS deposit (Herzig & Hannington, 1995).

Gold-rich VMS deposits

Gold-rich VMS deposits has been crudely defined as VMS deposits with a gold grade (in g/t) exceeding the total base metal grade (in %) (Poulsen & Hannington, 1996; Hannington, et al., 1999; Dubé, et al., 2007). Mercier-Langevin & Hannington (2011) refines the definition by basing classification on deviation from the world means in terms of gold grade and tonnage. In their classification, an auriferous deposit has a gold grade > 3.46 g/t (0.76 ± 2.70 g/t), while any VMS with a tonnage of >31 t Au (4.7 ± 26.3 t Au) is gold-anomalous. Deposits that fulfil both these criteria are considered gold-rich. Regardless of what classification is used, it is the gold content itself that sets this subgroup of VMS deposits apart from other types of VMS deposits. Depositional age does not appear to be a limiting factor, with gold-rich VMS deposits occurring in districts of all major geological time periods (Hannington, et al., 1999; Huston, 2000). VMS deposits in mafic and bimodal-felsic host rocks have an elevated average gold concentration (Franklin, et al., 2005; Galley, et al., 2007), and most gold-rich deposits are believed to have formed in an extensional arc environment (Mercier-Langevin & Hannington, 2011). In particular, gold-rich VMS deposits seem to be related to large volumes of transitional to calc-alkaline felsic volcanic rocks (Mercier-Langevin & Hannington, 2011).

Gold-rich modern black-smoker systems commonly occur in immature back arcs in island arc- or continental crust, as opposed to more mature arc systems with a geochemical signal closer to the relatively gold-poor mid-ocean ridges (Table 4 in Hannington, et al., 1999). Similarly to the ancient deposits, the presence of proximal andesitic to rhyolitic rocks seems to encourage accumulation of

Au (Hannington, et al., 1999). These gold-rich hydrothermal vent systems also tend to be enriched in As, Sb, Hg, Pb, and, in particular, Ag (Hannington, et al., 1999). Within a deposit, gold is usually enriched in either the outer Zn-Pb-rich parts or with Cu(-Bi) in the stockwork of the black-smoker system (Huston & Large, 1989). This zonation is connected to the solubility of Au in the hydrothermal fluid and the difference in temperature and pH within a system, where gold is carried as a sulphide complex at low temperatures (150 – 275° C) and as a chlorine complex at higher temperatures (275 – 350° C) (Huston & Large, 1989).

The source, solubility and precipitation of gold are key factors in deciphering anomalous gold content in VMS deposits. Within a deposit, variations in Au concentration can often be explained by shifts in gold solubility in the fluid phase. Factors controlling larger scale variations, however, are still debated (Huston, 2000). Possible factors includes high local or regional background concentrations of gold (such as in back-arc basins: Moss, et al., 2001; Pitcairn, 2011; or above mantle plumes: Webber, et al., 2013); subcritical phase separation of the hydrothermal fluid (i.e. sub-seafloor boiling): Butterfield, et al., 1990; Hannington, et al., 1999; input of gold-rich volatiles from shallow sub-seafloor intrusions: Sillitoe, et al., 1996; Huston, et al., 2011; unusually fertile magma source of related intrusions: Monecke & Mercier-Langevin, 2014. Further enrichment by zone-refining is also possible (Hannington et al., 1999). Some world-class VMS deposits in terms of gold grade are proposed to have formed as VMS-epithermal hybrid deposits in a shallow marine to subaerial environment (e.g. Boliden, Skellefte District, Sweden: Bergman Weihed, 1996; Eskay Creek, British Columbia, Canada: Roth, et al., 1999).

Remobilization of VMS deposits

Remobilization in ore geology can be loosely defined as changes in metal distribution in a pre-existing mineralization (Marshall & Gilligan, 1987; Marshall & Gilligan, 1993; Marshall, et al., 2000). Post-formational metamorphism and deformation are the most common and far-reaching mechanisms behind remobilization observed in modern deposits. Remobilization processes included solid-state mechanical transfer, fluid-state chemical transfer, and mixed-state transfer, where most systems experience multiple processes of different types acting in tandem (Marshall & Gilligan, 1987). Given that remobilization is the interplay between pre-existing mineralogy and changes in geologic environment, singling out specific features as the result of either ore-forming (mobilizing) or ore reworking (remobilizing) processes can be difficult. However, two common features observed in many VMS deposits can be directly ascribed to remobilization: (1) grain coarsening and within grain homogenization and (2) purging of dispersed trace- and non-stoichiometric elements in an ore body from their original host into in veins and pockets (Table 1 in Marshall, et al., 2000) (Craig & Vokes, 1992).

Mechanical translocation

Sulphides in general shift from brittle to ductile behaviour at 100-200° C, considerably lower temperature that silicate minerals, enabling massive sulphide bodies to behave as one low competence unit during deformation in low- to medium grade metamorphic environments (Marshall & Gilligan, 1993; Tomkins, 2007). Differences in competence between common sulphides may also cause fractionation of metals within a sulphide body, with galena being susceptible to translocation into low-strain sites while pyrite is generally resistant to any such movement (Figure 2 in Marshall & Gilligan, 1993). Chalcopyrite, pyrrhotite, and sphalerite all have intermediate competence between that of galena and pyrite, and the order of these minerals in terms of competence varies with temperature (Duckworth & Rickard, 1993; Marshall & Gilligan, 1987; Marshall & Gilligan, 1993). Deformation at lower temperatures can cause fracturing of sulphides, in particular pyrite (Craig & Vokes, 1993), effectively leading to a decrease in grain size.

Chemical translocation

Fluid-driven translocation of a VMS requires substantial fluid fluxes in contact with the sulphides to be efficient. Given the generally low permeability and lack of hydrous phases in massive sulphide bodies, pure fluid-driven processes (excluding melts) are generally insignificant for more massive VMS bodies (Marshall & Gilligan, 1987). However, coupled with deformation, fluid- and mixed-state translocation can be an important control on element distribution, as has been noted in various VMS deposits (Sulitjelma, Norway: Cook, 1996; Bleikvassli, Norway: Cook, et al., 1998; Montauban, Quebec, Canada: Tomkins, 2007). In the case of Sulitjelma, there is strong evidence for fluid-driven remobilization of Cu, Pb, Sb, Ni, Ag, and Au into discrete pockets of remobilized material (Cook, 1996). Precious metals in the Bleikvassli mine has also been concentrated during metamorphism (Moralev, et al., 1995). LA-ICP-MS studies of “invisible” gold in sulphides also indicate a release of Au during post-mineralization metamorphism (Larocque, et al., 1995; Wagner, et al., 2007). Additional mineralogical changes observed at higher grades of metamorphism include sphalerite exsolution from chalcopyrite (Sangster & Scott, 1976) and Ag-rich tetrahedrite being exsolved from galena (Plimer, 1987).

Sulphide melting

Sulphide melting has been proposed as a mechanism of ore remobilization in several ore deposits (e.g. Broken Hill, Australia: Lawrence, 1967; Mavrogenes, et al., 2001; Frost, et al., 2011; Challenger, Australia: Tomkins, 2002; Tomkins & Mavrogenes, 2002; Bleikvassli, Norway: Vokes, 1971; Lengenbach, Switzerland: Hofmann, 1994; Hofmann & Knill, 1996; Knill, 1996; Hettmann, et al., 2014; Monte Arsiccio, Italy: Biagioni, et al., 2013) and experimental studies has shown that mid- to high

grade metamorphic temperatures may cause melting of common sulphide mineral assemblages (e.g. Barton, 1971; Brett & Kullerud, 1967; Craig & Kullerud, 1967).

Several papers describing the mechanisms behind sulphide melting has been published recently (Frost, et al., 2002; Tomkins, et al., 2006; Tomkins, et al., 2007; Tomkins, 2007). To overcome the relatively high melting points of individual sulphides (see Table 1), multiple component systems and melt phase fluxing of solids are considered (Frost, et al., 2002). For example, Tomkins et al. (2006) outlines the conditions for melting of arsenopyrite, a potentially powerful initiator of sulphide melting at lower amphibolite facies (~560° C at 5 kbar: Clark, 1960). Melting of arsenopyrite is controlled by temperature and $f(S_2)$, a variable often buffered by the common pyrite-pyrrhotite system (Toulmin & Barton, 1964), and the As-rich melt formed from the arsenopyrite-pyrite-pyrrhotite assemblage is suggested to be able to further melting of other sulphide minerals.

Low-melting-point chalcophile elements

The role of low-melting-point chalcophile elements ("LMCE"), first described by Frost et al. (2002), is critical for sulphide anatexis below middle amphibolite facies. This group of elements, consisting of Ag, As, Bi, Hg, Sb, Se, Sn, Tl and Te (with Au being an associated element (Tomkins, 2002)) all have a melting point below 1000° C and are considered chalcophile. Mineral phases, many of them sulfosalts, containing one or more of these elements tend to have a low melting temperature (Table 1), even below 350° C in the case of realgar (AsS) and orpiment (As_2S_3), and melts formed from such minerals can acts as a flux for the local system by wetting surfaces of the solid phases.

Table 1, modified from Table 2 in Tomkins et al. (2007).

Components	Melting temperature at 1 kbar	Reference
Single minerals		
Dyscrasite	558	(Hansen & Aderko, 1958)
Arsenopyrite	670	(Clark, 1960)
Chalcopyrite	850	(Craig & Kullerud, 1967)
Galena	1114	(Freidrich, 1907)
Pyrrhotite	1195	(Freidrich, 1907)
Sphalerite	1680	(Freidrich, 1907)
Multiple minerals		
Arsenopyrite + pyrite	491	(Barton, 1969)
Pyrite + galena	719	(Brett & Kullerud, 1967)
Py + gn + cpy + sph	~730 (2kbar)	(Stevens, et al., 2005)
Po + gn + sph	800	(Mavrogenes, et al., 2001)
Pyrrhotite + galena	880	(Freidrich, 1907)
Sphalerite + galena	1040	(Freidrich, 1907)
Pyrrhotite + sphalerite	1180	(Freidrich, 1907)

Controversy regarding sulphide anatexis

The relevance of sulphide melting during regional metamorphism is disputed. Plimer (1987) argues that the experimental data used by Brett & Kullerud (1967) and Craig & Kullerud (1967), among others, does not represent natural systems, where sulphur- and oxygen fugacity, $f(S_2)$ and $f(O_2)$ respectively, along with water pressure, $P(H_2O)$, can be expected to be lower than in the experimental settings. Comparing the composition of a Fe-Cu-Pb-Zn-S massive sulphide with a theoretical melt generated from such a system has led some researchers to suggest that sulphide melting is rare (Skinner & Johnson, 1987; Marshall, et al., 2000). Spry et al. (2008) dissect the major arguments for a significant sulphide melt phase in the Broken Hill Zn-Pb-Ag deposit. Melting of LMCE-bearing sulfosalts, they argue, did occur, but P-T conditions were not enough to initiate melting of the common sulphide minerals, even with a sulfosalt melt phase present, as was suggested by (Mavrogenes, et al., 2001). Other features of the Broken Hill deposit that has been attributed to sulphide melting, such as dihedral angles (Frost, et al., 2002, later reinforced by Frost, et al., 2011) and sulphide inclusions in garnet (Frost, et al., 2002; Sparks & Mavrogenes, 2005), were also questioned Spry et al. (2008). It is worth noting that most of the criticism is focused on melting of the Broken Hill ore body, whereas melting of other deposits, such Lengenbach, Switzerland, or Monte Arsiccio, Italy, has, to date, been undisputed. However, since these latter deposits host anomalous concentrations of LMCE, they are difficult to compare with more common VMS deposits in regards of sulphide anatexis.

Geological setting

Fennoscandian shield

The Skellefte district is hosted in the Fennoscandian Shield, the oldest geological unit in Europe. The core of the shield is the Archean craton, a section made up by greenstone belts and granitoids intrusions in northern Norway, northern and eastern Finland, and the Kola Peninsula in Russia. The craton was formed through merging of two smaller cratons, the Kola- and Karelian cratons, around 2.69 Ga (Gaál & Gorbatschev, 1987), and continued growth of the shield proceeded through accretion of crustal material on the W-SW side of the craton. The oldest rocks recorded in the Fennoscandian shield are the trondhjemite gneiss of the Pudasjärvi belt in the Karelian craton, with an age of <3.5 Ga (Huhma, et al., 2004).

Continental rifting, with associated magmatic activity, initiated during early Paleoproterozoic (2.51-2.43 Ga) and is marked by multiple layered mafic igneous complexes in the vicinity of Archean granitoids (Alapieti & Lahtinen, 2002). Subduction with associated arc volcanism to the W-SW of the

craton, followed by collision with, and accretion onto, the craton itself is prominent between ca. 1.9-1.8 Ga (Gaál, 1990), an event referred to as the Svecofennian, or Svecokarelian, orogeny. The central part of the shield, the Svecofennian Domain, is dominated by island arc volcanic rocks and coeval alkaline granitoids, formed between 1.9-1.87 Ga (Lundqvist, et al., 1998). The Transscandinavian Igneous Belt formed further SW-W of the Fennoscandian domain in an extensional setting, mainly between 1.81-1.65 Ga, with the oldest recorded rock being 1.85 Ga (Gorbatschev, 2004). As the name indicates, this belt comprises mainly intrusive and extrusive magmatic rocks, and its extent NW-SE is currently unknown. During the Gothian Orogeny, the Southwest Scandinavian domain was accreted onto the shield, and was later deformed by the Hallandian- (1.5-1.4 Ga: Brander, et al., 2011), the Sveconorwegian- (1.1-0.92 Ga: Weihed, et al., 2005) and lastly the Caledonian Orogeny (0.6-0.4 Ga: Gaál & Gorbatschev, 1987). The Caledonian orogenic belt, which covers the westernmost part of the Scandinavian Peninsula, is allochthonous and, therefore, not included in the Fennoscandian Shield.

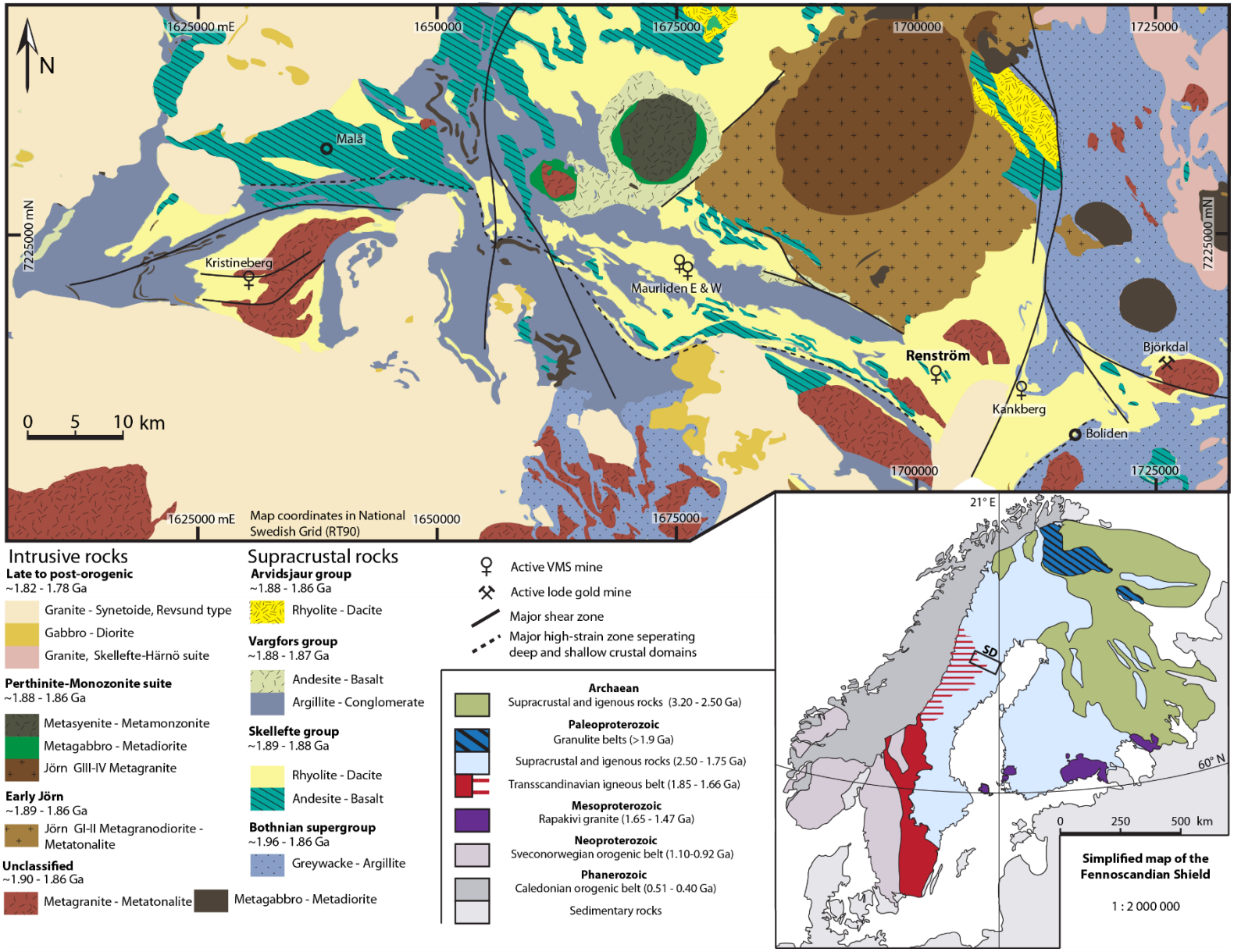

Figure 1. Small map: Simplified geology of the Fennoscandian Shield. SD: Skellfete district. Modified from Weihed et al. (2005), original map from Koistinen et al. (2001). Large map: Geology of the Skellefte district. Modified from Bauer et al. (2014), originally compiled based on Bergman Weihed (2001), Kathol et al. (2005) and Skyttä et al. (2012).

Skellefte district

The Skellefte district is a ca 120 x 30 km area of Paleoproterozoic (1.9-1.87 Ga) rocks hosted in the Fennoscandian Domain (Figure 1) (Allen et al., 1996). It stretches from the town of Boliden further W-NW and has been an important source of metals in Sweden throughout the latest century. Earlier studies (Weihed, et al., 1992; Allen, et al., 1996; Billström & Weihed, 1996) of the Skellefte district suggested formation in a volcanic arc setting that was later accreted onto the Karelian Craton. More recent studies propose either an extensional setting, between arcs, over a subduction zone (Nironen, 1997; Weihed et al., 2005) or a rift setting in an older basement (Skiöld & Rutland, 2006). The district is broadly defined by a belt of mainly volcanic rocks ("Skellefte group": Allen, et al., 1996), that hosts more than 79 known VMS deposits (Bauer, et al., 2014). This unit is overlain by sedimentary and extrusive rocks ("Vargfors group": Allen, et al., 1996), including breccia with clasts from the Skellefte group. Further N, the Skellefte group is overlain by red-brown volcano-sedimentary rocks of similar age as the Vargfors group ("Arvidsjaur group": Allen, et al., 1996; "Kiruna Arvidsjaur Porphyry Group": Liljequist & Svenson, 1974; Perdahl & Frietsch, 1993). Mafic to felsic intrusive rocks, mainly tonalities, adjacent to, and within, the Skellefte group makes out the "Jörn granitoids suit" (Allen, et al., 1996), and is believed to be comagmatic with the Skellefte group (Wilson, et al., 1987; Skiöld, et al., 1993). To the S, an extensive unit of metasedimentary, with some intrusive, rocks ("Bothnian Basin") delineates the southern border of the district. The district scale stratigraphy is immensely complex, and no unit can be continuously traced throughout the whole area (Allen, et al., 1996).

Three deformation events have shaped the district: D1, a period of crustal extension during which most of the VMS deposits were formed (Bauer, et al., 2014), preserved in pre-Skellefte group rocks (>1.9 Ga: Rutland, et al., 2001); D2, compressional deformation during the Svecofennian/Svecokarelian orogeny (1.879 – 1.867 Ga: Skyttä, et al., 2012) (Weihed et al., 1992; Allen et al., 1996); D3, E-W shortening between ca 1.82-1.80 Ga (Weihed, et al., 2002). Since D1 pre-dates the VMS deposition, only D2 and D3 have deformed the ore bodies in the area, being major controls on the current distribution of deposits. However, D2 and D3 are likely to have reactivated D1 faults, indicating that all three deformation events were crucial for ore distribution (Bauer, et al., 2011).

The main early folds, foliation and cleavages strikes parallel to the belt's extension. Plunge is moderately W in the W of the belt, moderately to steeply SE-NE in the E and shallow to moderate in the middle. Multiple faults, all striking roughly N, divide the belt into chunks and is believed to be caused by a secondary deformation event (D2 or D3) (Allen, et al., 1996). S_1 foliation, parallel to S_0, has been preserved in pumiceous rocks as crenulate stylolitic foliation, in chlorite-/sericite rocks as pervasive mica foliation and in lavas and intrusions as a spaced, weak foliation (based on McPhie, et

al., 1993). The district is characterized by moderate metamorphism, with greenschist facies in the centre to lower amphibolite facies in the E, W and S of the district (Berglund & Ekström, 1980; Allen, et al., 1996; Skiöld et al., 1993)).

VMS deposits in the Skellefte district

The Skellefte district has been a major source of Cu, Zn, Au, Ag, Pb, As, S, and Sb in Sweden ever since mining started in the Boliden deposit 1925 (Grip & Wirstam, 1970). Using the classification of Franklin et al. (2005), the Skellefte district is bimodal-felsic, with a strong spatial connection between deposits and submarine, felsic cryptodomes (Allen, et al., 1996; Gibson, et al., 2007). Suggested depositional setting for deposits in the district include deep-water seafloor, sub-seafloor replacement (e.g. Renström, Långdal, Petiknäs N: Allen, et al., 1996; Doyle & Allen, 2003) and shallow water-, possibly subaerial-, synvolcanic replacement (e.g. Boliden: Bergman Weihed, 1996). Deposits are strictly related to a period of extensional volcanism (Weihed, et al., 2005), reflected in a stratigraphic restriction with deposits generally occurring in the upper parts of the Skellefte group (Allen, et al., 1996). Allen et al. (1996) lists 4 different types of ore mineral assemblages: pyrite with streaks of disseminated sphalerite ± other ore minerals; sphalerite-pyrite-galena ± chalcopyrite; fine grained arsenopyrite ± pyrite-chalcopyrite; chlorite with pyrite-chalcopyrite veins and impregnations. Ore occurs as massive (50+ vol. % sulphides), semi-massive (25-50 vol. % sulphides) or impregnated (<25 % sulphides) ore bodies (Allen, et al., 1996).

The most common ore host is pumiceous volcaniclastic rocks, but hydrothermally altered breccia, fault zones and intrusive contacts also host deposits (Allen, et al., 1996). Thus, permeability seems to have been the major control on ore deposition. Recent studies have also shown a strong correlation between major shear zones and large deposits (Bauer, et al., 2014). Deposits often consist of one or more elliptical lenses. Main alteration halo is quartz-sericite-pyrite, generally in the form of an asymmetric envelope that extends mainly into the footwall. Pyrite, either disseminated or in the form of stringer networks, also reach further into the footwall. Dolomite-calcite-chlorite-talc ± tremolite alteration occurs in some deposits (e.g. Renström, Rävliden, Rävlidmyran, Rakkejaur, Långdal, Näsliden, Hälträsk), a strong indication of replacing rather than emplacing ore paragenesis, according to Allen et al. (1996).

Renström deposit

The Renström deposit is a Zn-Cu-Pb-Ag-Au VMS located 15 km W-NW of Boliden (Figure 1), with pre-production ore reserves of 9 Mt at 6.5 % Zn, 1.5 % Pb, 0.8 % Cu, 155 g/t Ag, and 2.8 g/t Au

(Duckworth & Rickard, 1993). The mine is currently the deepest mine in Sweden, and the discovery of a new ore zone extended the mine's target zone down to 1750 m below the surface, 430 m below the current depth of the mine (1320 m in 2004). The ore is mainly massive to semi-massive pyrite-sphalerite, but chalcopyrite and pyrrhotite also occur locally in stringers (Allen & Svenson, 2004). To date, 5 lenses of economic interest have been identified: the A and B lenses, the Deep A lens, the Deep Zone and the Simon lens (Figure 2), of which the latter is the ore body studied in the present study. The area is heavily deformed, making it stratigraphically and structurally complex, but all lenses occur in the same fold system (Allen & Svenson, 2004). All rock units in the area show moderate to strong foliation and lineation, and have been metamorphosed to greenschist facies (Duckworth & Rickard, 1993). The ore is hosted in a 20 to 70 m thick unit consisting of glassy silt-sandstone, basaltic to rhyolitic sills and domes, and compacted pumice (Allen & Svenson, 2004). Volcanic textural features can be traces from barren to mineralized rocks, indicating a replacing ore genesis, as suggested in Allen et al. (1996) and Doyle & Allen (2003). Evidence of deformation in the ductile regime can be found in both the host rock, as elongated fragments, and in the mineralized zone, as bands and almost tabular lenses (Duckworth & Rickard, 1993).

The Simon lens is located at the 950-1170 m levels (Figure 2), and host a probable reserve of 505 000 t (7.9 % Zn, 1.5 % Pb, 0.8 % Cu, 158 g/t Ag, and 3.6 g/t Au) (Kläre, 2001). The lens itself is a sub-vertical envelope of strong chlorite alteration, hosted in chlorite-quartz altered volcanic sediment. The sedimentary unit is made up by varying silt- and pumice-rich layers close to the mineralization. Multiple dacitic bodies intrude the hosting volcanic sediment in the stratigraphic lower parts of the unit. Within the chlorite envelope, numerous (>1 to 17 m wide, >20 to <240 m long) lenses of massive to semi-massive pyrite-sphalerite resides, following the general strike and dip the host rock. The lens is situated in the limb of a refolded synform that dips ~50° to the east (Kläre, 2001).

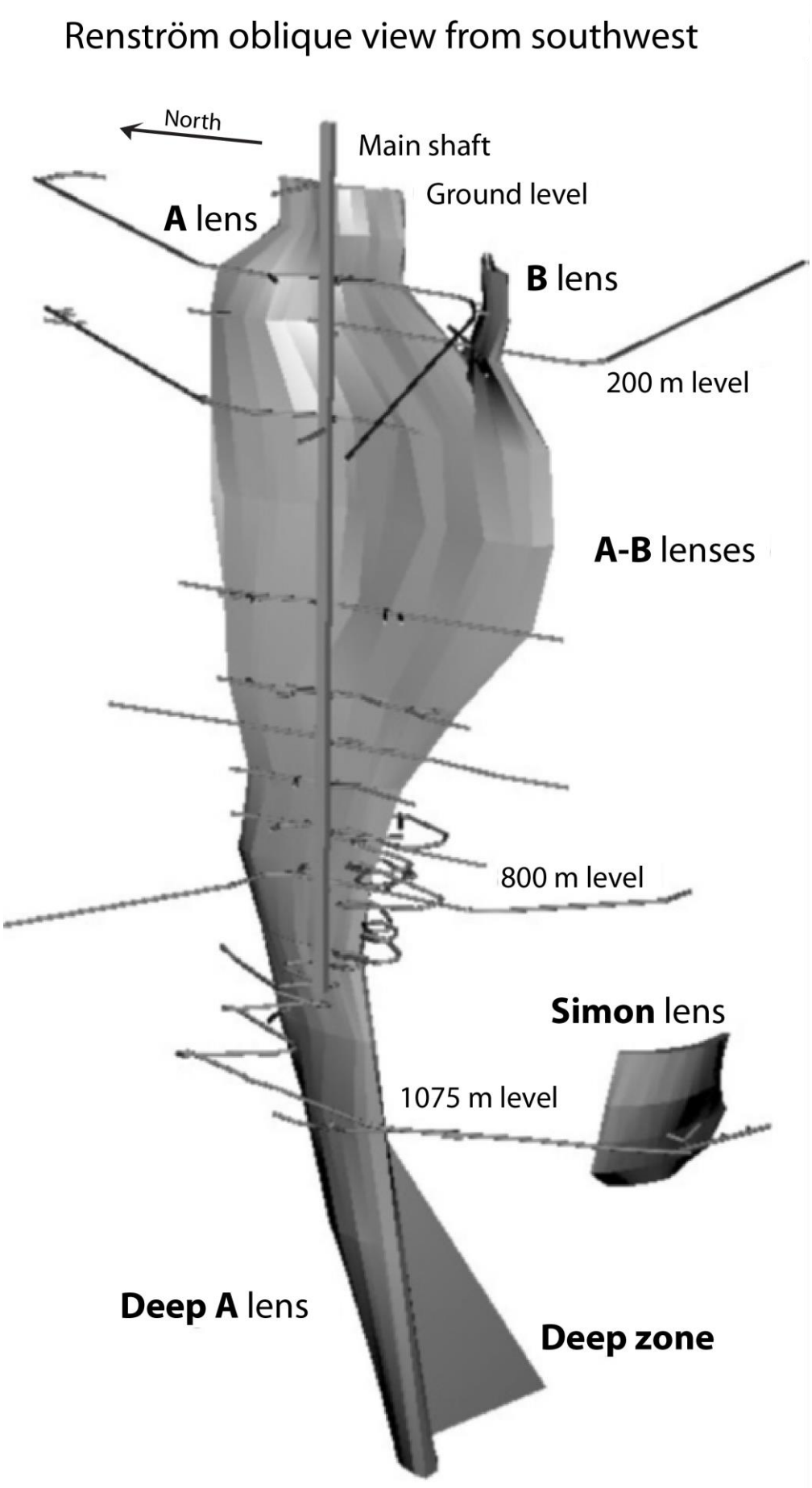

Figure 2. Schematic 3D model of the Renström deposit.. From Allen & Svenson (2004).

Sampling

Lithological description of the core

Drill core BH2559 is taken from the Simon lens of the Renström deposit, a mineralization within the same fold system as the main ore body but spatially detached (Figure 2). The core was taken sub-horizontally, tilting slightly upward and penetrating three lithological units in the now vertical stratigraphy, all of them altered to varying degrees. Parts of a fine-grained, dark-grey dacite intrusion covers the top meters of the core, followed by volcanic sediment with layers of pumice, a chlorite schist envelope and then back to a more silty volcanic sediment (Figure 3). The stratigraphic order is reversed, with dacite being the lowermost unit. Sections of grey to light grey altered pumice and distinct blue rounded quartz grains can be found within the volcanic sediment (Figure 4f). In other parts of the sedimentary unit, silicified silty layers occur with minor stringers of pyrite (Figure 4a). This marks the upper border of the chlorite schist envelope and the mineralized zone of the core. Within the chlorite schist, mineralization occurs as elongated parallel lenses of massive to semi-massive sphalerite and/or pyrite, with minor amounts of galena, chalcopyrite, pyrrhotite and arsenopyrite, as well as coarse dolomite and quartz. Going further upwards in the stratigraphy, the chlorite schist is sharply overlain by another section of volcanic sediment, impregnated by stringers of pyrrhotite ± pyrite and minor sphalerite. The abundance of sulphides gradually decrease further away from the mineralized zone. This section of volcanic sediment has abundant pumice-rich layers, and becomes siltier and more distinctly foliated towards the end of the core. Although mineralization is restricted to the chlorite schist, stringers and bands of pyrite and pyrrhotite can be found in the volcanic sediment, as well as minor amounts of sphalerite.

A suite of 88 samples were collected from the core, chosen to represent the variation in lithology, alteration and mineralisation styles, with positions in the core shown in Figure 3. Of these, all but one sample were polished down to 30 µm thin sections at Vancouver Petrographics. The last sample, CURT, was doubly polished and specifically selected for studies of fluid inclusions in sphalerite and dolomite (Figure 3).

Textural description of the core

All sections of the core show evidence of deformation, although the extent and type of deformation varies between units. The contact between the dacite and the upper volcanic sediment is gradational, with fragments of dacite occurring in the volcanic sediment (Figure 4). The foliation become gradually more distinct further down the volcanic sediment, with elongated clasts being common in the lower sections. Massive and fine-grained parts of the volcanic sediment can be found

at the bottom of this unit (Figure 4a). Elongated fragments from the volcanic sediment occur in the upper parts of the underlying chlorite schist (Figure 4b). Foliation in the chlorite schist is commonly well-developed and this unit is folded in places (Figure 4c). Brecciated fragments of dolomite occur in places (Figure 4d). Close to the lower contact of the chlorite schist, the foliation changes dip and becomes subparallel to the core itself (Figure 4e). The lower unit of volcanic sediment has abundant blue quartz and elongated pumice fragments (Figure 4f), while the siltier unit at the end of the core is absent of any such features.

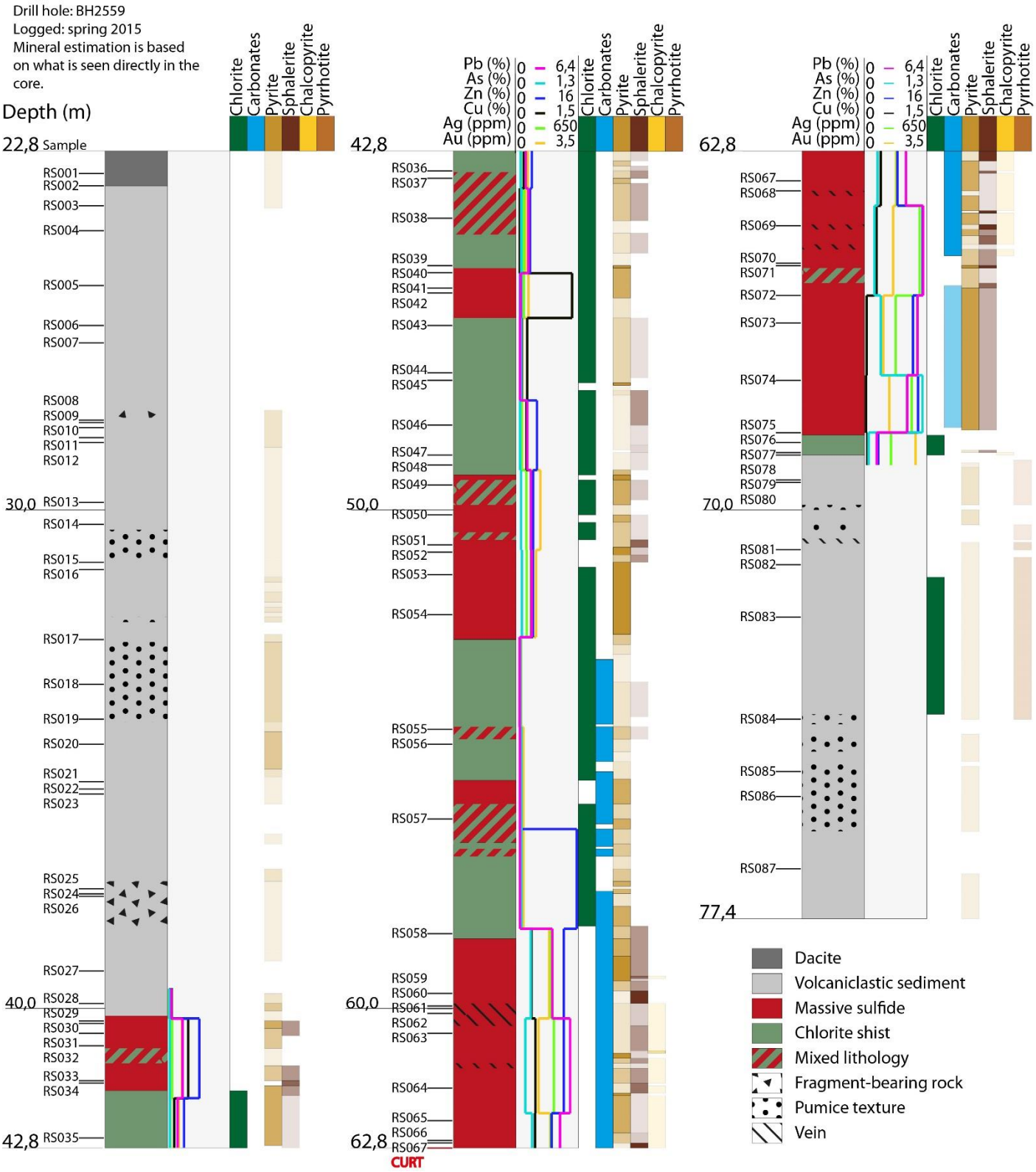

Figure 3. Log of drill hole BH2559 showing the lithological variation, the abundance of key alteration and ore minerals, and also whole rock concentrations of selected metals. The lithology and mineral abundances are estimated from visual observation of the core. Element concentrations are taken from whole rock assay data provided by Boliden (Table 6).

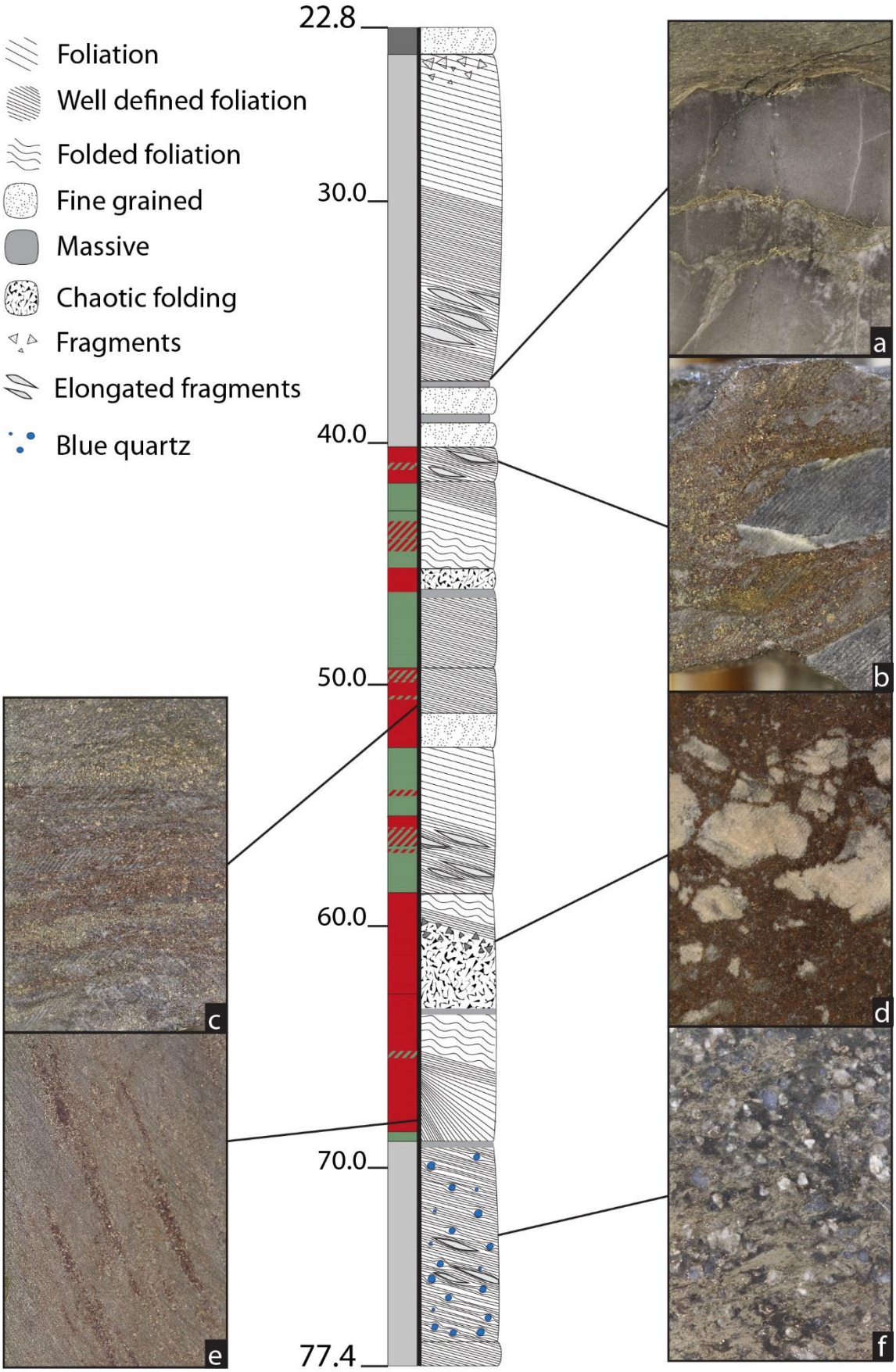

Figure 4. Structural log of the core. The left column is the lithological units presented in Figure 3. The right column is a sketch of the deformation textures observed in the core. Pictures a – f are ~25 mm wide and are taken along the core. Dip of foliation is only given in relation to the strike of the core and may not, therefore, represent the actual dip. ***a*** *Silicified blobs of quartzite in contact with silty volcanic sediment.* ***b*** *Elongated fragments in sulphide dominated matrix.* ***c*** *Varying bands of pyrite and sphalerite.* ***d*** *Fragments of dolomite in sphalerite.* ***e*** *Tilted bands of sphalerite in chlorite altered groundmass.* ***f*** *Foliated pumice with rounded blue quartz grains.*

Methods

Instrumental setup

Microscopy

Reflected and transmitted light microscopy has been the main tool for mineral identification and establishing mineral textural relationships. For unknown minerals grains in thin sections, a Philips XL-30- ESEM-FEG environmental scanning electron microscope ("ESEM"), equipped with an EDAX X-ray energy dispersive system ("EDS"), operating under high chamber vacuum, was used to obtain element concentrations. All samples were covered in a ~20nm thick layer of carbon before analysis to increase the conductivity of the sample.

Microprobe

Wave-length dispersive spectroscopy analysis for geothermometry of arsenopyrite was performed at the electron microprobe facility at Geocentrum, Uppsala University, using a Jeol JXA-8530F HyperProbe. Beam size was 1-2 µm, current was set to 20 kV, with a voltage of 20 nA. Standards and energy-lines used are listed in Table 2. All thin sections were carbon coated before analysis.

Table 2. Standards and energy-lines used for microprobe analysis.

Element	Standard	Energy-line
S	Pyrite, sphalerite, galena	K-α
Fe	Pyrite	K-α
Ni	Ni-sulphide	K-α
Cu	Cuprite	K-α
Zn	Sphalerite	K-α
As	Ga-arsenide	L-α
Ag	Silver	L-α
Cd	Cadmium	L-α
Sb	Stibnite	L-α
Pb	Galena	M-α

LA-ICP-MS

Trace element concentrations were measured using laser ablation inductively coupled plasma mass spectrometry ("LA-ICP-MS"), carried out at the Department of Earth Sciences, University of Gothenburg. An Agilent 8800QQQ Triple Quad ICP-MS, coupled with a New Wave NWR213 laser ablation system, were utilized for this analysis. For opaque phases, two runs with slightly different settings were performed. The first run, covering all common opaque minerals identified in the core, used the following settings: isotopes analysed: ^{34}S, ^{57}Fe, ^{66}Zn, ^{75}As, ^{78}Se, ^{95}Mo, ^{107}Ag, ^{111}Cd, ^{115}In, ^{121}Sb, ^{125}Te, ^{197}Au, ^{202}Hg, ^{208}Pb, ^{209}Bi; laser beam energy density: 4.3 J/cm^2; spot size: 20 µm; pulse

frequency: 5 Hz. For calibration, Pb_{208} (for galena) and Fe_{57} (for all other mineral phases) concentration of the Mass-1 standard, also known as PS-1, was used (Wilson, et al., 2002). The second run, focused on the Au content of dyscrasite, used a smaller spot size (10 µm) to avoid contamination from neighbouring minerals. To compensate for this loss of sampling material, analysis of ^{78}Se, ^{95}Mo, ^{111}Cd and ^{115}In were omitted for the second run, enabling longer sampling time for ^{197}Au instead. For the second run, ^{121}Sb concentration of Mass-1 was used as a standard.

Lab procedure for Pb-U dating of titanites followed the method described in (Cornell, et al., 2013), with the exception that the same facility as mentioned above was used instead of the Agilent 7500a quadrupole ICP-MS. For this analysis, spot size was set to 50 µm, frequency to 5 Hz with a surface energy of 4.1 J/cm^2. A flow of 950 ml He and 4 ml N_2 per minute was used during the procedure. GJ-1 was used as primary standard (Jackson, et al., 2004).

Fluid inclusions

Fluid inclusion studies was performed using a Horiba Instruments LabRAM HR 800 confocal laser Raman spectrometer with a multichannel air-cooled 1024 x 256 pixel charge-coupled device array detector. Laser was generated from an Ar-ion source, with a wavelength of 514 nm and a surface power of 5 mW. Focusing of the laser beam was done through an x100 objective lens, achieving a spot size of ~1 µm. The accuracy of the procedure was controlled through repeated analysis of a silicon wafer standard. LabSpec 5 software was utilized to convert obtained data to Raman spectra.

Geothermometry

The arsenopyrite geothermometer developed by Kretschmar & Scott (1976) builds on experimental studies by Clark (1960) and Barton (1969) in the Fe-As-S system, and has been applied to multiple ore bodies, including deposits in the Skellefte district (Berglund & Ekström, 1980). The refractory nature of arsenopyrite make it a robust tool up to lower amphibolite facies, after which the effect of pressure makes estimates inaccurate (Sharp, et al., 1985). The method relies on a sulphur fugacity buffered by the pyrite-pyrrhotite system (Toulmin & Barton, 1964; Barton, 1969), so only arsenopyrite grains in direct contact with both pyrite and pyrrhotite should be included when using the geothermometer.

Geochronology

U and Pb may be incorporated in titanite ($CaTiSiO_5$) during mineral growth, making the mineral a possible geochronometer. Titanite is the main Ti-host in weakly metamorphosed calcareous rocks, but Ti may go into ilmenite ($FeTiO_3$) at upper greenschist to lower amphibolite facies. Titanite has an estimated closure temperature above 660° C (Frost, et al., 2000), significantly higher than what has

been inferred for the Renström deposit (Berglund & Ekström, 1980). Instead of closure temperature marking the upper border of the mineral's usefulness as geochronometer, mineral growth governs the recorded U-Pb age of titanite (Scott & St Onge, 1995), making titanite an ideal tool for dating low to medium grade metamorphic events and deformation (Frost, et al., 2000).

Results

Mineralogy

Opaque minerals

Opaque minerals found in the core includes multiple common sulphides, two types of sulphosalts and rare species of Ag-rich phases. The term "opaque" relates to the mineral's appearance under transmitted light microscopy: they generally show up as compact phases with little to no light shining through the grain under plane polarized light.

Arsenopyrite

Arsenopyrite is fairly common throughout the core, and similarly to pyrite, it is not restricted to a specific alteration styles or host rocks, but can be found in all assemblages. The largest abundances of arsenopyrite are associated with abundant pyrite, and arsenopyrite is relatively uncommon in sections of sphalerite-dominated massive sulphide. Only rare isolated grains occur in unmineralized rock. Being a refractory mineral, arsenopyrite maintains it rhombic euhedral shape in all but one sample, where it has been fragmented and partially broken down by other common sulphide minerals (Figure 5d). Arsenopyrite in the core generally form large (< ca. 0.7 mm) crystals, particularly in the sulphide rich sections of the core, but aggregates of small (< ca. 20 µm) arsenopyrite crystals can be found in lower parts of the mineralized zone. Isolated minor grains of arsenopyrite have also been observed within chalcopyrite. Inclusions of pyrite in larger arsenopyrite occur, but growth of pyrite on the surface of arsenopyrite crystals is a more common texture, sometimes almost reaching full encapsulation of the arsenopyrite grain.

Chalcopyrite

Larger patches of chalcopyrite occur sporadically throughout the core, always associated with dolomite and abundant sulphides. On a microscopic scale, chalcopyrite can be found in most parts of the mineralized zone, often together with pyrrhotite and/or sphalerite. Chalcopyrite commonly occurs as anhedral ponds, but also exists as inclusions and crack infills in sphalerite. Chalcopyrite is of minor occurrence in sphalerite dominated samples, but is more common in samples with more or less equal amounts of pyrite and sphalerite, as well as in samples rich anhedral pyrrhotite. Moreover, chalcopyrite, along with pyrrhotite, sphalerite, galena and, to a lesser extent, pyrite, occur in veins

and patches of quartz, chlorite, and calcite (Figure 5c, f). Chalcopyrite as a thin rim on pyrrhotite in contact tetrahedrite and/or sphalerite is an existing, but rare, feature, only observed in sphalerite dominated samples (Figure 5c). Cubanite exsolutions in chalcopyrite has been noted in a few larger accumulations of chalcopyrite, of which all also have notable amounts of pyrrhotite in direct contact with the chalcopyrite.

Galena

In sphalerite dominated parts of the core, small silvery grains of galena can be observed with a hand-lens in the massive red-brown sphalerite. These grains do not form larger patches, but remain as individual crystals in the dark red groundmass. Under the microscope, galena is common as anhedral ponds between grains of sphalerite, penetrating the sphalerite structure along grain boundaries (Figure 5c, e). These ponds may be elongated along foliation. Galena is also abundant together with chalcopyrite-pyrrhotite(±sphalerite), either in the form of shapeless accumulations surrounding rounded pyrite or small sulphide packages in calcite or chlorite. Similarly to aforementioned sulphides, galena may also occur as isolated grains in quartz-, calcite-, and chlorite veins.

Pyrite

Pyrite is the most common sulphide in the core and occurs as two distinct types the naked eye: coarse grains in pyrite-quartz bands or lenses and smears of very fine grained pyrite, following foliation and commonly infilling spaces between grains (Figure 4a, c, e). In pyrite-dominated sections of the core, these two modes of occurrence often appear in contact with each other, with quartz making out the remainder of the rock. Streaks and bands of sphalerite may also occur in such areas.

Pyrite can be found more or less throughout the whole core varying in style and abundance from small disseminated grains to pure massive pyrite-quartz assemblages. Disseminated pyrite above and below the main mineralized zone are generally small eu- to subhedral single grains that show evidence of partial breakdown. Sizable pyrites in these areas have pressure shadows of calcite and/or sheet silicates. Larger accumulations of pyrite outside the main mineralized zone can be found with either quartz or chlorite in veins, following the general foliation of the rock. Within the mineralized zone, pyrite tends to show replacement textures with most other common sulphides, arsenopyrite excluded. In particular, caries textures with sphalerite infill in pyrite occur in more or less every sample where significant amounts of pyrite and sphalerite coexist (Figure 5e). Pyrites in such samples all have rounded edges. Sphalerite, pyrrhotite, galena and chalcopyrite often surround and fill cracks in larger pyrite grains, particularly in the lower parts of the mineralized zone (Figure 5a). In the middle of the mineralized zone, a section of essentially pure pyrite and quartz exists, showing little to no signs of alteration (Figure 5b). The massive pyrite in this area seems to be the result of

amalgamation of smaller pyrite crystals. In the outer parts of this pyrite-quartz zone, calcite, with associated biotite and amphibole, intrude through the quartz and enable precipitation of sphalerite, chalcopyrite and pyrrhotite in cracks, and between grains, of pyrite.

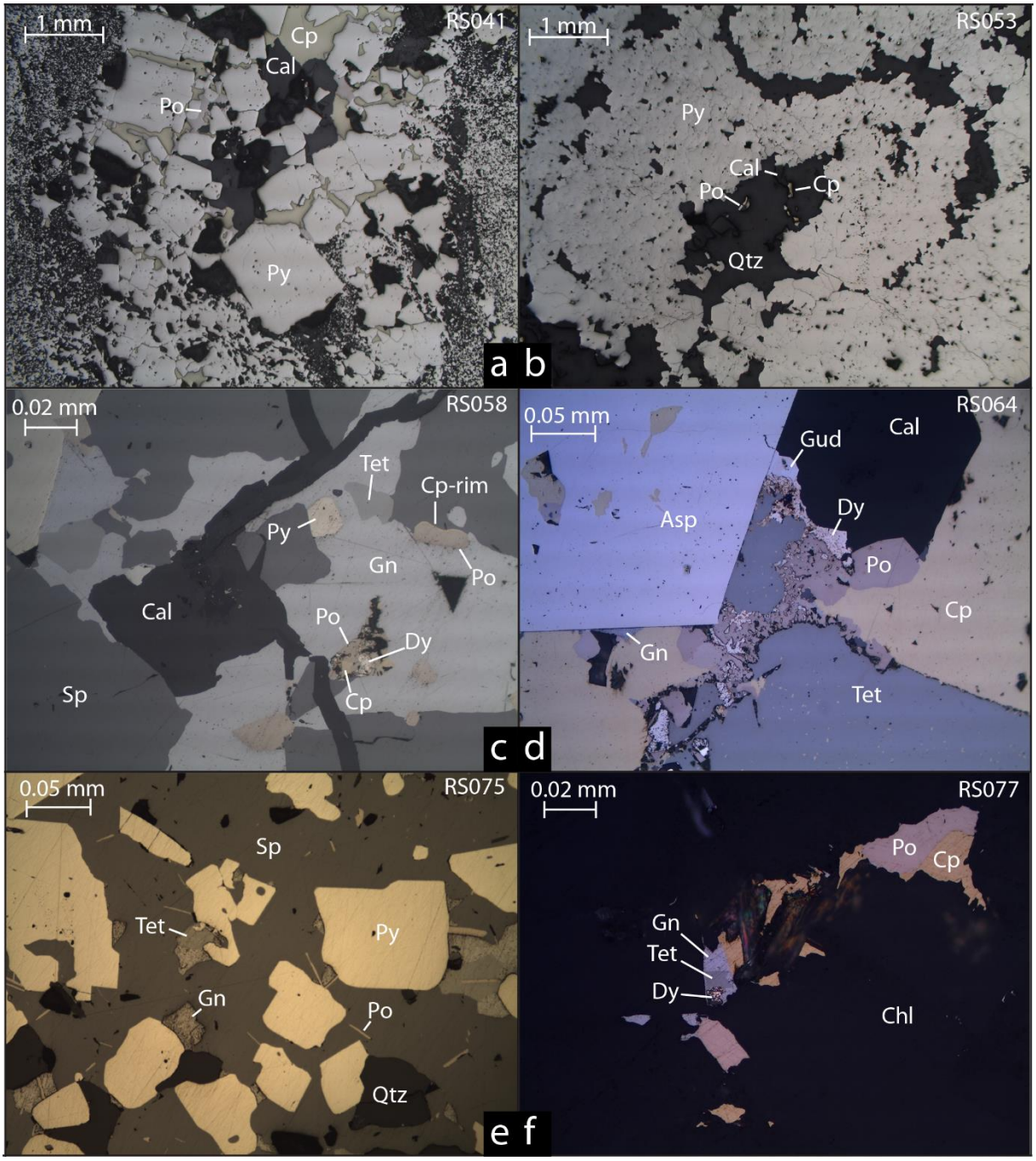

Figure 5. Sulphide assemblages under reflected light. ***a*** *Vein of coarse pyrite (Py) and calcite (Cal), with infillings of chalcopyrite (Cp) and pyrrhotite (Po). The vein cuts through fine grained pyrite and quartz (Qtz).* ***b*** *Massive pyrite-quartz assemblage with minor chalcopyrite and pyrrhotite associated with intrusive calcite.* ***c*** *Pond of galena (Gn), pyrrhotite, and tetrahedrite (Tet) in a massive sphalerite (Sp) and pyrite assemblage. Calcite- filled crack cuts the sulphide assemblage, facilitating breakdown of tetrahedrite into pyrrhotite, chalcopyrite and dyscrasite (Dys). A thin rim of chalcopyrite occur in the contact between sphalerite and pyrrhotite.* ***d*** *Breakdown of tetrahedrite into multiple component along grain boundaries in a arsenopyrite-rich chalcopyrite-assemblage. Dyscrasite and pyrrhotite form a symplectic-like intergrowth, while chalcopyrite form inclusions in tetrahedrite. Gudmundite (Gud) occur as small grains in contact with calcite.* ***e*** *Massive sphalerite with rounded grains of pyrite and quartz, euhedral sticks of pyrrhotite, and ponds of galena and tetrahedrite. Pyrite show a typical caries replacement texture, with mainly sphalerite being the replacing component.* ***f*** *Inclusions of pyrrhotite-chalcopyrite-galena-tetrahedrite, with minor dyscrasite, in massive chlorite (Chl).*

Pyrrhotite

A few grains of pyrrhotite has been observed directly in the core, but based on changes in magnetism along the core, pyrrhotite is inferred to be fairly common in the lower sections of the mineralized zone and the underlying units (Figure 3). No other minerals with significant magnetism has been observed.

There are two distinct forms of pyrrhotite found in samples: elongated euhedral crystals of varying size (<0.1 mm long) in massive sphalerite (Figure 5e), and anhedral patches commonly occurring with chalcopyrite, galena, and minor amounts of sphalerite (Figure 5a, f). The pyrrhotite "sticks" in sphalerite-dominated samples are not restricted to the massive sphalerite itself, but may also be found in galena, tetrahedrite, and/or boulangerite. Growth of pyrrhotite on the surface of pyrite is a common feature in such samples. Pyrrhotite past the mineralized zone commonly form pressure shadows on larger grains (quartz, feldspar or pyrite) or fill out parts of quartz- or calcite veins. Further out from the mineralized zone, veins of pyrrhotite and pyrite occur, notably absent of calcite. The silty layers at the bottom of the core has elongated impregnations of pyrrhotite parallel to the foliation (Figure 6f). Rows of pyrrhotite grains in the contact between calcite and chalcopyrite has been observed in multiple samples, as well as pyrrhotite crack infill in chalcopyrite.

Sphalerite

Sphalerite is the second most common sulphide in the core and is the dominant species in parts of the mineralized zone. Bands or streaks of sphalerite are common in sulphide rich sections (Figure 4e), but massive sphalerite with blobs of dolomite can also be found (Figure 4d). Some parts of the core is almost entirely made up by pyrite and sphalerite in the form of varying layers dominated by either sulphide (Figure 4c).

On a microscopic level, sphalerite occurs as anhedral patches and ponds. In samples dominated by the mineral (>50 % of the total volume), sphalerite makes out the bearing structures of the rock (Figure 5e). In such samples, there is extensive evidence of sphalerite replacement of pyrite. In all but the most sphalerite rich parts of the core, the mineral tends to form bands of varying thickness parallel to the general foliation. Sphalerite in the mineralized zone are most commonly associated with euhedral pyrrhotite, ponds of galena and rounded pyrites (Figure 5c, e), but outside this zone, sphalerite is more common as bands with associated rounded pyrite or in veins with associated anhedral chalcopyrite-pyrrhotie±galena±pyrite.

Tetrahedrite

Tetrahedrite has not been observed with the naked eye in the core, but is commonly observed in thin sections rich in sphalerite and galena. The mineral forms anhedral patches in sphalerite together with

galena and, more rarely, boulangerite ($Pb_5Sb_4S_{11}$) (Figure 5e). It may also be found together with chalcopyrite, pyrrhotite, sphalerite, and galena in veins of chlorite or calcite, especially in the lower parts of the mineralized zone (Figure 5f). Larger grains of tetrahedrite are uncommon, and the few examples found have all shown varying degrees of breakdown into multiple other components. Tetrahedrite in sphalerite-pyrite-galena-pyrrhotite samples are the least altered (Figure 5e), while tetrahedrite in more complex assemblages, such as chalcopyrite-pyrite-pyrrhotite-galena-calcite(±arsenopyrite), tend to break down into chalcopyrite-pyrrhotite-dyscrasite(±gudmundite) (Figure 5d). Particularly, abundant calcite seems to be a catalyst for tetrahedrite breakdown. While stable tetrahedrite is essentially free of inclusions, large grains experiencing breakdown tend to be dotted with small inclusions of chalcopyrite±gudmundite±arsenopyrite, and also rimmed with anhedral pyrrhotite-dyscrasite (Figure 5d).

Minor opaque phases

Dyscrasite (Ag_3Sb) has been noted in 10 out of 87 samples, although never in any significant quantities. The antimonide occurs as ~5-20 µm ivory-white anhedral grains in reflected light that easily oxidize to a more red-blue hue along the edges. All observed dyscrasite grains occur with calcite (Figure 5c). Dyscrasite seems to form in direct contact with, or in proximity of, pyrrhotite, chalcopyrite, tetrahedrite, and/or gudmundite, often with more than one of these minerals present. Dyscrasite may also occur as isolated grains in mineralized calcite veins, as noted in the chlorite rich lower parts of the mineralized zone. A notable texture specific for breakdown of tetrahedrite is a dyscrasite-pyrrhotite intergrowth, almost symplectic in nature (Figure 5d). In favourable areas, with plenty of unstable tetrahedrite, larger (>0.1 mm), irregularly shaped bodies of dyscrasite may form.

Gudmundite (FeSbS) is a small (~10-30 µm) uncommon pale blue-grey sulphide that has been observed in a few mineralized samples. All observations of gudmundite has been in direct contact with calcite (Figure 5d). In sphalerite-rich samples, gudmundite grows on surfaces of pyrite or, less commonly, galena in calcite-filled cracks. In samples with abundant chalcopyrite, gudmundite can be found together with other breakdown products of tetrahedrite, as listed above. The mineral commonly form as sub- to anhedral rhombic crystals that may be confused with arsenopyrite.

Boulangerite ($Pb_5Sb_4S_{11}$) is a rare light green-grey anhedral sulphosalt that coexists with tetrahedrite and galena in sphalerite dominated samples. Boulangerite tend to form stretched out grains and, similarly to its two companion minerals, fills out the space between sphalerite and pyrrhotite grains.

Additionally, two small (<10 µm) grains of eugenite ($Ag_{11}Hg_2$) have been observed as inclusions in sphalerite, and two inclusions of tennatite ($Cu_6[Cu_4(Fe,Zn)_2]As_4S_{13}$) has been noted in pyrite.

Alteration minerals

The alteration assemblage observed in the Renström deposit can be attributed to (at least) two major events: mineralization in a VMS-environment and post-mineralization regional metamorphism at greenschist facies. Distinguishing between these two events is problematic, and certain minerals are likely to have developed during both events. In this study, the term “alteration mineral” covers all minerals not classified as opaque minerals.

Amphiboles

The amphiboles in these samples lie on the actinolite-tremolite series and they occur in the upper half of the core as rhombic and often partially fragmented grains. The colour is green to pale green or even colourless in plane polarized light, with the paler species occurring closer to the mineralized zone (Figure 6c). Inclusions of pyrite, smaller than the surrounding pyrite grains, are fairly common in amphiboles, and sulphides often cut through, or intrude along cleavage planes (Figure 6c). Amphiboles partially altered to calcite also occur with calcite in the massive quartz-pyrite assemblages. A distinctly different style of amphibole occurs in a quartz-amphibole vein in the upper volcanic sediment, where the amphibole sits as thin green needles in radiating clusters in a quartz groundmass, partially intruded by calcite (Figure 17a). In this vein, only amphiboles close to the calcite show any signs of alteration.

Biotite

Albeit not the most frequently occurring mineral, biotite can still be found in most sections of the core. However, it is less abundant within the mineralized zone, where it can only be found as isolated eu- to subhedral grains surrounded by sulphides. Outside the mineralized zone, biotite occurs as small to large anhedral patches, commonly stretched out in bands that follow the general foliation. Small inclusions of pyrite occur in biotite, but pyrite following the shape of euhedral biotite grains is a more common feature, particularly in pyrite rich samples. Distribution of euhedral biotite in the lower parts of the core is restricted to calcite veins, where it occurs with pyrite, pyrrhotite and sphalerite. Bands of sphalerite often have plenty of eu- to subhedral grains of what is assumed to be biotite in varying shades of brown incorporated in them, although complete encapsulation of the silicate is uncommon (Figure 6b).

Calcite

Calcite is a common mineral occurring as veins and intrusions in all sections of the core, cross-cutting foliation at some places while following it at other. Individual grains vary in shape and appearance, ranging from large euhedral crystals with clear twinning (Figure 6d) to microcrystalline anhedral masses (Figure 6f). Calcite seems to be focused in areas that have experienced high strain, as

indicated by mineral orientation and stretching. Plenty of different minerals are spatially related to calcite, either occurring directly in calcite veins or in contact with them. A good example of this can be seen in the pyrite-quartz zone, where biotite and amphibole only occur in contact with calcite. Similarly, grains of chalcopyrite, pyrrhotite and sphalerite in the same section can be continuously traced back to calcite intrusions in quartz, and no sulphides other than pyrite can be found disconnected from these veins (Figure 5b). In samples dominated by sphalerite-dolomite, cracks filled with calcite cut through grains of dolomite, sphalerite and galena (Figure 5c). Veins of calcite also cut through larger patches of dolomite in the chalcopyrite-dolomite rich sections of the core. Calcite veining can be traced from the mineralized zone far out into the stratigraphically overlaying volcanic sediment (Figure 6f), and it is related to these veins that most of the sulphides in this part of the core exist (Figure 17d). Calcite can also been seen cutting through larger sections of chlorite.

Chlorite

Most of the core shows chlorite alteration, even visible to the naked eye, though it is focused in the mineralized zone of the core. The most common mode of occurrence of chlorite is as small anhedral grains spread out through the groundmass of a sample, a feature that can be observed in more or less the whole volcanic sediment (Figure 6f). In heavily sheared zones, euhedral, fan-like chlorite grains can be found in clusters of sulphides, forming pressure shadows on mainly pyrite. Chlorite alteration commonly creeps along the edge of sulphide clusters, commonly replacing other sheet silicates. Veins of more or less pure chlorite can be found in selected parts of the core, whereas larger areas of mainly chlorite are restricted to the lower parts of the mineralized zone. Common sulphides, such as galena and sphalerite, penetrate these fan-like grains along the chlorite cleavage (Figure 5f).

Dolomite

Dolomite is restricted to the mineralized zone, specifically the sphalerite-rich parts of it, where it is a fairly common mineral (Figure 5d). However, outside this area, dolomite cannot be observed in any significant amounts. Depending on the mineral assemblage related to dolomite, two types can be found: in sphalerite-dominated areas, rounded isolated pockets of dolomite in sphalerite are common, whereas larger accumulations of dolomite, making out the bearing mass of certain samples, commonly show a fan- or tallus-like texture.

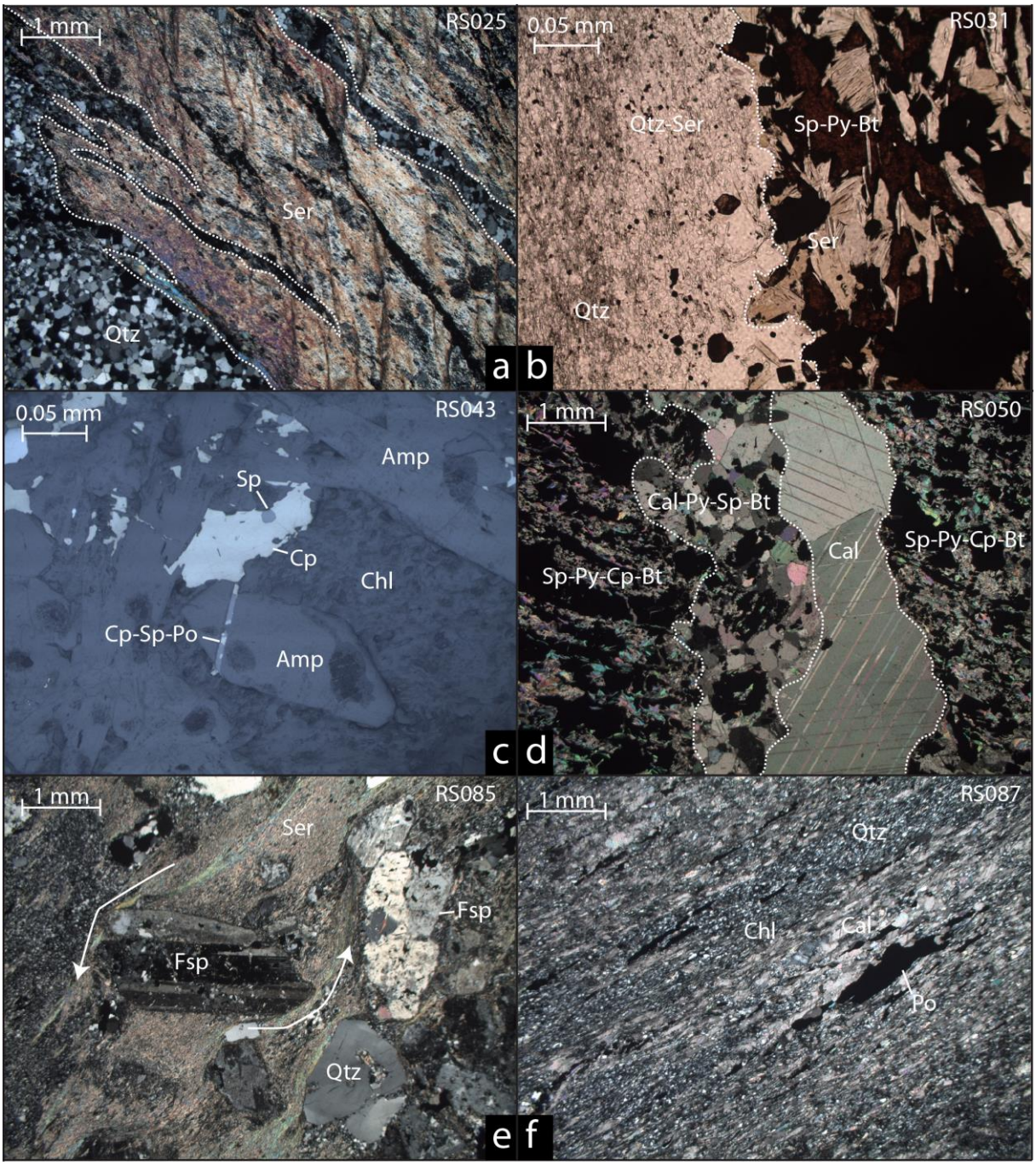

*Figure 6. Alteration minerals found in the core under plane- (a) and cross-polarized (b,d,e,f) light, as well as reflected light (c). **a** Foliated and partially folded sericite (Ser) with slivers of quartz (Qtz). Shifting birefringence of sericite is due to varying thickness of the thin section. **b** Contact between a band of sphalerite (Sp) and pyrite (Py), with euhedral biotite (Bt), and medium-grained quartz, overprinted with fine sericite. **c** Partially broken amphiboles (Amp) in a chlorite- (Chl) dominated groundmass, with sphalerite and pyrrhotite cutting through the amphibole fabric and intrude along cleavage of the grains. **d** Calcite (Cal) vein cutting through a foliated assemblages of sphalerite-pyrite (Py)-chalcopyrite (Cp), with associated eu- to subhedral biotite. **e** Rounded and rotated porphyroclasts of feldspars (Fsp) and quartz in a fine-grained groundmass of quartz and sericite. Rotational movement of feldspar is indicated by the white arrows. **f** Heavily foliated sample from the silty bottom layer of the core, with slivers of pyrrhotite in an assemblage of fine quartz and chlorite with bands of flattened carbonate grains.*

Quartz

Quartz is a common mineral, occurring in different shapes and varieties throughout the core. In the volcanic sediment, quartz can be found as porphyroclasts (Figure 6e), veins, accumulation of grains or as a fine grained groundmass (Figure 6b, f), whereas quartz in the mineralized zone are more common as rounded isolated pockets in sulphide assemblages or infill between pyrite grains (Figure 5e). Thin veins of pure quartz in the upper and lower parts of the core tend to be folded and/or cut by calcite veins. Coarse quartz forming veins and bands with pyrite close to the border of the mineralized zone are often elongated parallel to foliation, while quartz in pyrite-dominated areas show little signs of deformation (Figure 5b). Thicker veins of quartz have sets of parallel cracks interpreted as joints that strike subparallel to the strike of the vein itself. Heavily silicified parts of the volcanic sediment are made up by bands of fine grained quartz and massive coarse grained quartz, with stringers and pods of pyrite and sericite occurring in-between (Figure 5a). In the lower unit of volcanic sediment, larger porphyroclasts of quartz and feldspars with pressure-shadows of chlorite, calcite, and/or pyrrhotite are abundant (Figure 6e). Cracks of these grains tend to be filled with finer grained quartz.

Sericite and muscovite

Although extensive sericite-alteration is indicated in hand samples by a silky texture on fractured surfaces, individual minerals cannot be identified without visual aid. In addition to fine-grained anhedral sericite alteration in groundmass (Figure 6a, e), eu- to subhedral, commonly elongated, grains of muscovite can also be found in selected samples, often related to bands and blobs of sulphides. Sericite is often concentrated as “flows” in samples, areas with signs of extensive deformation (Figure 6e). Small, thin, pale green needles overprinting porphyritic feldspar and quartz has been identified as sericite, but identification is not certain (Figure 6b). Elongated grains of muscovite generally follow the foliation, but variation in grain orientation is common within muscovite rich samples. Muscovite often has preserved reaction textures with both chlorite and biotite, but which direction the reaction is going cannot be definitely established.

Titanite

Titanite ($CaTiSiO_5$, also called sphene) is an uncommon mineral in the core, occurring mainly in fine-grained parts of pyrite-rich samples. The grains are generally ~20-30 µm thick, eu- to subhedral and rhombic, often with pyrite inclusions. One notable exception is two pairs of well-defined elongated crystals in a sphalerite-dominated sample, where each crystal has the approximate dimensions of 70*70*400 µm . Knots of ilmenite breaking down to titanite can be found throughout the core, even in sulphide-rich samples.

Tourmaline

Tourmaline in the core is rare, and has only been observed in 3 samples. Grains found are all blocky with a clear dark to light green zonation and sits in the fine grained groundmass, in veins or in stretched accumulations of pyrite, implying that its distribution is not controlled by features existing today. A pair of tourmaline grains has inclusions, or possibly infill, of pyrite.

Opaque mineral geochemistry

Distribution of precious metals

Gold in the core has an uneven distribution, varying within the mineralized zone from 0.1 to 3.0 ppm (μ = 0.9 ± 0.8 ppm) (Table 6). The distribution of Au also varies greatly both between and within different mineral species. Of the common sulphides, arsenopyrite has an elevated Au-concentration with an average of 0.3 ppm (n = 15) and peak concentration of 72.88 ppm (Figure 7). Gudmundite has a similar average concentration (0.4 ppm, n = 3), but a significantly lower peak concentration (0.947 ppm). Pyrite, pyrrhotite, sphalerite, and tetrahedrite all have an average concentration around 0.1 ppm, while chalcopyrite and galena has even lower averages, 0.04 and 0.02 ppm respectively. Dyscrasite is the only mineral analysed with an average concentration of Au higher than the average whole rock analysis, with 189.7 ppm (n = 37) and a peak measurement of 6781.31 ppm, or ~0.7 % Au (Figure 7). As indicated by the standard deviation for dyscrasite (± 1113 ppm), the average concentration of Au is heavily skewed by one measurement, and excluding this peak gives an average of 6.6 ± 8.0 ppm Au for dyscrasite.

Whole rock concentration of silver varies strongly in the mineralised zone, ranging from 2 to 609 ppm (μ = 167.7 ± 200.5 ppm) (Table 6). As indicated by Figure 3, silver is concentrated in the lower parts of the mineralized zone. Two minerals presented here contain stoichiometric silver: Ag-rich tetrahedrite and dyscrasite. Tetrahedrite has an average of 22.8 ± 7.6 wt % Ag (n = 17, peak at 32.7 wt %) and can be considered a fairly abundant mineral, with some samples consisting of up to 1-2 vol % tetrahedrite. The average Ag-concentration in dyscrasite is 65.9 ± 9.9 wt % (n = 37, peak at 78.8 wt %). Of the common sulphides, galena has a significant enrichment in Ag, with an average of 0.1 ± 0.07 % (n = 12, peak at 0.27 wt %). Gudmundite is also rich in Ag (μ = 0.5 ± 0.9 wt %, n = 3) but, like Au in dyscrasite, the average concentration is skewed by one high measurement of 1.5 wt %. Arsenopyrite, chalcopyrite, pyrite and sphalerite all have relatively low concentrations of Ag (Asp: μ = 17.6 ± 34.9 ppm, n = 15; Cp: μ = 16.2 ± 7.5 ppm, n = 15; Py: μ = 36.1 ± 114.4 ppm, n = 16; Sp: μ = 69.6 ± 151.5 ppm, n = 17). Pyrrhotite have significant spread of concentrations, going from 0.1 wt % to 0.6 ppm (μ = 304.4 ± 517.4 ppm, n = 4).

Distribution of other minor and trace elements

Levels of mercury are generally low in all minerals, but one mineral with stoichiometric Hg have been identified in sample RS060: eugenite ($Ag_{11}Hg_2$). Dyscrasite has a relatively high concentration of mercury (μ = 5.9 ± 4.6 wt %, n = 6) (Figure 8), with a peak measurement of 13.6 wt % Hg. Sphalerite has the second highest concentration of mercury, with an average of 241.5 ± 78.7 ppm (n = 17), while the other common sulphide minerals have concentration <15 ppm. Many minerals have stoichiometric Sb (Figure 8), of which the most common is tetrahedrite. Dyscrasite, gudmundite and boulangerite ($Pb_5Sb_4S_{11}$) all have high concentrations of Sb, but given their relatively low abundance, they are deemed to be minor sources of the element. Of the common sulphides, galena has the highest concentration of antimony (μ = 857.8 ± 427.5 ppm, n = 12), while arsenopyrite, pyrrhotite, pyrite, chalcopyrite, and sphalerite have concentrations in the range 10-150 ppm.

Concentrations of bismuth is below 1 ppm for most opaque minerals, with galena (μ = 22.5 ± 17.7 ppm), dyscrasite (μ = 3.5 ± 7.2 ppm) and pyrite (μ = 2.9 ± 7.9 ppm) being the exceptions. Likewise, only sphalerite has an indium concentration above 1 ppm (μ = 1.2 ± 1.3 ppm). Arsenopyrite and tetrahedrite have a relative enrichment of molybdenum, with 19.3 ± 55.3 ppm and 9.4 ± 24.3 ppm respectively, compared to concentrations at or below 1 ppm for the other analysed phases. Galena has a relative enrichment of Se (μ = 455.5 ± 256.8 ppm), while the other minerals all have concentrations <100 ppm. Te is generally low in all minerals.

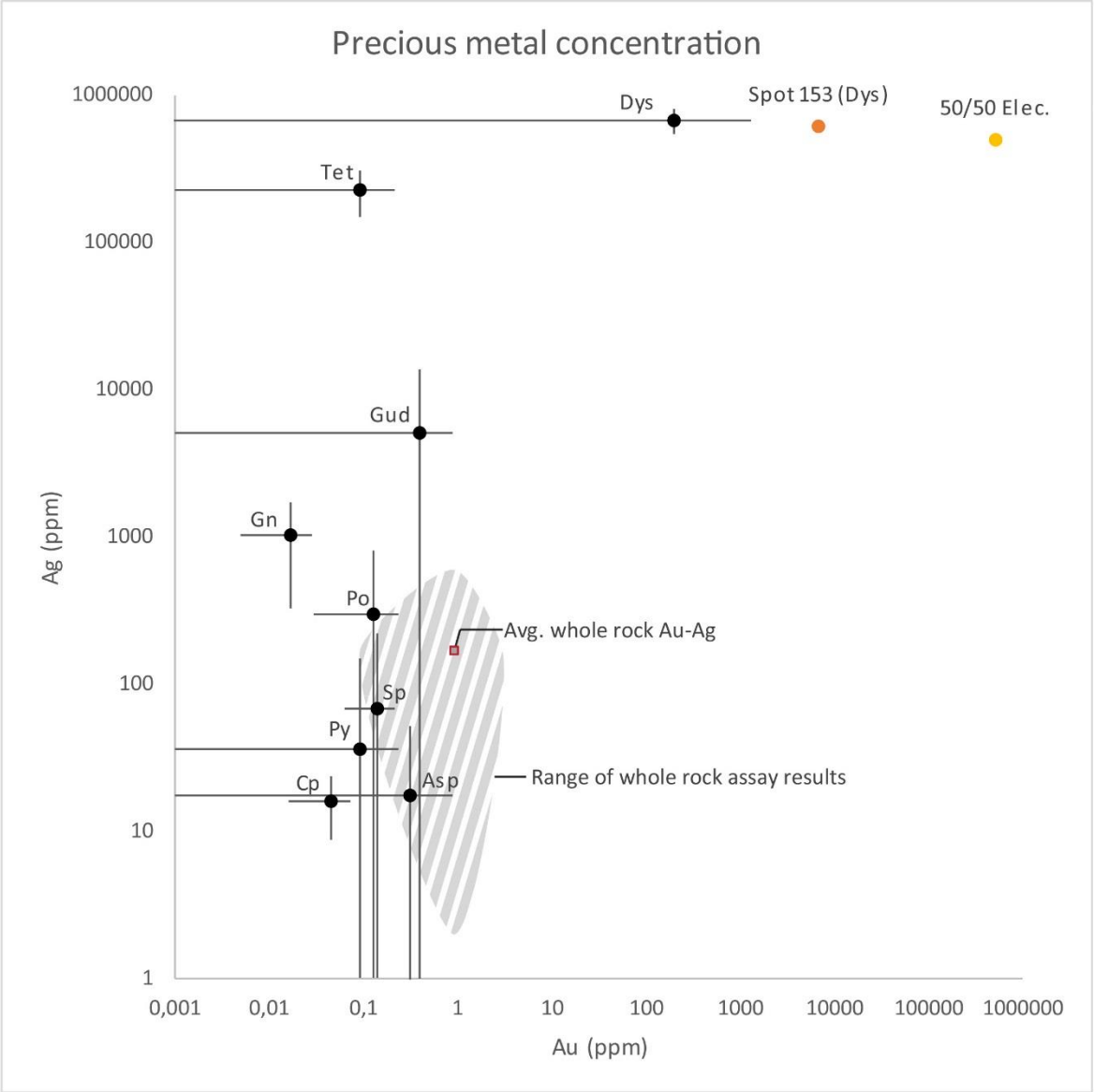

Figure 7. Concentration of Ag and Au in analysed opaque phases. Asp: arsenopyrite; Cp: chalcopyrite; Dys: dyscrasite; Gn: galena; Gud: gudmundite; Po: pyrrhotite; Py: pyrite; Sp: sphalerite; Tet: tetrahedrite. The orange dot is the highest measured concentration of gold, ~0.7 wt %, found in sample RS060. The yellow dot is a hypothetical electrum with 50 % Au and 50 % Ag.

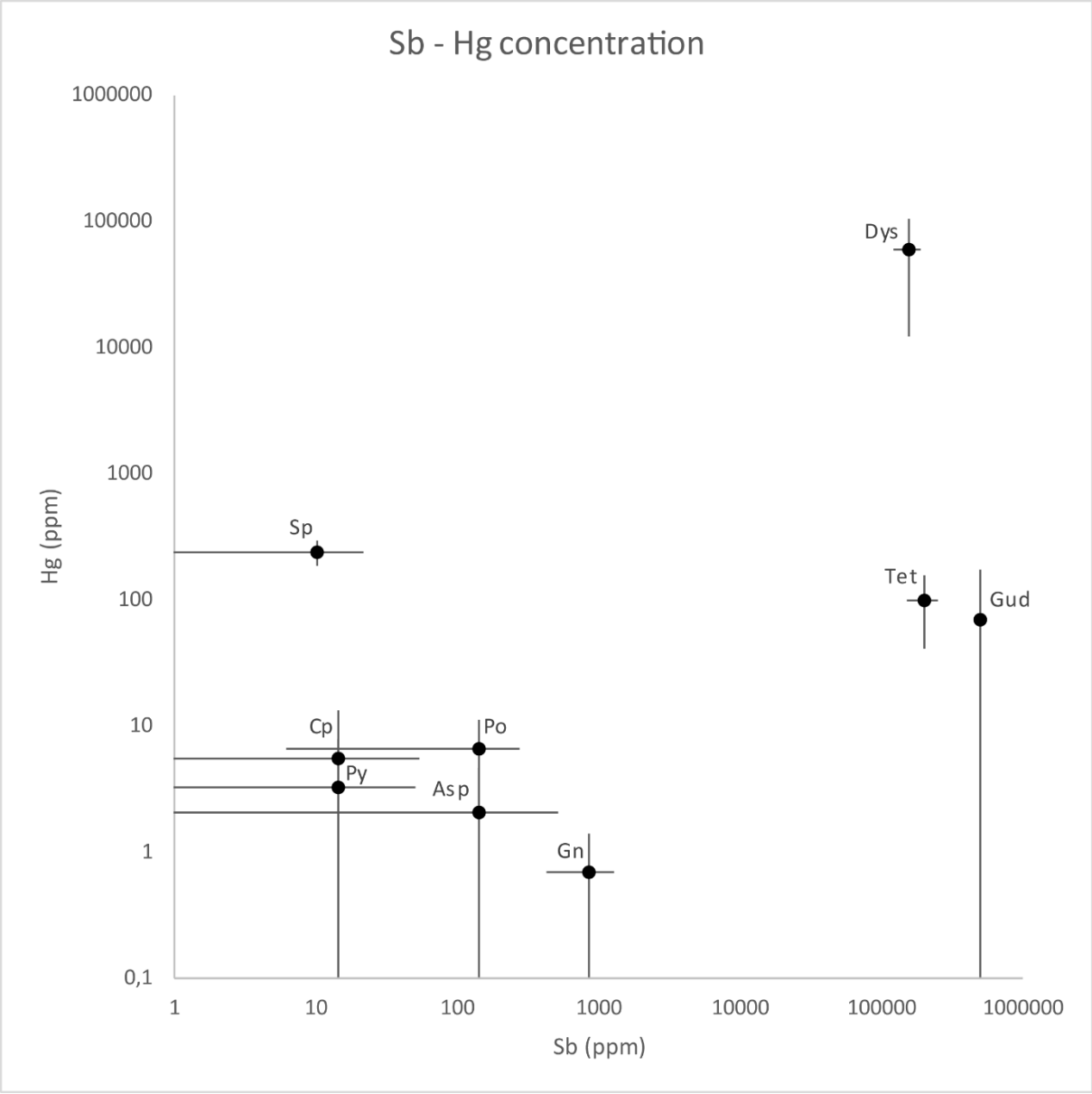

Figure 8. Concentration of Hg and Sb in analysed opaque phases. Asp: arsenopyrite; Cp: chalcopyrite; Dys: dyscrasite; Gn: galena; Gud: gudmundite; Po: pyrrhotite; Py: pyrite; Sp: sphalerite; Tet: tetrahedrite.

Composition of tetrahedrite group minerals

The tetrahedrite group of minerals, also called fahlore, have the general formula $(Cu,Ag)_6Cu_4(Fe,Zn,Cu,Hg,Cd)_2(Sb,As,Bi,Te)_4(S,Se)_{13}$ (Johnson, et al., 1986). The majority of the tetrahedrite group minerals analysed have a composition between tetrahedrite and Ag-rich tetrahedrite (Figure 9), with high Ag (μ = 23.9 ± 6.1 wt. %, n = 16), low Zn (μ = 1.5 ± 1.0 wt. %, n = 16) and Hg, Cd, Bi, Te and Se all <100 ppm. One grain of tennantite has been analysed, with 22.6 wt % As and significantly higher Zn (4.5 wt. % compared to μ = 1.5 ± 1.0 wt %) at the expense of Fe (3.3 wt % compared to μ = 5.4 ± 1.7 wt %) and lower Ag (4.2 wt % %) than the average for the group (μ = 22.8 ±

7.6 wt %). Excluding the tennantite, the tetrahedrite group minerals can be divided into two groups based on the Ag concentration, a factor that correlates well with the amount of alteration experienced by the mineral (Figure 9). Unaltered grains, most of them in massive sphalerite samples, plot within the Ag-rich tetrahedrite field, with Sb > As at % and Ag / Cu > 0.3 at %, and have an average Ag concentration of 31.3 ± 1.9 wt. % (n = 6). Altered grains tend to have a lower Ag content (μ = 19.5 ± 1.8 wt %, n = 10), and a slightly higher Sb (21.4 ± 2.3 wt % compared to 20.4 ± 2.0 wt %).

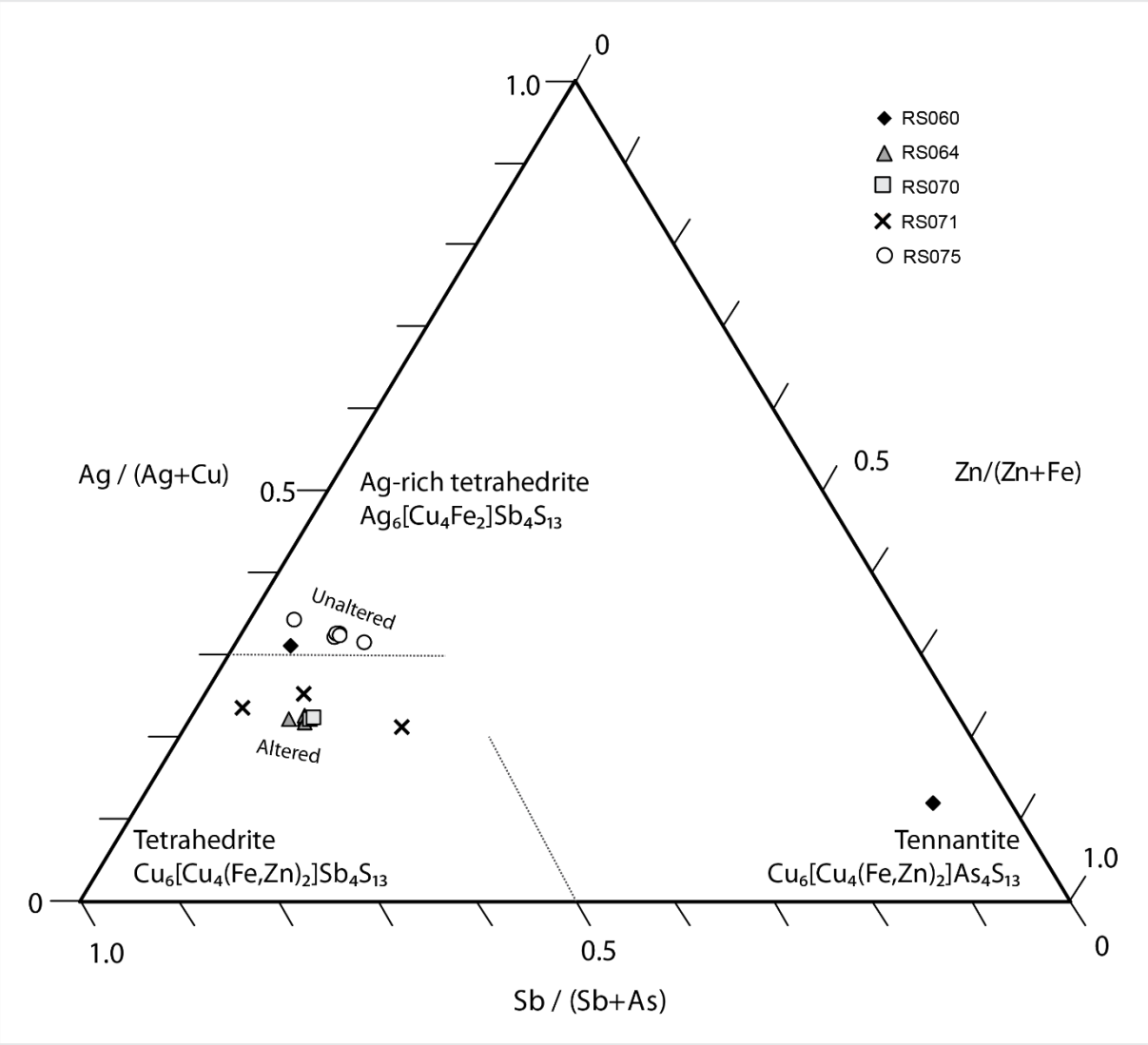

Figure 9. Composition of tetrahedrite-group minerals. Dashed lines indicate the border between end-members. Altered and unaltered indicates whetever or not the mineral show any replacement textures. Diagram was made with the Tri-Plot spreadsheet (Graham & Midgley, 2000).

Fluid inclusions

CURT, a sample from the massive sphalerite-dolomite assemblage was investigated for fluid inclusions (Figure 3). The sample contains primarily sphalerite with islands of dolomite, but also

patches of galena, partially rounded pyrite, chalcopyrite, and minor sulphosalts. Fluid inclusions were found in the central parts of dolomite, while sphalerite was notably absent of any such inclusions (Figure 11.). Inclusions occur as euhedral rhombohedra voids in the dolomite, often small (<10 µm), and with two or three phases liquid-vapour phases inside (Figure 11). Microthermometric studies indicate that the dolomite formed from a H_2O-CO_2 fluid with a salinity of 3-5.5 eq. wt % (Ca,Na)Cl (Table 18). Homogenization temperature is estimated to 282 – 296° C, with a pressure of 0.3 kbar based on the lowest CO_2 concentration found in inclusions.

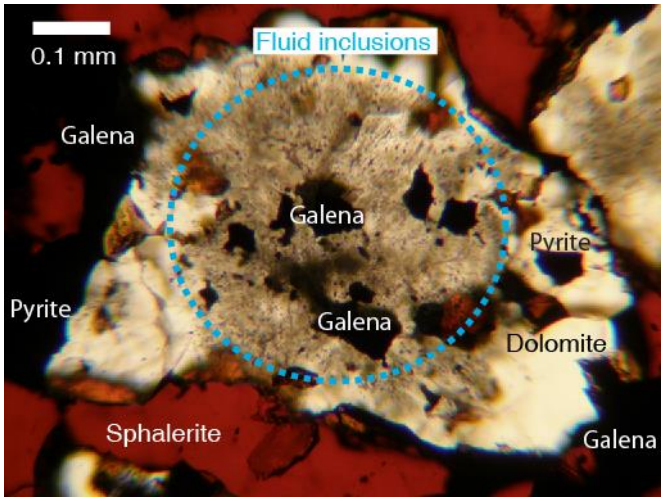

Figure 11. Dolomite with fluid inclusions, surrounded by sphalerite, pyrite and galena. Picture is taken from sample CURT.

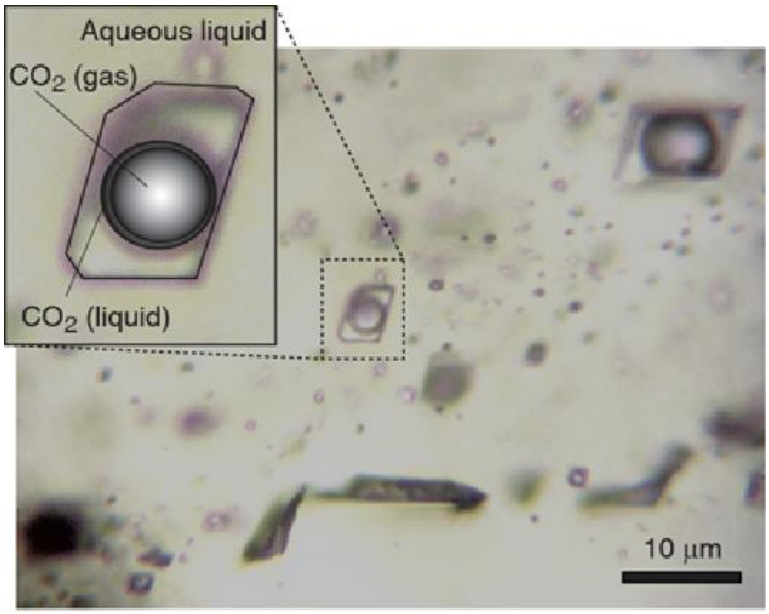

Figure 10. Close up picture of fluid inclusions in dolomite.

Geothermometry

A total of 38 microprobe analyses of arsenopyrite in sample RS077 were conducted. Of these, 7 grains displayed the criteria necessary for the grains to be suitable for geothermometry; they were in contact with both pyrite and pyrrhotite, and had a total concentration of 100.0 ± 1.0 % and a total concentration of minor components (e.g. Zn, Cu or Sb) below 1 %. These measurements have an average of 31.3 ± 0.5 at % As, yielding a temperature of 379 ± 29° C following the calibration described in Kretschmar and Scott (1976) (Figure 12).

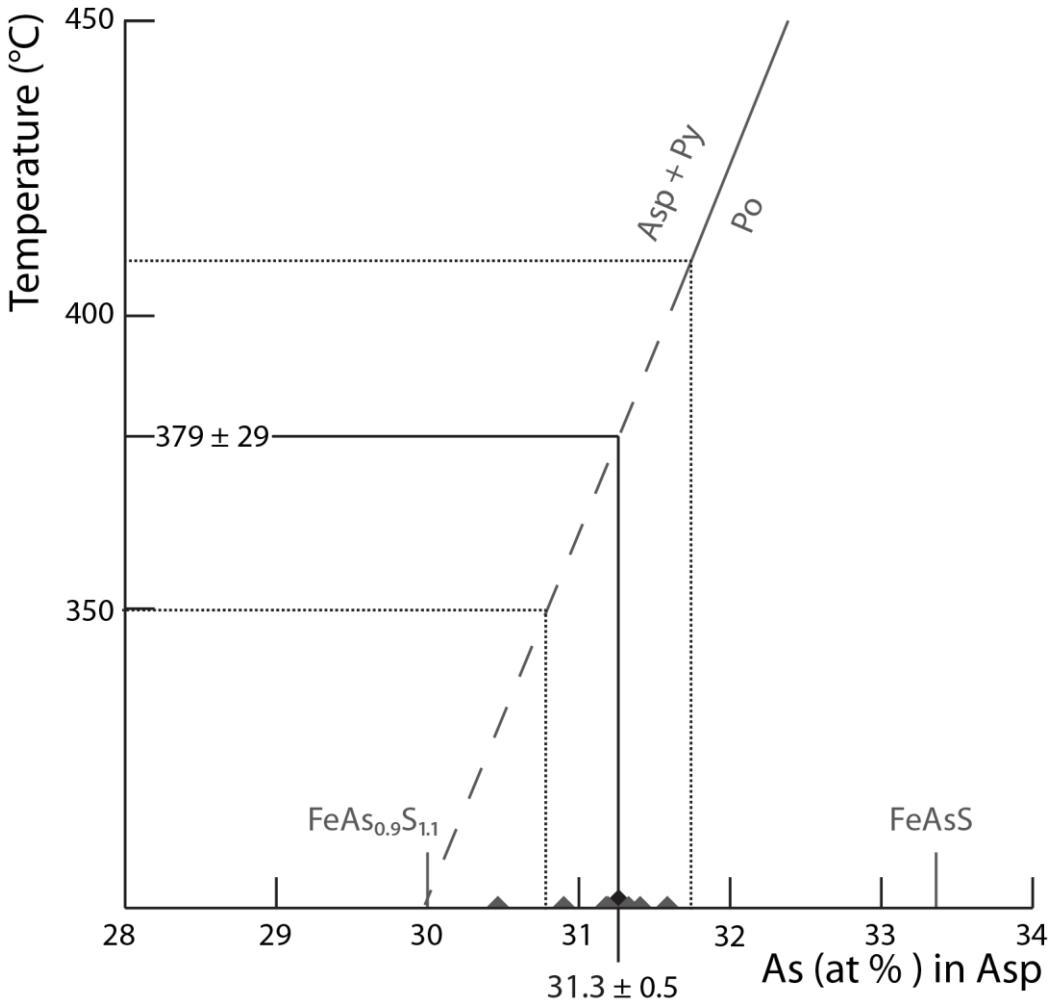

Figure 12. Temperature – As (at %) plot. Samples are indicated with grey triangles on the X-axis. After (Kretschmar & Scott, 1976).

Geochronology

In sample RS075, two titanite pairs was found: one with quartz in the silicate dominate part of the sample and one with quartz and pyrite in the massive sphalerite-galena-pyrite assemblage. Rounded grains of quartz are spread out in both the sulphide- and silicate-rich parts of the sample. Carbonates, chlorite and sericite are abundant in the silicate parts of the sample, but only carbonates penetrate into the outer areas of the massive sulphide. All four grains of titanite are euhedral to subhedral. No preferred orientation of grains has been observed in any parts of the sample. In the massive sulphide, titanite grows around grains of pyrite, while sphalerite seems to follow the elongated titanite euhedra. In total, 6 LA-ICP-MS measurements were performed on the two grains in the massive sulphide (Figure 14), yielding an average concentration of 3.9 ppm U and 1.0 ppm Th (Table 20).Plotting the $^{207}Pb/^{206}Pb$ ratio versus the $^{238}U/^{206}Pb$ ratio on a Tera-Wasserburg diagram yields lower intercept age of 1855 ± 35 Ma, with a mean square weighted deviation of 1.2 (Figure 13b). However, if all common Pb is assumed to be incorporated into the grain at the time of mineral growth, the intercept can be fixed at $^{207}Pb/^{206}Pb$ = 1.0, yielding an age of 1816 ± 28 Ma and a mean square weighted deviation of 0.50 (Figure 13a). The latter method neglects lab contamination of common Pb. However, since titanite readily incorporates Pb into the crystal structure, it is reasonable to assume that all common Pb measured was incorporated at the time of crystal growth.

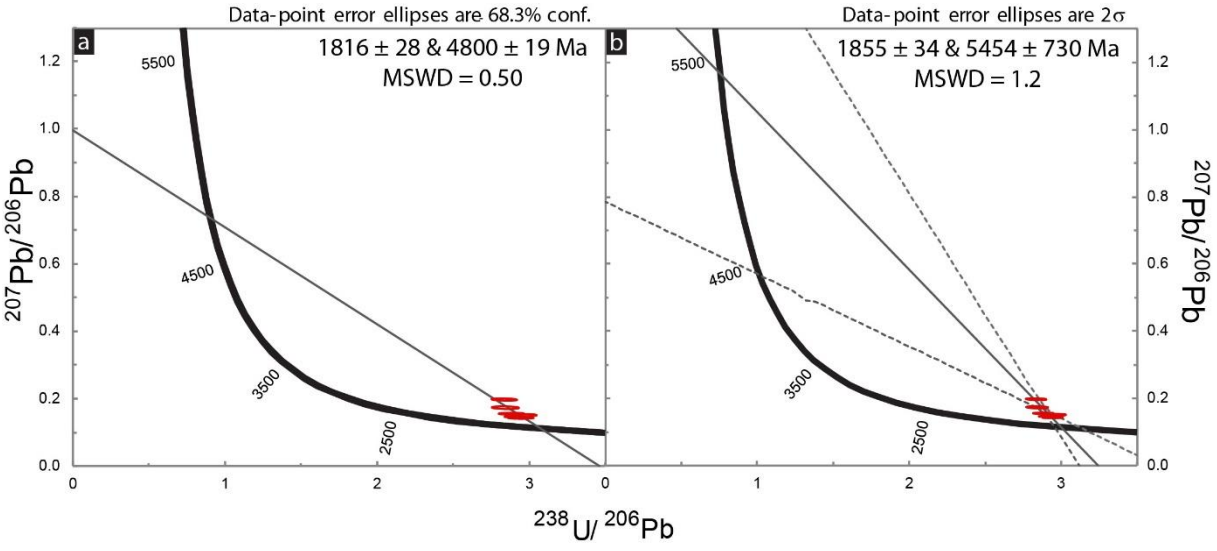

Figure 13. Tera-Wasserburg diagram for analysed U-Pb ratios in titanite. After Tera & Wasserburg (1972).

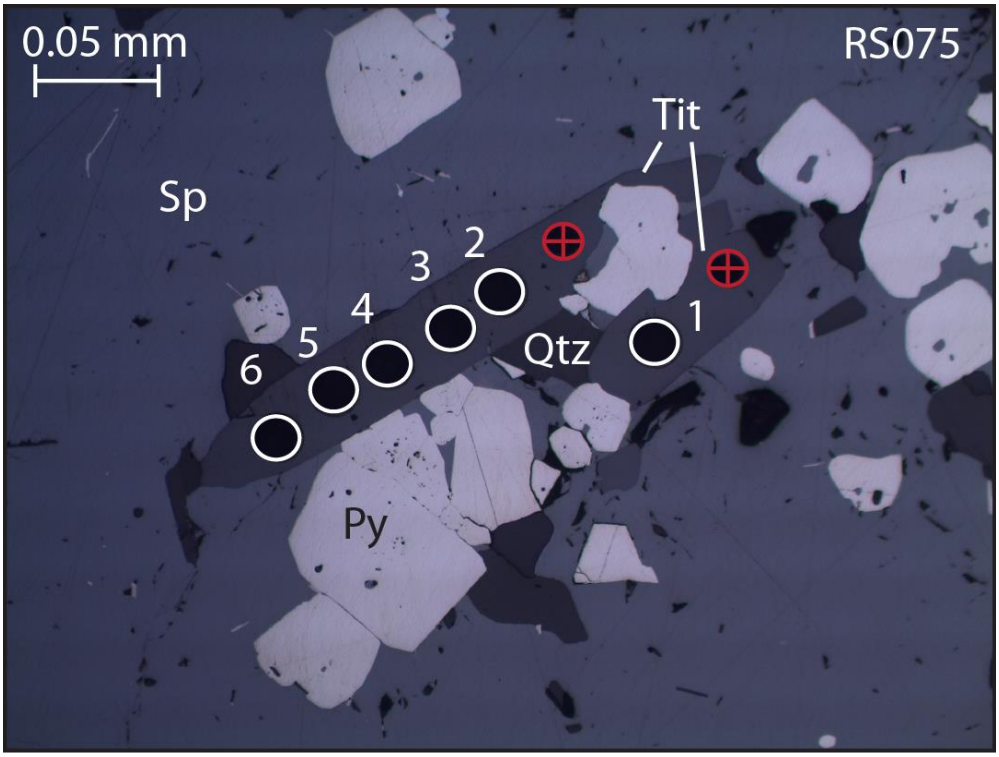

Figure 14. Titanite grains analysed for geochronology. Red circles with crosses are test measurements. White circles with corresponding numbers indicate measurement number (Table 20). Py: pyrite; Qtz: quartz; Sp: sphalerite.

Discussion

Mineral paragenesis

For the sake of discussing the paragenetic sequence of the deposit, only processes producing a net increase in the abundance of a mineral are taken into account. This means that processes only causing translocation of a mineral are excluded from the model in Figure 15. Some of the minerals in the deposit, such as chlorite, could have formed both during mineralisation and metamorphism and so their position in the paragenesis is uncertain. The paragenesis presented here is not exhaustive but is based on the most clearly observed textures.

What can now be observed in the mineralized zone is essentially the result of two major ore-forming events: sub-seafloor hydrothermal convection during which the main ore body was formed, and regional metamorphism which caused extensive reworking of existing minerals and formation of new minerals. Deformation textures are the key to differentiate between these two events; the regional metamorphism was accompanied by extensive deformation overprinting and partial recrystallization of the mineralogy formed during the former event. However, early metamorphic minerals would also

have been reworked by deformation to some extent during peak metamorphism, so mineral- and environmental association must also be applied to distinguish between different events.

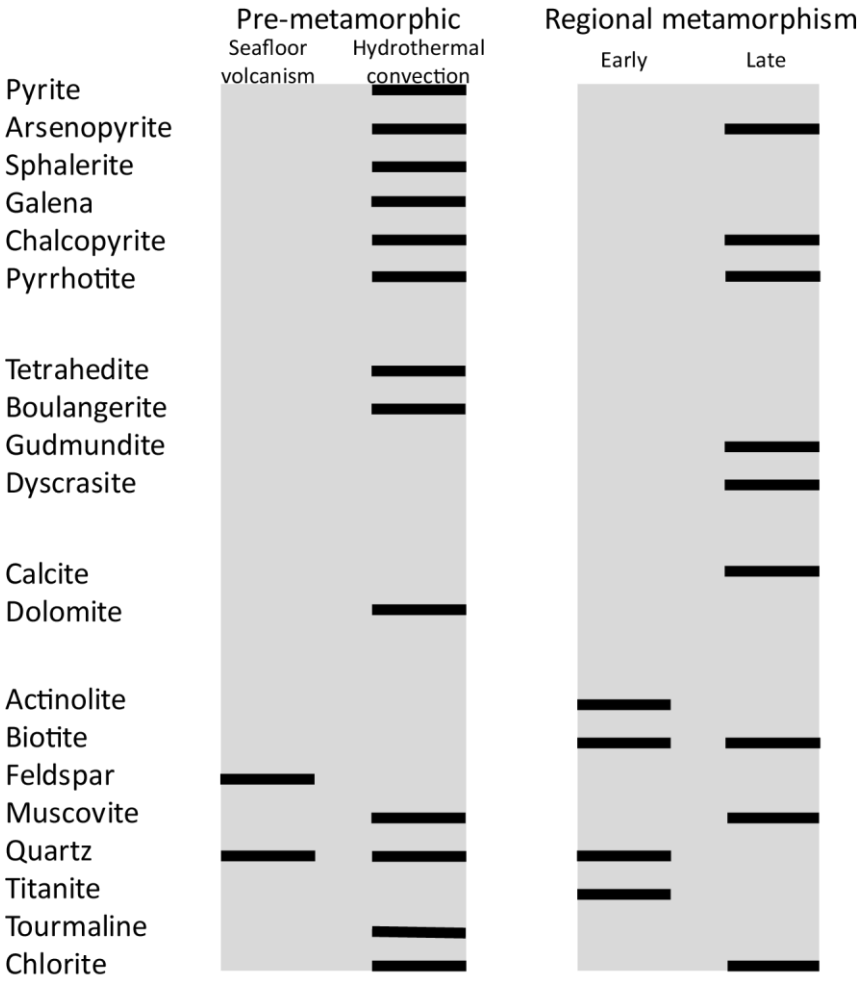

Figure 15. Mineral paragenesis of the Simon lens. Black lines indicate net growth of a mineral in the system as a whole during a certain event (i.e. excluding recrystalization).

Pre-metamorphism

Several mineral phases are interpreted to be partially or completely of pre-metamorphic origin. This assumption is based on textural relations, such as overprinting deformation textures, and the geological environment associated with the mineral.

Opaque minerals

All common sulphides are likely to have formed during the main massive sulphide mineralisation event, and their current mineral association may partially reflect the original metal zonation in the VMS-environment, heavily overprinted by later regional metamorphism. An example of metal zonation in a similar type of deposit is shown in the schematic diagram in Figure 16. Larger (>30 µm)

euhedral grains of arsenopyrite are one of the earliest sulphides formed, with sphalerite and pyrite commonly following the shape of the arsenopyrite grain. Inclusions of pyrite inside arsenopyrite points towards simultaneous growth of both minerals (Figure 17c) in the early stages of hydrothermal alteration. Disseminated pyrite, common in most parts of the core outside the mineralized zone, are likely to be of pre-metamorphic origin; dispersed pyrite is common around VMS ore bodies, while regional metamorphism is more likely to form concentrated assemblages of pyrite related to areas of high fluid flow. The euhedral sticks of pyrrhotite in sphalerite (Figure 5e) is very different in character compared to the retrograde pyrrhotite related to calcite veining (Figure 17d), indicating formation unrelated to metamorphism, possibly through exsolution from a galena-sphalerite assemblage. The chalcopyrite-dolomite association noted in the core may very well reflect a pre-metamorphic zonation, as indicated in Figure 16. Tetrahedrite-group minerals and boulangerite may have formed either directly with pyrite, sphalerite, and galena (Figure 16) or by exsolution from galena upon cooling, as described in Gasparrini & Lowell (1985) and Sack & Goodell (2002).

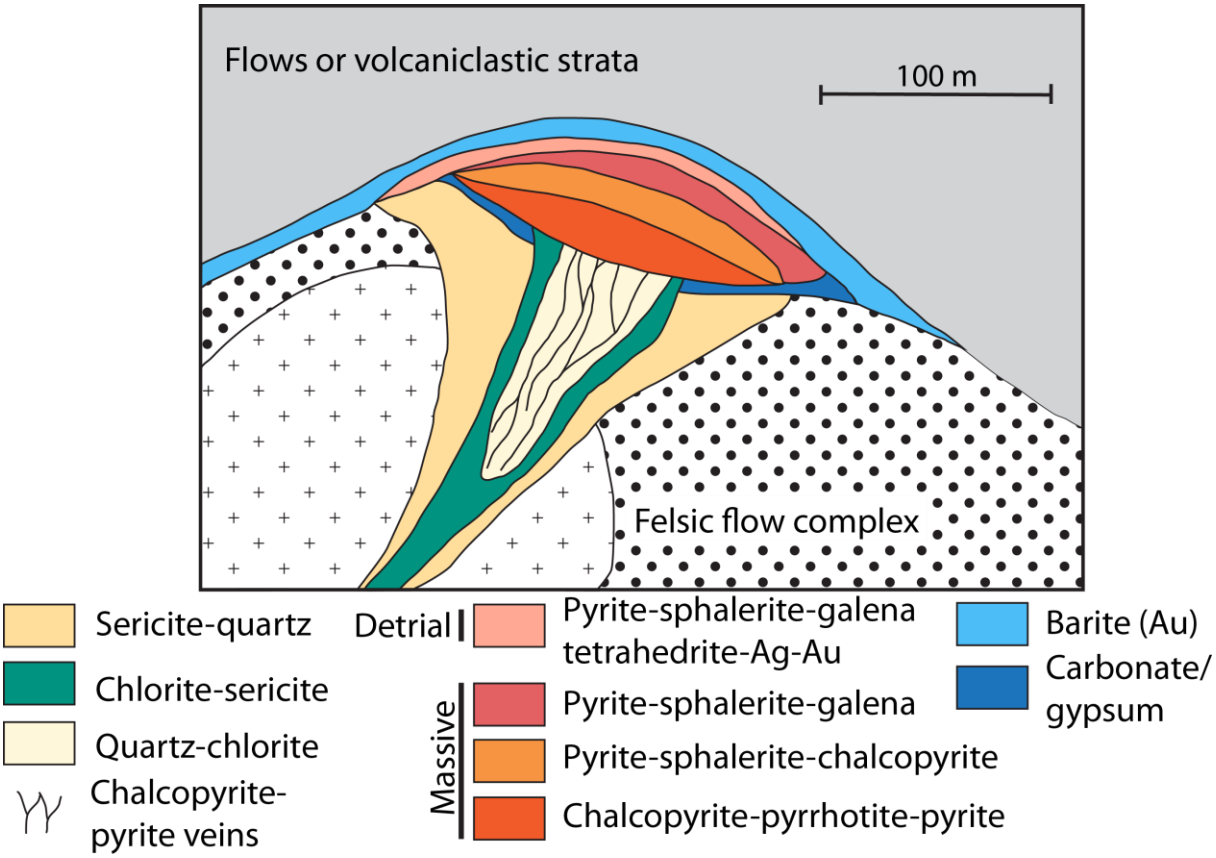

Figure 16. Generalized mineral zonation of a exhalative bimodal-felsic VMS deposit. Note that geometry of a replacement-type VMS deposit most likely differs, but a similar mineral associate can be expected. Modified from Galley et al.(2007).

Alteration minerals

Due to metamorphic replacement, only some alteration minerals can safely be ascribed to the sub-seafloor hydrothermal convection. Large and rounded quartz and feldspar grains in the metavolcanic sedimentary rock are interpreted to be porphyroclasts from seafloor volcanism (Figure 6e), pre-dating the ore-forming hydrothermal activity and thus being the oldest grains identified in the core. Chlorite, dolomite, muscovite (in the form of sericite), and quartz are all common alteration phases in the VMS-environment (Figure 16) (e.g. Hannington, et al., 2005; Galley, et al., 2007), and fragmented and foliated masses of these minerals may be ascribed to extensive hydrothermal alteration. The few grains of tourmaline found in the samples lack any observable mineral- or textural association, and their current distribution is thus deemed to reflect early processes, such as the hydrothermal circulation (Shanks III, 2012).

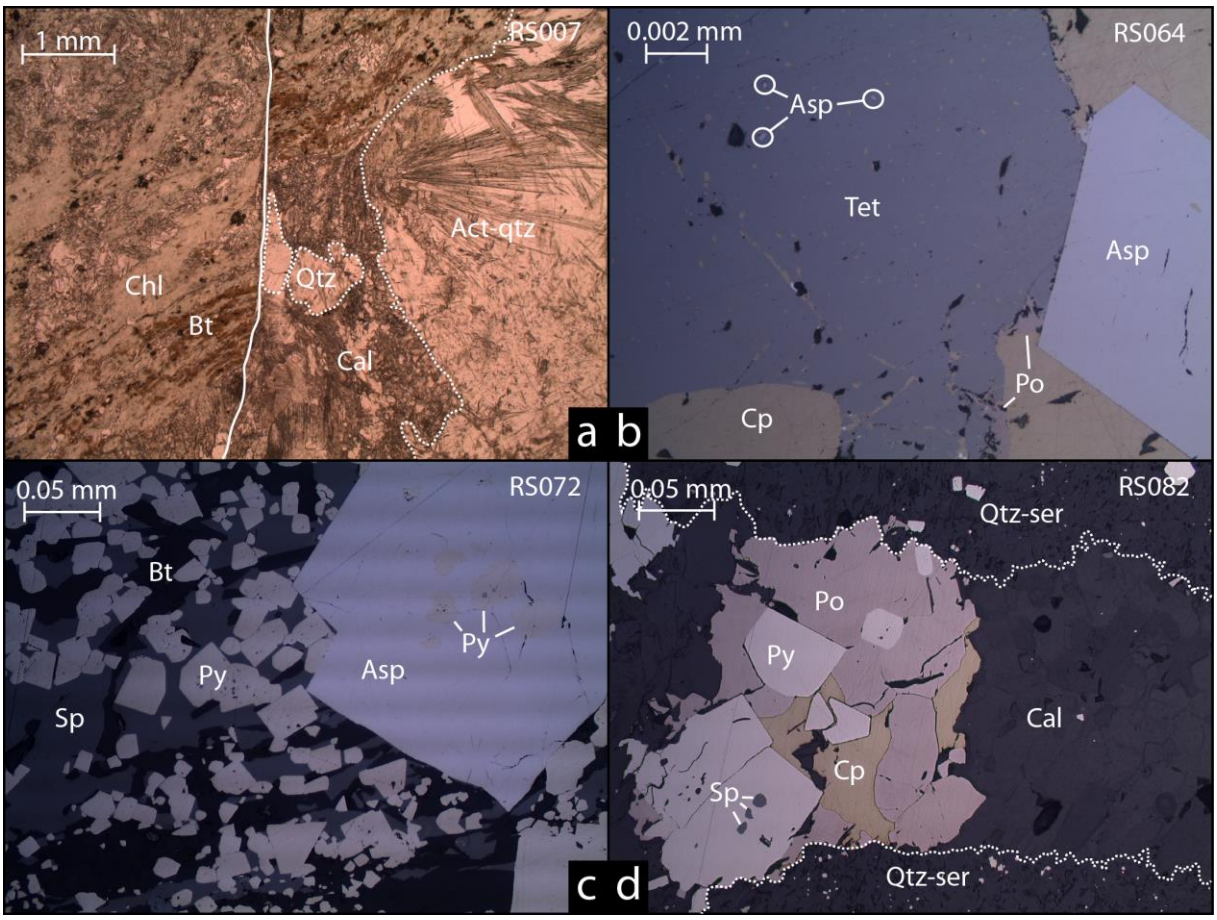

Figure 17. Microscope pictures of remobilized sections in plain polarized- (a, b) and reflected (c, d) light. ***a*** *Vein of actinolite (Act) and quartz (Qtz) fractured and displaced, with calcite (Cal) infiltrating along the crack. Displacement is indicated by the biotite (Bt) assemblage in the chlorite-dominated (Chl) border zone. Solid white line marks out the fracture. Dashed white line deliniated the border between actinolite-quartz and intrudcing calcite.* ***b*** *Tetrahedrite (Tet) partially breaking down in a chalcopyrite (Cp) dominated assemblage. Small inclusions of arsenopyrite (Asp) and chalcopyrite is common in the tetrahedrite.* ***c*** *Euhedral arsenopyrite with inclusions of pyrite (Py) in an assemblage of sphalerite (Sp), biotite and pyrite. Note how both sphalerite and pyrite follow the shape of biotite.* ***d*** *Pyrite, pyrrhotite (Po) and chalcopyrite, with minor sphalerite, in a calcite vein cutting through a quartz-sericite (Ser) groundmass.*

Regional metamorphism

Even if extensive evidence for deformation, and thus also mechanical remobilization, of the massive sulphide assemblage in the core have been noted (Figure 4), the extent and character of deposit-scale mechanical remobilization during metamorphism cannot be established based on the semi-2-dimensional information gained from a single core. Therefore, only small scale effects of mechanical metamorphic remobilization will be evaluated in this report.

Opaque minerals

Of all the opaque minerals investigated in this study, grains of arsenopyrite appears the most refractory, largely unaffected by the regional metamorphism. However, arsenopyrite grains analysed with electron microprobe have an As concentration indicating equilibrium temperature between

black smoker systems (350° C: Hannington, et al., 2005) and peak metamorphism (~400° C: Berglund & Ekström, 1980), so it is safe to assume that all opaque phases have been affected by the regional metamorphism to some extent. Pyrrhotite in the lower section of the mineralized zone and in the lower volcanic sediment is spatially associated with calcite veining, and commonly grow in pressure shadows of porphyroblasts and porphyroclasts of pyrite, quartz, and feldspar. This indicates late stage formation related to the metamorphic hydrothermal system. Pyrite and sphalerite are not common in calcite veins, but still occur with chalcopyrite and pyrrhotite in places (Figure 17d). Grain coarsening through merging of smaller grains is common for pyrite, in particular in pyrite-quartz assemblages (Figure 5b), but larger porphyroblasts of pyrite related to calcite indicate that pyrite also grew in the metamorphic hydrothermal system (Figure 17d). Sphalerite surrounding prograde and peak metamorphic minerals, such as biotite and titanite (Figure 14 and Figure 17c), are believed to have undergone plastic deformation during the regional metamorphism, and the banded or foliated nature of sphalerite in multiple samples can also be explained by this mechanism.

Ample evidence for breakdown of tetrahedrite-group minerals has been found in samples from various parts of the mineralized zone (Figure 5c, d, f and Figure 17b). Generally, tetrahedrite in contact with, or in the proximity of, calcite seems to be unstable, indicating a fluid-dominated replacement process. Given the retrograde association of calcite, this process is thought to have taken place during the waning phases of metamorphism. Additional support for this interpretation is the presence of gudmundite as a product of the breakdown, a mineral that is unstable above 280 ± 10° C (Clark, 1966), significantly lower than peak metamorphism. In addition to gudmundite, dyscrasite, pyrrhotite, and chalcopyrite are also common products of this breakdown (Figure 5c, d). Small isolated grains of arsenopyrite in unstable tetrahedrites (Figure 17b), although spatially disconnected from the other products of the process, have also been inferred to be the direct result of retrograde breakdown of tetrahedrite, and their rarity can be ascribed to the generally low concentration of As in the tetrahedrites.

Metamorphic metal zonation

Kläre (2001) suggested that a high Cu / low Zn zonation partly related to tectonic remobilization existed in the Simon lens, overprinting the original VMS-related zonation of similar character (Figure 16). The current study is in agreement with this observation; the distribution of chalcopyrite, the main Cu-host, is largely controlled by calcite veining, while sphalerite has mainly been redistributed by solid-state mechanical remobilization. Since pyrite and sphalerite are both minor phases in these calcite veins, it is suggested that fluid-dominated chemical remobilization transported Cu from the massive sphalerite-pyrite assemblage into high-strain zones, where fluid flow was likely focused, causing the Cu / Zn fractionation observed. However, since the main mineralization event likely

produced a Cu / Zn zonation, with chalcopyrite precipitating in the centre and sphalerite forming further out of the ore body, the extent of the metamorphic remobilization zonation cannot be established. The heterogeneous distribution of gold in the lens has also been attributed to the tectonic remobilization (Kläre, 2001). The highest assay gold results are obtained from the end of the mineralized zone (Figure 3), the most deformed section of the core (Figure 4). The highest concentrations of gold has also been measured in minerals related to the calcite veining (Figure 7), supporting the suggestion that the regional metamorphism concentrated Au from the massive sulphides into more discrete veins and pockets.

Sulphide melting

Tomkins (2007) noted that precious metals in the Montauban deposit, a metamorphosed exhalative VMS deposit of similar mineralogy as the Renström deposit, were concentrated in small pockets and veinlets interpreted as the result of partial sulphide melting of the massive sulphide ore body. Au-rich dyscrasite, gudmundite, and arsenopyrite were common minerals found in these small accumulations (Figure 18b), reflecting a preferable fractionation of Ag, As, Au, and Sb into the suggested sulphide melt. Only one assemblage of similar composition and character has been noted in the core (Figure 18a), more specifically in sample RS064, a sample with plenty of euhedral arsenopyrite grains, anhedral chalcopyrite and tetrahedrite, and the largest amount of dyscrasite noted in any sample (Figure 5d). Within the hosting dolomite, a larger patch of chalcopyrite and arsenopyrite form an intergrowing texture, where arsenopyrite grows along specific crystal faces (Figure 18a). Gudmundite sits at the contact to the surrounding dolomite, while dyscrasite is restricted to the calcite patches found within the assemblage. An arsenic-rich unidentified mineral forms jagged grains pointing into the calcite (Figure 18a). Only minor amounts of sphalerite and no Fe-rich sulphide can be found in this section of the sample, pointing towards an enrichment of LMCE (Frost, et al., 2002) compared to Fe-Zn.

One of the main arguments for sulphide melting (as opposed to hydrothermal alteration) at Montauban is the lack of alteration mineralogy related to melt assemblages (Tomkins 2007). In the area described above, calcite is abundant, indicating the presence of a fluid (Figure 18a). Whether the area described above represents the onset of melting is not clear, but there is clearly an association with a hydrothermal fluid and it is perhaps more likely that the alteration was fluid-driven remobilization. The presence of fractured grains of arsenopyrite could explain the enrichment of As in the remobilised phases. Furthermore, the peak metamorphic temperature recorded at Montauban is 650° C (Bernier, et al., 1987), significantly higher then what is estimated for Renström (379 ± 29° C : this study). Only samples from the Monte Arsiccio mine in Italy are interpreted to have partially melted at temperatures lower than what Renström has experienced (Biagioni, et al., 2013), but the

anomalous Tl-rich pyrite ore at Monte Arsiccio makes comparisons between these two deposits weak. In conclusion, it is deemed unlikely that any sulphide melting took place in the Simon lens during the regional metamorphism, although local mineral assemblages may have had the ability to form melts at relatively low temperatures.

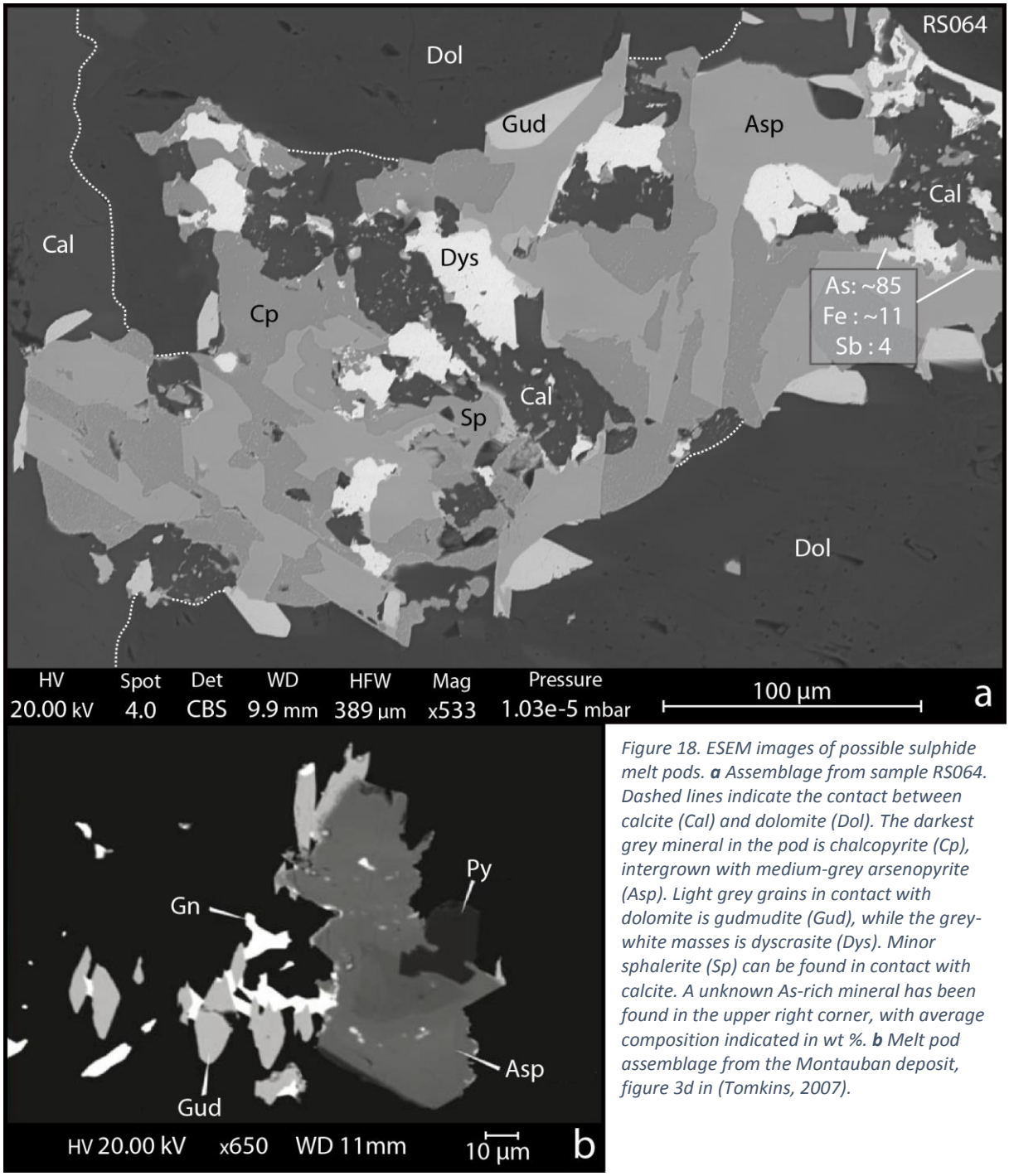

*Figure 18. ESEM images of possible sulphide melt pods. **a** Assemblage from sample RS064. Dashed lines indicate the contact between calcite (Cal) and dolomite (Dol). The darkest grey mineral in the pod is chalcopyrite (Cp), intergrown with medium-grey arsenopyrite (Asp). Light grey grains in contact with dolomite is gudmudite (Gud), while the grey-white masses is dyscrasite (Dys). Minor sphalerite (Sp) can be found in contact with calcite. A unknown As-rich mineral has been found in the upper right corner, with average composition indicated in wt %. **b** Melt pod assemblage from the Montauban deposit, figure 3d in (Tomkins, 2007).*

Alteration minerals

Most of the alteration minerals from the main ore forming event were likely completely replaced during the regional metamorphism. As mentioned above, the original hydrothermal alteration assemblage was most likely dominated by chlorite, dolomite, quartz, and sericite, but the formation of clay minerals through argillic alteration, such as kaolinite and ilmenite, cannot be ruled out (Hannington, et al., 2005).

Euhedral biotite, commonly surrounded by various sulphides (Figure 6b), is likely to have formed from sericite, the main potassium host, before extensive reworking of the massive sulphide assemblage. Anhedral biotite, on the other hand, is of retrograde origin, often found along grain contacts in highly deformed zones. Actinolite is also found in two variants: a quartz-actinolite vein, where the amphibole occurs as radiating needles (Figure 17a), and as more blocky mineral grains, commonly associated with calcite and quartz. The former group has been fractured and partially replaced by chlorite and calcite, indicating formation during the early stages of metamorphism. Similarly, the latter group of amphiboles also show later replacement textures, mainly with calcite or chlorite, but also with common sulphides (Figure 6c). Growth of chlorite during metamorphism seems to be mainly through replacement of other sheet silicates, such as biotite and muscovite, but also of the aforementioned amphiboles. Larger patches of muscovite are restricted to local low-pressure zones, such as in pressure shadows of pyrite porphyroblasts and in contact with larger accumulations of pyrite-sphalerite. Although both chlorite and muscovite (as sericite) are dominant alteration species in larger parts of the core, determining if these accumulations are of a metamorphic or pre-metamorphic origin has not been possible. Calcite is the mineral with the strongest association with later stage alteration, commonly found cross-cutting other minerals and textures (Figure 5c, Figure 17a, d). However, abundant anhedral calcite found in high-strain zones, indicate growth both during peak- and retrograde metamorphism. Although no clear evidence for calcite replacement of dolomite has been observed, the process is indicated by the thickest calcite veins found in dolomite-rich areas. Most titanite occur as smaller grains in chlorite-sericite-calcite-altered groundmass, but titanite found in massive sulphide has sphalerite growing around it, while still following the shape of pyrite (Figure 14). Sphalerite is assumed to have deformed mainly, but not exclusively (Figure 5c), in the ductile regime. Therefore, it is suggested that titanite grew during peak metamorphism and was later surrounded by plastically deformed sphalerite. The sulphides may have preserved the titanite from the partial retrograde alteration observed in other titanite grains.

Distribution of precious metals

As indicated in Figure 3 and Figure 4, Ag and Au are both enriched in deformed sections of the core. Both of these metals have been remobilized and concentrated during the regional metamorphism, but their behaviour appears to be decoupled as they are hosted in different minerals.

Distribution of gold

Figure 7 implies that of all the analysed sulphide minerals, only dyscrasite has sufficient gold abundance to be a viable host mineral for the gold in the whole rock. In the most sulphide rich section of the mineralized zone (~58 – 69 m in Figure 3), gold is enriched with an average gold grade of 1.72 ppm. With an average concentration of 189.7 ppm Au, 0.009 vol % dyscrasite would be needed to account for the whole rock gold concentrations. This abundance of dyscrasite is lower than has been observed in several samples from this zone. Kläre (2001) reported electrum as a common alloy in the ore, often found together with abundant sphalerite. No electrum has been observed in this study, but given the heterogeneous distribution of the metal in the Simon lens (Kläre, 2001), it remains possible that it happened not to be present in the sample material investigated. Only 3.4×10^{-6} vol % electrum with a 50/50 Au/Ag would be needed to account for the whole rock Au concentrations, indicating that when present, electrum is an important host for Au. However, the ~0.7 wt % Au measured in one of the dyscrasite grains is a strong indication that dyscrasite may be a significant host of gold in the Simon lens. Dyscrasite with as much as 14.8 % has been reported from the remobilized Montauban VMS deposit (Tomkins, 2007), indicating the potential of dyscrasite as a gold-hosting mineral.

Distribution of silver

Four mineral phases have significant (Ag grade > whole rock assay results: Table 6) concentrations of Ag: dyscrasite, tetrahedrite, gudmundite, and galena, listed in descending order from richest to poorest. Of these, dyscrasite and gudmundite are rare, never making up more than ~0.01 vol % of a sample. Galena and tetrahedrite, on the other hand, are fairly common minerals, making them suitable candidates to be the main hosts of silver in the Simon lens. Although breakdown of tetrahedrite results in depletion of Ag of the tetrahedrite (Figure 9), the formation of dyscrasite in proximity of the tetrahedrite grains seem to compensate for this loss, making the process isochemical in regards of Ag at a local scale. Thus, even if retrograde processes seem to concentrate Ag into discrete mineral phases such as dyscrasite and gudmundite, the distribution of Ag in the Simon lens is still largely controlled by pre-metamorphic factors.

Geochronology

Metamorphic titanite commonly has lower concentrations of U and common Pb than magmatic titanite (Frost, et al., 2000), and the ~ 3.9 ppm measured in the samples (Table 20) lies in the lower end of the uranium concentration spectra of titanite. The acquired age of 1816 Ma falls within the estimated age of the latest major deformation event (D3 at 1.82 – 1.80 Ma: Weihed, et al., 2002), and peak metamorphism from previous studies is estimated to have taken place around 1.82 Ga (Weihed, et al., 2002). Textural observations, such as penetrative calcite veins, indicate that Ca was mobile during the latest metamorphic event, while Ti can be considered immobile during low to medium grade metamorphism (Van Baalen, 1993). The age recorded could therefore be interpreted as the age of titanite replacement of pre-existing Ti-bearing minerals, such as ilmenite, rutile, and/or titanite, facilitated by a Ca-rich fluid. Although sample RS075 show no signs of deformation, there is extensive evidence of alteration in that section of the core. Given the heavily deformed nature of the lower section of the mineralized zone as a whole (Figure 4), it is deemed reasonable to assume that the age obtained from titanite indicates retrograde regional metamorphism at 1.816 Ga.

Geothermometry

Previous geothermometry studies performed on arsenopyrite in the district by Berglund & Ekström (1980) indicate an equilibrium temperature around 400° C (Table 3). Similarly, geochemical investigations of kobellite-rich sulphosalts from the Boliden deposit indicate formation around 350 – 450° C (Wagner & Jonsson, 2001). The obtained temperature of 379 ± 29° C from arsenopyrite in sample RS077 is in agreement with these studies. Common greenschist facies minerals observed in the core, such as late chlorite veins and minor actinolite, also support this estimation. Similarly to sample RS075, which was used for geochronology, sample RS077 show little signs of deformation, even though it is taken from one of the more deformed sections of the core. Although arsenopyrite is a relatively refractory mineral, the extensive reworking of massive sulphide assemblages, along with related growth of retrograde minerals under greenschist conditions, indicate that As in arsenopyrite was reset during peak metamorphism.

Table 3. Arsenopyrite geothermometry estimates from the Skellefte district. From Berglund & Ekström, 1980).

Location	Pressure	Temperature	Distance to Renström
Näsliden		360-420° C	52 km
Rakkejaur	6 kbar	360-425° C	
Kankberg		360-475° C?	9 km
Långsele	6 kbar	~400° C	
Boliden		430° C	14 km

Fluid inclusions

Broman (1987) carried out a district-wide study of fluid inclusions in sphalerite, quartz and calcite from massive sulphide ores in the Skellefte district, covering 6 mines including Renström. The ore-forming fluids were reported to contain Ca, Na, and Cl, with a salinity of 4 ± 2 eq wt % NaCl. The inclusions were divided into two groups based on homogenization temperature, 210° C and 295° C, interpreted to represent different stages of growth in the VMS-environment (Broman, 1987). Only inclusions of the latter group were reported from Renström. Measurements in this study fall very much in line with previous estimates, with essentially the same salinity and homogenization temperature (Table 18). The carbonate phase reported as calcite in (Broman, 1987) was identified with visual means only, and recent investigations with Raman-spectrometry indicate that inclusions in dolomite rather than calcite were analysed (Broman, personal communication, 2015).

Dolomite in the core generally shows brittle deformation, as opposed to the often plastically deformed surrounding massive sulphides. No dolomite textures points towards growth during metamorphism, and the mineral is interpreted to have formed in the 1.89-1.87 Ga (Lundström & Persson, 1999) VMS-environment. Although changes in fluid inclusions during deformation, such as leakage of a phase, cannot be completely ruled out, it is deemed unlikely, given the overall homogenous chemistry and phase relations of the inclusions. Thus, the fluid inclusions found in dolomite is believed to represent a hydrothermal fluid related to the ore-forming hydrothermal convection.

Summary

A summary of the hydrothermal events that have affected the Simon lens is listed below in chronological order:

- Volcanism on the seafloor produces a volcanic sediment with larger clasts of quartz and feldspar.
- Hydrothermal convection cells are initiated when rifting causes normal faulting of the oceanic crust.
- Hydrothermal fluids penetrating a permeable section in contact with the volcanic sedimentary rock underneath the seafloor heavily alters the host rock, partially replacing it with arsenopyrite, pyrite, sphalerite, galena, chalcopyrite, and pyrrhotite, forming massive sulphide bodies. Tetrahedrite and boulangerite may either have formed during this phase or later upon cooling of galena.
- In tandem with sulphide precipitation, extensive chlorite-alteration creates an envelope around the mineralisation. Sericite, quartz, and dolomite are also formed by the

hydrothermal fluids, and fluid inclusion results presented in this study indicate dolomite is formed at 292 ± 4° C. This homogenization temperature is in agreement with earlier fluid inclusion studies of carbonates in the district (Broman, 1987).

- As the geodynamic environment shifts from extension to compression, the massive sulphide bodies are heavily deformed, causing both folding and shearing. Deformation is more extensive in the sulphide bodies than in the surrounding host rock (Årebäck, et al., 2005).
- Peak regional metamorphism at greenschist facies takes place around ~1820 Ma (Weihed, et al., 2002). Grains of titanite in the Simon lens analysed in this study yield a U-Pb age of 1816 ± 28 Ma, indicating peak metamorphism around that period. Grains of arsenopyrite in the lens also analysed in this study record a peak metamorphic temperature at 379 ± 29° C, in line with previous estimation for the area (Berglund & Ekström, 1980).
- Remobilization during the regional metamorphism may have reinforced pre-metamorphic zonation of Cu and Zn, where Cu, as chalcopyrite, has been remobilized mainly by fluids while Zn, as sphalerite, has been remobilized by solid-state mechanical processes. Au, and to a lesser extent Ag, has been redistributed by fluid-dominated processes from the massive pyrite-sphalerite assemblage to areas of high fluid flow. Dyscrasite, formed through fluid-driven breakdown of tetrahedrite during retrograde metamorphism, is possibly a important host of Au, alongside electrum (Kläre, 2001).
- Partial sulphide melting, a process that has gained attention in recent years (e.g. Tomkins, 2007; Tomkins, et al., 2007), has likely not taken place at the Simon lens, although local enrichement of LMCE could possibly enable melts at temperatures <500° C. A texture observed in a chalcopyrite-arsenopyrite-tetrahedrite assemblage could represent the onset of fluid mediated melting, but more research would be needed to validate this.

Conclusions

The latest major metamorphic event have caused remobilization of metals in the Simon lens of the Renström deposit. By investigating how different events have affected the ore body, changes in metal distribution can be tracked, generating valuable information for near-mine exploration and ore processing. In this study, a paragenetic sequence covering minerals formed during metamorphic and pre-metamorphic conditions in the Simon lens have been established. Au in this model has been concentrated in minerals forming under retrograde metamorphism by fluid-dominated process, while most of the Ag is hosted in minerals formed during the seafloor hydrothermal convection. Sb, and partially also Hg and Cu, have also been remobilized by metamorphic fluids, while Zn and Fe in the form of sphalerite and pyrite has mainly been remobilized by solid-state mechanical processes.

No convincing evidence of sulphide melting has been found in the core. Arsenopyrite geothermometry indicate peak metamorphism at 379 ± 29° C, which took place at 1816 ± 28 Ma, based on the U-Pb age from titanite. Fluid inclusions in dolomite indicate that dolomite formed exclusively in the VMS-environment around 292 ± 4° C , while the other carbonate found in the core, calcite, is of metamorphic origin.

Acknowledgments

I would like to thank the following groups and individuals: Dr Iain Pitcairn for supervising this project, guiding me through the process and engaging in fruitful discussions; Curt Broman for performing the fluid inclusions studies; Thomas Zack for the U-Pb dating of titanite; Rodney Allen and Jakob Fahlgren at Boliden AB for proving valuable insights regarding the Renström deposit; Stiftelsen Stockholms Geologer for financing parts of the project through the Gavelinfonden scholarship; Karin Hendahl, Gerhard Makowsky, Eva Gustafsson, Mathilda Nyzell, Kajsa Markdahl, and Camilla Olsson for helpful discussions and input along the way. Finally, I would like to thank the whole Department of Geological Sciences at Stockholm University for the last seven years. It has been a wonderful time.

References

Alapieti, T. & Lahtinen, J., 2002. Platinum-group element mineralization in layered intrusions of northern Finland and the Kola Peninsula, Russia. in: L. J. Cabri, ed. *The Geology, Geochemistry, Mineralogy and Mineral Beneficiation of Platinum-group Elements.* Ottawa(Ontario): Canadian Institute of Mining, Metallurgy and Petroleum, pp. 507-546.

Allen, R. L. & Svenson, S.-Å., 2004. 1.9 Ga Volcanic Stratigraphy, Structure, and Zn-Pb-Cu-Au-Ag Massive Sulfide Deposits of the Renström Area, Skellefte District, Sweden. *Society of Economic Geologists Guidebook,* Volym 33, pp. 65-88.

Allen, R. L., Weihed, P. & Svensson, S. Å., 1996. Setting of Zn-Cu-Au-Ag Massive Sulfide Deposits in the Evolution and Architecture of a 1.9 Ga Marine Volcanic Arc, Skellefte District, Sweden. *Economic Geology,* Volym 91, pp. 1022-1053.

Barrie, C. T. & Hannington, M. D., 1999. Classification of volcanic-associated massive sulfide deposits based on host rock composition. *Reviews in Economic Geology,* Volym 8, pp. 2-12.

Barrie, C. T., Hannington, M. D. & Bleeker, W., 1999. The Giant Kidd Creek Volcanic-Associated Massive Sulfide Deposit, Abitibi Subprovince, Canada. *Reviews in Economic Geology,* Volym 8, pp. 241-253.

Barton, P. B., 1969. Thermochemical study of the system Fe-As-S. *Geochimica et Cosmochimica Acta,* Volym 33, pp. 841-857.

Barton, P. B., 1971. The Fe-Sb-S system. *Economic Geology,* Volym 66, pp. 121-132.

Bauer, T. E., Skyttä, P., Allen, R. L. & Weihed, P., 2011. Syn-extensional faulting controlling structural inversion - Insights from the Paleoproterozoic Vargfors syncline, Skellefte mining district, Sweden. *Precambrian Research,* Volym 191, pp. 166-183.

Bauer, T. E., 2014. Correlation between distribution and shape of VMS deposits and regional deformation patterns, Skellefte District, northern Sweden. *Mineralium Deposita,* Volym 49, pp. 555-573.

Berglund, S. & Ekström, T. K., 1980. Arsenopyrite and Sphalerite as T-P Indicators in Sulfide Ores from Northern Sweden. *Mineralium Deposita,* Volym 15, pp. 175-187.

Bergman Weihed, J., 2001. Paleoproterozoic deformation zones in the Skellefte and Arvidsjaur areas, northern Sweden. i: P. Weihed, red. *Economic Geology Research.* Uppsala: Sveriges Geologiska Undersökning, pp. 46-68.

Bergman Weihed, J., Bergström, U., Billström, K. & Weihed, P., 1996. Geology and tectonic evolution of the Paleoproterozoic Boliden Au-Cu-As deposit, Skellefte District, northern Sweden. *Economic Geology,* Volym 91, pp. 1073-1097.

Bernier, L., Pouliot, G. & MacLean, W. H., 1987. Geology and metamorphism of the North Montauban Gold Zone: a metamorphosed polymetallic exhalative deposit, Grenville Province, Quebec. *Economic Geology,* Volym 82, pp. 2076-2090.

Biagioni, C., 2013. Mobilization of Tl-hg-As-Sb-(Ag,Cu)-Pb sulfosalt melts during low-grade metamorphism in the Alpi Apuane (Tuscany, Italy). *Geology,* 41(7), pp. 747-750.

Billström, K. & Weihed, P., 1996. Age and provenance of host rocks and ores of the Paleoproterozoic Skellefte District, northern Sweden. *Economic Geology,* Volym 91, pp. 1054-1072.

Brander, L., Söderlund, U., Lundqvist, L. & Appelquist, K., 2011. Time-constrains for the 1.47-1.40 Ga Hallandian orogeny in Fennoscandia. i: *The Mesoproterozoic Hallandian Event - a region-scale orogenic event in the Fennoscandian Shield.* Göteborg: Göteborgs Universitet, Paper V, manuscript.

Brett, R. & Kullerud, G., 1967. The Fe-Pb-S system. *Economic Geology,* Volym 62, pp. 345-369.

Broman, C., 1987. Fluid inclusions of the massive sulphides in the Skellefte district, Sweden. *Chemical Geology,* Volym 61, pp. 161-168.

Butterfield, D. A., 1990. Geochemistry of hydrothermal fluids from Axial Seamount hydrothermal emissions study vent field, Juan de Fuca Ridge: Subseafloor boiling and subsequent fluid-rock interaction. *Journal of Geophysical Research,* Volym 95, pp. 12,895 - 12,921.

Clark, A. H., 1966. Heating experiments on gudmundite. *Mineralogical Magazine,* Volym 68, pp. 332-352.

Clark, L. A., 1960. The Fe-As-S system: phase relations and applications. *Economic Geology,* Volym 55, pp. 1345-1381.

Cook, N. J., 1996. Mineralogy of the sulphide deposits at Sulitjelma, northern Norway. *Ore Geology Reviews,* Volym 11, pp. 303-338.

Cook, N. J., Spry, P. G. & Vokes, F. M., 1998. Mineralogy and textural realtionships among sulphosalts and related minerals in the Bleikvassli Zn-Pb-(Cu) deposit, Nordland, Norway. *Mineralium Deposita,* Volym 34, pp. 35-56.

Cornell, D. H., Brander, L., Zack, T. & Kristoffersen, M., 2013. The Plat Sjambok Anorthosite and its tonalitic country rocks: Mesoproterozoic pre-tectonic intrusions in the Kaaien Terrane, Namaqua-Natal Province, southern Africa. *International Geology Review,* 55(12), pp. 1471-1489.

Craig, J. R. & Kullerud, G., 1967. The Cu-Fe-Pb-S system. *Yearbook of the Carnegie Institution of Washington,* Volym 65, pp. 344-352.

Craig, J. R. & Vokes, F. M., 1992. Ore mineralogy of the Appalachian-Caledonian stratabound sulfide deposits. *Ore Geology Review,* Volym 7, pp. 77-123.

Craig, J. R. & Vokes, F. M., 1993. The metamorphism of pyrite and pyritic ores: an overview. *Mineralogical Magazine,* Volym 57, pp. 3-18.

Doyle, M. G. & Allen, R. L., 2003. Subsea-floor replacement in volcanic hosted massive sulfide deposits. *Ore Geology Reviews,* 23(3-4), pp. 183-222.

Dubé, B., 2007. Gold-rich volcanogenic massive sulphide deposits. i: W. D. Goodfellow, red. *Mineral Deposits of Canada: a Synthesis of Major Deposits Types, District Metallogeny, the Evolution of Geological Provinces, and Exploration Methods.*Geological Association of Canada, Mineral Deposits Division, Special Publications 5, pp. 75-94.

Duckworth, R. C. & Rickard, D., 1993. Sulphide mylonites from the Renström VMS deposit, Northern Sweden. *Mineralogical Magazine,* Volym 57, pp. 83-91.

Franklin, J. M., Gibson, H. L., Jonasson, I. R. & Galley, A. G., 2005. Volcanogenic Massive Sulphide Deposits. i: J. W. Hedenquist, J. F. H. Thompson, R. J. Goldfarb & J. P. Richards, red. *Economic Geology 100th Anniversary Volume.* Littleton(Colorado): Society of Economic Geologists, pp. 523-560.

Franklin, J. M., Sangster, D. M. & Lydon, J. W., 1981. Volcanic associated massive sulfide deposits. i: *Economic Geology 75th Anniversary Volume.* Littleton(Colorado):The Economic Geology Publishing Company, pp. 485-627.

Freidrich, K., 1907. The binary systems FeS-ZnS and FeS-PbS. *Metallurgie,* Volym 4, pp. 479-485.

Frost, B. R., Chamberlain, K. R. & Schumacher, J. C., 2000. Sphene (titanite): phase relations and role as a geochronometer. *Chemical geology,* Volym 172, pp. 131-148.

Frost, B. R., Mavrogenes, J. A. & Tomkins, A. G., 2002. Partial Melting of Sulfide Ore Deposits during Medium- and High-Grade Metamorphism. *Canadian Mineralogist,* Volym 40, pp. 1-18.

Frost, B. R., Swapp, S. M. & Mavrogenes, J., 2011. Textural Evidence for Extensive Melting of the Broken Hill Orebody. *Economic Geology,* Volym 106, pp. 869-882.

Gaál, G., 1990. Tectonic styles of Early Proterozoic ore deposition in the Fennoscandian Shield. *Precambrian Research,* Volym 46, pp. 83-114.

Gaál, G. & Gorbatschev, R., 1987. An outline of the Precambrian evolution of the Baltic Shield. *Precambrian Research,* Volym 35, pp. 15-52.

Galley, A., Hannington, M. D. & Jonasson, I., 2007. Volcanogenic Massive Sulphide Deposits. i: W. D. Goodfellow, red. *Mineral Deposits of Canada: A Synthesis of Major Deposit-Types, District Metallogeny, the Evolution of Geological Provinces, and Exploration Methods.* Geological Association of Canada, Mineral Deposits Division, Special Publications, pp. 141-161.

Gasparrini, C. & Lowell, G. R., 1985. Silver-bearing inclusions in "Argentiferous" galena from the Silvemine district in southeast Missouri. *Canadian Mineralogist,* Volym 23, pp. 99-102.

Gibson, H. L., Allen, R. L., Riverin, T. E. & Lane, T. E., 2007. The VMS model: advances and application to exploration targeting. i: B. Milkereit, red. *Proceedings of the Fifth Decennial International Conference on Mineral Exploration.* Toronto(Ontario): Decennial Mineral Exploration Conferences, pp. 713-730.

Gibson, H. L. & Gamble, A. P. D., 2000. A reconstruction of the volcanic environments hosting Archean seafloor and subseafloor VMS mineralization at the Potter Mine, Munro township, Ontario, Canada. i: J. B. Gemmel & J. Pongratz, red. *Volcanic Environments and Massive Sulfide Deposits.* Hobart: CODES, pp. 65-66.

Goodfellow, W. D. & Peter, J. A., 1996. Sulphur isotope composition of the Brunswick No. 12 massive sulphide deposit, Bathurst Mining Campm: implications for ambient environment, sulphur source and ore genesis. *Canadian Journal of Earth Science,* Volym 33, pp. 231-251.

Goodfellow, W. D., Peter, J. M., Winchester, J. A. & van Staal, C. R., 2003. Ambient marine environment and sediment provenance during formation of massive sulfide deposits in the Bathurst mining camp: importance of reduced bottom waters to sulfide precipitation and preservation. *Economic Geology Mongraph,* Volym 11, pp. 129-156.

Gorbatschev, R., 2004. 1. The Transscandinavian Igneous Belt - Introduction and Background. i: K. Högdahl, U. B. Andersson & O. Eklund, red. *The Transscandinavian Igneous Belt (TIB) in Sweden: a review of its character and evolution.* Espoo: Geological Survey of Finland, pp. 9-15.

Graham, D. J. & Midgley, N. G., 2000. Graphical representation of particle shape using triangular diagrams: an Excel spreadsheet method. *Earth Surface Processes and Landforms,* 25(13), pp. 1473-1477.

Grip, E. & Wirstam, Å., 1970. The Boliden sulfide deposit: A review of geo-investigations carried out during the lifetime of the Boliden mine, Sweden (1924-1967). *Sveriges Geologiska Undersökning: Serie C, Avhandlingar och uppsatser,* Volym 651, p. 68.

Hannington, M. D., Bleeker, W. & Kjarsgaard, I., 1999. Sulphide mineralogy, geochemistry and ore genesis of the Kidd Creek Deposit: Part II. The bornite zone. *Economic Geology Monograph,* Volym 10, pp. 225-266.

Hannington, M. D., de Ronde, C. E. J. & Peterson, S., 2005. Sea-Floor Tectonics and Submarine Hydrothermal Systems. i: J. W. Hedenquist, J. F. H. Thompson, R. J. Goldfarb & J. P. Richards, red. *Economic Geology 100th Anniversary Volume.* Littleton(Colorado): The Economic Geology Publishing Company, pp. 111-142.

Hannington, M. D., Galley, A. G., Herzig, P. M. & Petersen, S., 1998. Comparision of the TAG mound and stockwork complex with Cyprous-type massive sulfide deposits. *Proceedings of the Ocean Drilling Program, Scientific Results,* Volym 158, pp. 389-415.

Hannington, M. D., Poulsen, K. H., Thompson, J. F. H. & Sillitoe, R. H., 1999. Volcanogenic Gold in the Massive Sulfide Environment. i: C. T. Barrie & M. D. Hannington, red. *Volcanic-Associated Massive Sulfide Deposits: Processes and Examples in Modern and Ancient Settings.* Littleton(Colorado): The Economic Geology Publishing Company, pp. 325-356.

Hansen, M. & Aderko, K., 1958. *Constitution of Binary Alloys.* New York: McGraw-Hill.

Herzig, P. M. & Hannington, M. D., 1995. Polymetallic massive sulfides at the modern sea-floor. A review. *Ore Geology Reviews,* Volym 10, pp. 95-115.

Hettmann, K., 2014. Thallium geochemistry in the metamorphic Lengenbach sulfide deposit, Switzerland: Thallium-isotope fractionation in a sulfide melt. *American Mineralogist ,* Volym 99, pp. 793-803.

Hofmann, B. A., 1994. Formation of a sulfide melt during Alpine metamorphism of the Lengenbach polymetallic sulfide mineralization, Binntal, Switzerland. *Mineralium Deposita,* Volym 29, pp. 439-442.

Hofmann, B. A. & Knill, M. D., 1996. Geochemistry and genesis of the Lengenbach Pb-Zn-As-Tl-Ba mineralization, Binn valley, Switzerland. *Mineralium Deposita,* Volym 31, pp. 319-339.

Huhma, H., Mutanen, T. & Whitehouse, M., 2004. Oldest rocks of the Fennoscandian Shield: the 3.5 Ga Siurua trondhejmite gneiss in the Archaean Pudasjärvi granulite belt, Finland. *GFF,* Volym 126, p. 10.

Humphris, S. E., 1995. The internal structure of an active sea floor massive sulphide deposit. *Nature,* Volym 377, pp. 713-716.

Huston, D. L., 2000. Gold in volcanic-hosted massive sulphide deposits: distribution, genesis, and exploration. i: S. G. Hagemann & P. E. Brown, red. *Gold in 2000.* Littleton: Society of Economic Geologists, Inc, pp. 400-426.

Huston, D. L. & Large, R. R., 1989. A chemical model for the concentration of gold in volcanogenic massive sulphide deposits. *Ore Geology Reviews,* Volym 4, pp. 171-200.

Huston, D. L., Relvas, J. M. R. S., Gemmell, J. B. & Drieberg, S., 2011. The role of granites in volcanic-hosted massive sulphide ore-forming systems: an assessment of magmatic-hydrothermal contributions. *Mineralium Deposita,* Volym 46, pp. 473-507.

Hutchington, R. W., 1973. Volcanogenic sulfide deposits and their metallogenic significance. *Economic Geology,* Volym 78, pp. 1223-1246.

Jackson, S. E., Pearson, N. J., Griffin, W. L. & Belousova, E. A., 2004. The application of laser ablation-inductively coupled plasma-mass spectrometry to in situ U–Pb zircon geochronology. *Chemical Geology,* 211(1-2), pp. 47-69.

Johnson, N. E., Craig, J. R. & Rimstidt, J. D., 1986. Compositional trends in tetrahedrite. *Canadian Mineralogist,* Volym 24, pp. 385-397.

Kathol, B., 2005. *Regional geological and geophysical maps of the Skellefte District and surrounding areas. Bedrock map.,* Uppsala: Geological Survey of Sweden.

Kläre, J., 2001. *Report on the geology of the Simon mineralization at Renström between 950-1170 meter levels,* Boliden: Boliden AB, unpublished reports.

Knill, M. D., 1996. The Pb-Zn-As-Tl-Ba-mineralization at Lengenbach, Binn valley, Switzerland. *Geotechnische Serie, Schweizerische Geotechnische Kommission,* Volym 90, p. 74.

Koistinen, T., 2001. *Geological Map of the Fennoscandian Shield, Scale 1: 2 000 000,* Geological surveys of Finland, Norway, and Sweden and the North-West Department of Natural Resrouces of Russia.

Kretschmar, U. & Scott, S. D., 1976. Phase relations involving arsenopyrite in the system Fe-As-S and their applications. *Canadian Mineralogist,* Volym 14, pp. 364-386.

Large, R. R., 1992. Australian volcanic-hosted massive sulfide deposits: features, styles and genetic models. *Economic Geology,* Volym 87, pp. 471-510.

Larocque, A. C. L., Hodgson, C. J., Cabri, L. J. & Jackman, J. A., 1995. Ion-microprobe analysis of pyrite, chalcopyrite and pyrrhotite from the Mobrun VMS deposit in Northwestern Quebec: Evidence for metamorphic remobilisation of gold. *Canadian Mineralogist,* Volym 33, pp. 373-388.

Laurila, T. E., Hannington, M. D., Petersen, S. & Garbe-Schoenberg, C. D., 2014. Trace metal distribution in the Atlantis II Deep (Red Sea) sediments. *Chemical Geology,* Volym 386, pp. 80-100.

Lawrence, L. J., 1967. Sulfide neomagmas and highly metamorphosed sulfide ore deposits. *Mineralium Deposita,* Volym 2, pp. 5-10.

Liljequist, R. & Svenson, S.-Å., 1974. Exceptionally well preserved Precambrian ignimbrites and basic lavas in N. Sweden. *Geologiska Föreningen i Stockholms Förhandlingar,* Volym 96, pp. 221-229.

Lundqvist, T., Vaasjoki, M. & Persson, P.-O., 1998. U-Pb ages of plutonic and volcanic rocks in the Svecofennian Bothnian Basin, central Sweden, and their implications for the Paleoproterozoic evolution of the basin. *GFF,* Volym 120, pp. 357-363.

Lundström, I. & Persson, P. B. U., 1999. Indication of early deformational events in the the north-eastern part of the Skellefte field. Indirect evidence from geological and radiometric data from the Stavaträsk-Klintån area, Boliden map-sheet. i: S. Bergman, red. *Radiometric dating results 4.* Uppsala: Sveriges Geologiska Undersökning, pp. 52-69.

Lydon, J. W., 1988. Ore deposits models; volcanogenic massive sulphide deposits: Part 2. Genetic Models. *Geoscience Canada,* Volym 15, pp. 43-65.

Marshall, B. & Gilligan, L. B., 1987. An introduction to remobolization: information from ore-body geometry and formation of ore deposits. *Reviews in Economic Geology,* Volume 2, pp. 87-131.

Marshall, B. & Gilligan, L. B., 1993. Remobilization, syn-tectonic processes and massive sulfide deposits. *Ore Geology Reviews,* Volym 8, pp. 39-64.

Marshall, B., Vokes, F.-M., Larocque & L, A. C., 2000. Regional metamorphic remobilization: upgrading and formation of ore deposits. *Economic Geology,* Volym 11, pp. 19-38.

Mavrogenes, J. A., MacIntosh, I. W. & Ellis, D. J., 2001. Partial melting of the Broken Hill galena-sphalerite ore - experimental studies in the system PbS-FeS-ZnS-(Ag2S). *Economic Geology,* Volym 96, pp. 205-210.

McPhie, J., Doyle, M. & Allen, R. L., 1993. *Volcanic textures: A guide to the interpretation of volcanic rocks.* Hobart(Tasmania): Centre of Ore Deposits and Exploration Studies, University of Tasmania.

Mercier-Langevin, P. & Hannington, M. D., 2011. The gold content of volcanogenic massive sulfide deposits. *Mineralium Deposita,* Volym 46, pp. 509-539.

Miller, A. R., 1966. Hot brines and recent iron deposits in deeps of the Red Sea. *Geochimica et Cosmochimica Acta,* Volym 30, pp. 341-359.

Monecke, T. & Mercier-Langevin, P., 2014. Gold in the Massive Sulfide Environment: A Comparision of Ancient and Modern Seafloor Hydrothermal Systems. *Acta Geologica Sinica,* Volym 88, pp. 190-191.

Moralev, G. V., Larsen, R. B. & Bjerkgård, T., 1995. *Distribution of precious metals in the Bleikvassli Zn-Pb Sedex type deposit, Nordland Norway,* Trondheim: Norge Geologiske Undersøkelse.

Moss, R., Scott, S. D. & Binns, R. A., 2001. Gold content of eastern Manus Basin volcanic rocks: implication for enrichment in associated hydrothermal precipitates. *Economic Geology,* Volym 96, pp. 91-107.

Nironen, M., 1997. The Svecofennian Orogen: a tectonic model. *Precambrian Research ,* Volym 86, pp. 21-44.

Ohmoto, H. H., 1996. Formation of volcanogenic massive sulfide deposits: the Kuroko perspective. *Ore Geology Review,* Volym 10, pp. 135-177.

Oudin, E. & Constantinou, G., 1984. Black smoker chimney fragments in Cyprus sulfide deposits. *Nature,* Volym 308, pp. 349-353.

Perdahl, J.-A. & Frietsch, R., 1993. Petrochemical and petrological characteristics of 1.9 Ga old volcanics in nothern Sweden. *Precambrian Research,* Volym 64, pp. 239-252.

Peter, J. M. & Scott, S. D., 1999. Windy Craggy, notherwestern British Columbia: the world's largest Besshi-type deposit. *Reviews in Economic Geology,* Volym 8, pp. 261-295.

Pitcairn, I. K., 2011. Background concentration of gold in different rock types. *Applied Earth Science,* Volym 120, pp. 31-38.

Plimer, I. R., 1987. Remobilization in high-grade metamorphic environments. *Ore Geology Reviews,* 2(1-3), pp. 231-245.

Poulsen, K. H. & Hannington, M. D., 1996. Volcanic-associated massive sulphide gold. i: R. O. Eckstrand, W. D. Sinclair & R. I. Thorpe, red. *Geology of Canadian Mineral Deposit Types.* Geological Society of America, pp. 183-196.

Roth, T., Thompson, J. F. H. & Barrett, T. J., 1999. The precious metal-rich Eskay Creek deposit, northwestern British Columbia. i: C. T. Barrie & M. D. Hannington, red. *Volcanic-associated massive sulfide deposits: Processes and examples in modern and ancient settings.* Littleton(Colorado): Society of Economic Geologists, pp. 357-373.

Rutland, R. W. R., Skiöld, T. & W, P. R., 2001. Age of deformation episodes in the Paleoproterozoic domain of nothern Sweden, and evidence for a pre-1.9 Ga crustal layer. *Precambiran Research,* Volym 112, pp. 239-259.

Sack, R. O. & Goodell, P. C., 2002. Retrograde reactions involving galena and Ag-sulphosalts in a zoned ore deposit, Julcani, Peru. *Mineralogical Magazine,* 66(6), pp. 1043-1062.

Sangster, D. F. & Scott, S. D., 1976. Precambrian strata-bound massive Cu-Zn-Pb sulfide ores in North America. i: K. H. Wolf, red. *Handbook of strata-bound and stratiform ore deposits.* Amsterdam: Elsevier, pp. 129-222.

Sawkins, F. J., 1976. Massive sulphide deposits in relation to geotectonics. *Geological Association of Canada, Special Papers,* Volym 14, pp. 221-240.

Sawkins, F. J., 1990. Integrated tectonic-genetic model for volcanic-hosted massive sulfide deposits. *Geology,* Volym 18, pp. 1061-1064.

Scott, D. J. & St Onge, M. R., 1995. Constraints on Pb closure temperature in titanite based on rocks from the Ungava Orogen, Canada; implications for U-Pb geochronology and P-T-t path determinations. *Geology,* Volym 23, pp. 1123-1126.

Shanks III, W. C. P., 2012. Hydrothermal Alteration. i: W. C. P. Shanks III & R. Thurston, red. *Volcanogenic Massive Sulfide Occurence Model.* U.S. Geological Survey Scientific Investigations Report 2010–5070—C, pp. 165-180.

Sharp, Z. D., Essene, E. J. & Kelly, W. C., 1985. A Re-Examination of the Arsenopyrite Geothermometer: Pressure Considerations and Applications to Natural Assemblages. *Canadian Mineralogist,* Volym 23, pp. 517-534.

Sillitoe, R. H., Hannington, M. D. & Thompson, J. F., 1996. High sulfidation deposits in the volcanogenic massive sulfide environment. *Economic Geology,* Volym 91, pp. 204-212.

Skinner, B. J. & Johnson, C. A., 1987. Evidence for movement of ore materials during high-grade metamorphism. *Ore Geology Reviews,* Volym 2, pp. 191-204.

Skiöld, T. & Rutland, R. R. W., 2006. Successive ~1.94 Ga plutonism and ~1.92 Ga deformation and metamorphism south of the Skellefte district, northern Sweden: Substantiation of the marginal basin accretion hypothesis of Svecofennian evolution. *Precambrian Research,* 148(3-4), pp. 181-204.

Skiöld, T., 1993. Chronology of Proterozoic orogenic processes at the Archaean continental margin in northern Sweden. *Precambrian Research,* Volym 64, pp. 225-238.

Skyttä, P., 2012. Pre-1987 Ga development of crustal domains overprinted by 1.87 Ga transpression in the Paleoproterozoic Skellefte district, Sweden. *Precambrian Research,* Volym 206-207, pp. 109-136.

Skyttä, P., 2013. Structural evolution of the VMS-hosting Kristineberg area, Sweden - constrains from structural analysis and 3D-modelling. *Solid Earth Discussions,* Volym 4, pp. 1281-1315.

Solomon, M., 1976. "Volcanic" massive sulfide deposits and their host rocks- an review and an explanation. i: K. A. Wolf, red. *Handbook of Strata-Bound and Stratiform Ore Deposits: II. Regional Studies and Specific Deposits.* Amsterdam: Elesvier, pp. 21-50.

Sparks, H. A. & Mavrogenes, J. A., 2005. Sulfide melt inclusions as evidence for the existence of a sulfide partial melt at Broken Hill, Australia. *Economic Geology,* Volym 100, pp. 773-779.

Spry, P. G., Plimer, I. R. & Teale, G. S., 2008. Did the Broken Hill (Australia) Zn-Pb-Ag deposit melt?. *Ore Geology Reviews,* Volym 34, pp. 233-241.

Stevens, G., Prinz, S. & Rozendaal, A., 2005. Partial melting of the assemblage sphalerite + galena + pyrrhotite + chalcopyrite + sulfur: implications for high-grade metamorphosed massive sulfide deposits. *Economic Geology,* Volym 100, pp. 781-786.

Tera, F. & Wasserburg, G. J., 1972. U-Th-Pb systematics in lunar highland samples from the Luna 20 and Apollo 16 missions. *Earth and Planetary Science Letters,* 17(1), pp. 36-51.

Tomkins, A. G., 2002. Evolution of the Granulite-Hosted Challanger Gold Deposit, South Australia: Implications for Ore Genesis. *PhD thesis, Australian National University, Canberra, Australia.*

Tomkins, A. G., 2007. Three mechanisms of ore re-mobilisation during amphibolite facies metamorphism at the Montauban Zn-Pb-Au-Ag deposit. *Mineralium Deposita,* Volym 42, pp. 627-637.

Tomkins, A. G., Frost, B. R. & Pattison, D. R. M., 2006. Arsenopyrite melting during metamorphism of sulfide ore deposits. *Canadian Mineralogist,* Volym 44, pp. 1045-1062.

Tomkins, A. G. & Mavrogenes, J. A., 2002. Mobilization of Gold as a Polymetallic Melt during Pelite Anatexis at the Challanger Deposit, South Australia: A Metamorphosed Archea Gold Deposit. *Economic Geology,* Volym 97, pp. 12-49-1271.

Tomkins, A. G., Pattison, D. R. M. & Frost, B. R., 2007. On the Initiation of Metamorphic Sulfide Anatexis. *Journal of Petrology,* 48(3), pp. 511-535.

Tornos, F., 2006. Environment of formation and styles of volcanogenic massive sulfides: the Iberian Pyrite Belt. *Ore Geology Reviews,* Volym 28, pp. 259-307.

Tornos, F., Peter, J. M., Allen, R. & Conde, C., 2015. Controls on the siting and style of volcanogenic massive sulphide deposits. *Ore Geology Reviews,* Volym 68, pp. 142-163.

Toulmin, P. I. & Barton, P. B., 1964. A thermodynamic study of pyrite and pyrrhotite. *Geochimica et Cosmochimica Acta,* Volym 28, pp. 641-671.

Wagner, T. & Jonsson, E., 2001. Mineralogy of sulfosalt-rich vein-type ores, Boliden massive sulfide deposit, Skellefte district, norhern Sweden. *Canadian Mineralogist,* Volym 39, pp. 855-872.

Wagner, T., Klemd, R., Wenzel, T. & Mattsson, B., 2007. Gold upgrading in metamorphosed massive sulide ore deposits: Direct evidence from laser-ablation-inductively coupled plasma-mass spectrometry analysis of invisible gold. *Geology,* Volym 35, pp. 775-778.

Van Baalen, M. R., 1993. Titanium mobility in metamorphic systems: a review. *Chemical Geology,* Volym 110, pp. 233-249.

Wasström, A., Agmalm, G. & Nilsson, P., 1999. *Åkulla Östra mine investigation, geology,* Boliden: GP99021, Prospekteringen, Boliden AB.

Webber, A. P., Robert, S., Taylor, R. N. & Pitcairn, I. K., 2013. Golden Plumes: Substantial gold enrichment of oceanic crust during ridge-plume interaction. *Geology,* Volym 41, pp. 87-90.

Weihed, P., 2005. Precambrian geodynamics and ore formation: The Fennoscandian Shield. *Ore Geology Reivews,* Volym 27, pp. 273-322.

Weihed, P., Bergman, J. & Bergström, U., 1992. Metallogeny and tectonic evolution of the Early Proterozoic Skellefte District, northern Sweden. *Precambrian Research,* Volym 58, pp. 143-167.

Weihed, P. B. K., Persson, P.-O. & Bergmann Weihed, J., 2002. Relationship between 1.90-1.85 Ga accretionary processes and 1.82-1.80 Ga oblique subduction at the Karelian cration margin, Fennoscandian Shield. *GFF,* Volym 124, pp. 163-180.

Wilson, M. R., 1987. Jörn: An early Proterozoic intrusive complex in a volcanic arc environment, north Sweden. *Precambrian Research,* Volym 36, pp. 201-225.

Wilson, S. A., Ridley, W. I. & Koenig, A. E., 2002. Development of sulfide calibration stadards for the laser ablation inductively-coupled plasma mass spectrometry technique. *Journal of Analytical Atomic Spectrometry,* Volym 17, pp. 406-409.

Vokes, F. M., 1971. Some aspects of the regional metamorphic mobilization of pre-existing sulfide deposits. *Mineralium Deposita,* Volym 6, pp. 122-129.

Zierenberg, R. A., 1998. The deep structure of a sea-floor hydrothermal deposit. *Nature,* Volym 392, pp. 485-488.

Årebäck, H., Barett, T. J., Abrahamsson, S. & Fagerström, P., 2005. The Paleoproterozoic Kristineberg VMS deposit, Skellefte district, northern Sweden, part I: geology. *Mineralium Deposita,* Volym 40, pp. 351-367.

Appendix

Table 4. Sample lithology and mineral assemblage, part 1. Cp: chalcopyrite; Sp: sphalerite; Po: pyrrhotite; Py: pyrite; Gn: galena; Asp: arsenopyrite; Carb: carbonate; Qtz: quartz; Fsp: feldspar; Chl: Chlorite; Bt: bitotite; Amp: amphibole.

Sample	Depth	Unit	Cp	Sp	Po	Py	Gn	Asp	Carb	Qtz	Fsp	Chl	Bt	Amp
1	22.25	Dacite				X			X	X		X	X	
2	23.5	Dacite				X			X	X		X		
3	23.9	Dacite							X					
4	24.4	Volc. Sed.				X						X	X	
5	25.5	Volc. Sed.							X					
6	26.3	Vein	X			X			X	X		X	X	X
7	26.65	Vein				X								
8	28.2	Volc. Sed.			X	X						X		
9	28.25	Volc. Sed.				X								x
10	28.35	Volc. Sed.										X	X	X
11	28.55	Volc. Sed.				X				X	?			x
12	28.65	Volc. Sed.				X				X	?			x
13	29.85	Pumice				X			X		X			
14	30.29	Volc. Sed.				X			X	X				
15	31.05	Volc. Sed.				X				X			?	
16	31.2	Vein				X			X	X				
17	32.6	Volc. Sed.				X			X	X				X
18	33.5	Pumice				X		X	X	X				
19	34.2	Pumice							X				X	
20	34.7	Volc. Sed.				X			X	X				
21	35.45	Qtzite				X				X				
22	35.6	Vein				X				X				
23	35.7	Vein	X			X				X				X
24	37.7	Volc. Sed.				X				X			?	?
25	37.6	Vein	X			X				X				
26	37.75	Qtzite							X	X				
27	39.25	Volc. Sed.												
28	39.9	Volc. Sed.		X		X						X		X
29	40.25	Sp-MS	X	X		X				X				X
30	40.3	Sp-MS	X	X	X	X?				X				?
31	40.5	Sp-MS	X	X		X				X				X
32	40.75	Volc. Sed.	X	X	X	X				X				
33	41.45	Sp-MS	X	X	X	X	X	X	X					?
34	41.5	Sp-MS	X	X	X	X	X							
35	42.6	Volc. Sed.	X	X		X	X		X					X
36	43.2	Py-MS		X		X			X					X
37	43.35	Sp-MS	X	X	X	X	X							X
38	44.15	Mass. Sul.	X	X	X	X	X			X				x
39	45.1	Py-MS	X	X		X	X		X					
40	45.24	Chlp	X	X	X	X			X					?
41	45.55	Py-MS	X	X	X	X	Minor		X	X				
42	45.65	Py-MS	X	X	X	X			X	X				
43	46.3	Volc. Sed.	X		X	X								X
44	47.25	Py-MS				X			X			X		

Table 5. Sample lithology and mineral assemblage, part 2. Cp: chalcopyrite; Sp: sphalerite; Po: pyrrhotite; Py: pyrite; Gn: galena; Asp: arsenopyrite; Carb: carbonate; Qtz: quartz; Fsp: feldspar; Chl: Chlorite; Bt: bitotite; Amp: amphibole.

Sample	Depth	Unit	Cp	Sp	Po	Py	Gn	Asp	Carb	Qtz	Fsp	Chl	Bt	Amp
45	47.4	Sp-MS	X	X	X	X								
46	48.3	Sp-MS	X	X	X	X	X		X					
47	48.9	Sp-MS		X		X	X		X					?
48	49.1	Sp-MS	X	X	X	X	X		X					?
49	49.5	Py-MS	X	X	X	X	X	X	X	X				?
50	50.7	Mass. Sul.	X	X	X	X			X	X				X
51	50.85	Mass. Sul.	X	X	X	X	X	Mino	X					x
52	51.3	Py-MS	X	X		X			X	X				
53	52.1	Py-MS	X	Mino	X	X	Minor		X	X				
54	54.4	Py-MS		X	X	X			X					?
55	54.7	Volc. Sed.				X								
56	56.2	Volc. Sed.	X	X	X	X								X
57	58.5	Mass. Sul.	X	X	X	X	X		X					?
58	59.7	Sp-MS		X	X	X	X		X					
59	59.95	Volc. Sed.		X		X	X		X					
60	60.0	Mass. Sul.	X	X	X	X	X							
61	60.1	Vein		X		X	X		X					
62	60.5	Cp-MS	X	X	X	X	X		X					
63	61.6	Sph-MS	X	X	X	X	X	x	X					
64	62.25	Cp-MS	X			X	X	X	X					
65	62.65	Py-MS	X	X	X	X	X		X					
66	62.7	Mass. Sul.	X	X		X	X		X					
67	63.4	Mass. Sul.	X	X		X	X	X	X					
68	63.6	Mass. Sul.	X	X	X	X	X	?	X					
69	64.3	Cp-MS	X	X	X	X	X	X	X					
70	65.05	Mass. Sul.	X	X		X	X		X					
71	65.1	Volc. Sed.	X			X	X	X	X					
72	65.7	Sp-MS	X	X		X		X	X					X
73	66.25	Py-MS	X	X		X	X	X	X					
74	67.4	Py-MS		X		X	X							
75	68.45	Sp-MS		X		X	X		X	X				
76	68.65	Vein							X	X		?		
77	68.85	Sp-MS	X	X	X				X	X		X		
78	68.9	Vein	X	X	X	X		X	X	X				
79	69.4	Volc. Sed.			X	X			X	X				
80	69.45	Volc. Sed.				X			X	X				
81	70.8	Volc. Sed.			X	X			X	X				
82	71.1	Volc. Sed.			X	X			X					
83	72.15	Pumice			X	X			X	X				
84	74.2	Pumice			X	X	X		X	X				
85	75.25	Pumice	X		X	X			X	X	X			
86	75.75	Pumice			X				X	X				
87	77.2	Pumice			X				X	X				
CURT	62.8	Sp-MS		X					x					

Table 6. Whole rock assay data for drill hole BH2559.

From - To (m)	Au (ppm)	Ag (ppm)	Cu (%)	Zn (%)	Pb (%)	As (%)
39,6 - 40,2	0,10	2	0,06	0,33	0,01	
40,2 - 41,8	0,64	30	0,40	6,79	1,20	0,02
41,8 - 43,55	0,49	14	0,12	3,40	0,67	0,02
43,55 - 45,25	0,36	49	0,41	2,89	0,97	0,04
45,25 - 46,15	0,53	46	1,37	0,17	0,12	0,04
46,15 - 47,8	0,17	5	0,20	0,57	0,04	0,03
47,8 - 49,2	0,15	22	0,17	4,84	0,86	0,01
49,2 - 50,8	1,26	75	0,29	3,77	1,24	0,03
50,8 - 52,55	0,96	80	0,30	3,71	1,35	0,05
52,55 - 54,35	0,09	3	0,01	0,07	0,01	0,02
54,35 - 56,4	0,22	3	0,01	0,04	0,02	0,04
56,4 - 58,4	0,23	6	0,03	0,05	0,03	0,04
58,4 - 60,2	1,81	354	0,31	15,90	3,64	0,25
60,2 - 62,1	1,15	387	0,41	12,25	5,61	0,13
62,1 - 63,9	1,86	353	0,40	8,88	4,50	0,28
63,9 - 65,7	1,69	609	0,29	15,80	6,37	0,21
65,7 - 67,3	1,09	341	0,04	13,15	5,76	0,35
67,3 - 68,45	1,46	520	0,02	14,55	4,64	1,28
68,45 - 69,1	3,03	288	0,06	3,61	1,28	0,08

*Table 7. Major and trace element concentration of **arsenopyrite** from LA-ICP-MS analysis. Concentration is given in parts per million (ppm).*

Sample	S34	Fe57	Cu63	Zn66	As75	Se78	Mo95	Ag107	In115	Sb121	Te125	Au197	Hg202	Pb208	Bi209	Total
RS060	242814,86	382161,88	34,16	27,76	373143,59	75,85	0,20	135,22	0,23	1412,46	0,53	0,35	1,72	206,91	0,02	1000016
RS060	287188,41	366218,44	40297,29	25,46	303330,25	16,75	<0,127	450,17	0,29	589,62	0,11	72,88	5,20	1822,28	0,10	1000017
RS064	217294,61	346913,03	15,78	53,27	435262,63	40,77	201,88	8,31	0,22	181,61	0,98	0,46	0,72	41,98	<0,0090	1000016
RS064	223378,72	346245,09	26,60	3,62	430224,09	30,16	1,88	4,92	0,21	89,10	2,00	2,13	0,89	6,84	0,03	1000016
RS064	222522,59	350436,94	1,15	1,43	427012,50	<16,50	0,11	2,75	0,20	30,18	2,59	0,21	<0,22	5,54	<0,0084	1000016
RS064	216631,36	353944,72	3,29	0,93	429387,59	20,18	<0,059	4,63	0,22	10,03	0,53	0,01	10,13	2,61	0,01	1000016
RS070	235718,81	365012,88	0,48	1,82	399190,50	4,82	13,48	3,74	0,26	26,87	0,60	0,08	3,12	38,62	<0,0079	1000016
RS070	251531,47	372699,69	1,77	1,65	375755,13	5,91	0,26	0,15	0,19	18,61	0,11	0,07	1,91	0,26	<0,0086	1000017
RS070	249654,02	367795,63	0,55	1,50	382535,53	2,34	2,87	0,51	0,23	18,53	0,94	0,06	2,60	0,98	<0,0096	1000016
RS070	273666,94	371963,63	2,86	<0,79	339711,66	4,92	0,16	8,06	0,20	61,41	0,97	0,04	1,67	14594,80	0,07	1000017
RS071	228958,77	358791,31	2,42	18,04	412087,66	96,13	5,30	26,83	0,24	19,54	7,06	0,03	0,85	1,30	0,00	1000015
RS071	230069,94	374514,00	5,75	1237,55	394078,91	15,28	0,02	22,01	0,23	27,88	<0,20	0,57	1,49	35,52	0,01	1000009
RS071	232019,30	356005,72	44,32	6,80	411846,34	30,60	24,57	7,84	0,18	20,91	0,96	0,34	0,24	8,29	0,01	1000016
RS071	220581,48	354778,16	1,52	4,51	424638,78	<19,14	0,16	0,30	0,63	9,35	0,31	0,02	0,48	0,61	<0,0099	1000016
RS071	308631,38	356271,69	13,12	60,74	334747,28	<17,95	0,17	21,67	0,18	36,18	<0,23	0,03	0,89	232,55	0,02	1000016
Average:	239533,88	361252,46	10,98	109,20	397830,16	29,72	19,31	17,64	0,24	140,19	1,47	0,31	2,05	1084,06	0,02	
StdDev:	25416,16	11153,90	14,24	339,63	32957,15	30,84	55,33	34,93	0,11	368,99	1,90	0,55	2,57	3889,41	0,02	

*Table 8. Major and trace element concentration of **boulangerite** from LA-ICP-MS analysis. Concentration is given in parts per million (ppm).*

Sample	S34	Fe57	Cu63	Zn66	As75	Se78	Mo95	Ag107	In115	Sb121	Te125	Au197	Hg202	Pb208	Bi209	SUM
RS075	201552,3	<4.15	2,52	5,29	4,69	214,65	<0.0297	220,31	0,104	200131	6,53	<0.0048	15,66	599910,4	13,86	1002077

*Table 9. Major and trace element concentration of **chalcopyrite** from LA-ICP-MS analysis. Concentration is given in parts per million (ppm).*

Sample	S34	Fe57	Cu63	Zn66	As75	Se78	Mo95	Ag107	In115	Sb121	Te125	Au197	Hg202	Pb208	Bi209	SUM
RS060	419058,3	270499,6	309919,1	460,16	46,09	13,6	0,27	9,52	1,226	1,13	<0,53	<0,0151	<2,57	1,87	<0,019	1000011
RS060	417679,8	271681,1	310128	428,56	69,2	9,74	0,17	8,48	1,249	0,95	<0,55	<0,0172	<0,94	3,17	<0,026	1000010
RS060	432454,2	269842,8	296456,3	1207,68	23,9	12,38	<0,26	6,57	1,118	1,27	<1,23	<0,024	<0,94	3,27	0,044	1000009
RS064	411206,5	276935,8	311152,1	676,46	<37,59	<54,48	<0,32	19,51	0,037	7,85	<1,04	<0,0187	2,66	3,52	<0,030	1000004
RS064	409599,2	279376,3	310510,9	333,31	147,92	<52,65	<0,139	29,98	0,052	8,86	0,42	0,0394	<1,03	2,14	0,033	1000009
RS064	419618,9	269757,2	310125,6	408,84	70,84	7,05	<0,246	13,04	0,061	3,04	<0,64	<0,0152	1,08	1,34	<0,034	1000007
RS070	415025,5	277687,4	305895,2	488,64	155,03	7,69	<0,32	30,66	0,092	153,83	<0,66	0,0143	4,92	562,33	<0,019	1000011
RS070	420893,5	272090,1	306613,7	249,98	149,68	<5,37	<0,219	9,2	0,025	4,09	1,77	0,026	<0,88	2,37	<0,028	1000014
RS071	418455,6	276756,2	304404,6	348,02	28,62	<50,55	0,19	15,56	<0,084	3,8	<0,73	<0,0185	<0,70	2,31	<0,022	1000015
RS071	414316,4	277418,5	307940,4	220,18	85,64	<54,50	<0,209	25,73	0,259	4,95	<0,50	<0,0174	<0,70	2,44	<0,029	1000014
RS071	440520	268054,2	290868,4	376,41	97,8	<43,21	0,173	16,97	0,226	3,5	<0,45	0,0289	1,14	75,01	<0,025	1000014
RS071	406877,9	282060,9	310565,9	409,77	79,75	<50,65	<0,166	13,16	0,278	3,4	<0,65	0,0321	<0,71	2,58	<0,024	1000014
RS071	422234,9	270086,1	307177,9	413,58	55,92	<50,67	<0,194	14,66	0,235	4,84	<0,73	<0,0198	21,58	3,08	<0,0186	1000013
RS075	425431,5	281287,5	292587,3	221,65	<1,77	<55,98	<0,19	17,39	0,727	9,15	<0,64	0,087	1,9	456,08	<0,032	1000013
RS075	398444,8	286135	314908,9	506,73	<1,34	<44,62	<0,168	12,78	1,011	1,06	<0,94	0,082	<0,79	1,77	0,044	1000012
Average:	418121,1	275311,2	305950,3	449,998	81,638	9,936667	0,17	16,214	0,471143	14,11467	1,095	0,044243	3,41	74,88533	0,040333	
StdDev:	10165,37	5458,882	7093,883	240,4872	44,10874	2,104896	0,009605	7,475797	0,482266	38,74479	0,954594	0,028547	7,330012	178,4482	0,006351	

*Table 10. Major and trace element concentration of **cubanite** from LA-ICP-MS analysis. Concentration is given in parts per million (ppm).*

Sample	S34	Fe57	Cu63	Zn66	As75	Se78	Mo95	Ag107	In115	Sb121	Te125	Au197	Hg202	Pb208	Bi209	SUM
RS064	394593,9	382237,2	222404,5	482,39	53,08	4,48	<0.215	202,07	0,98	2,54	<0.75	<0.0150	<1.48	28,26	<0.022	1000009

*Table 11. Major and trace element concentration of **dyscrasite** from LA-ICP-MS analysis. Concentration is given in parts per million (ppm). Empty cells indicate that the element was not measured for that sample.*

Sample	S34	Fe57	Cu63	Zn66	As75	Se78	Mo95	Ag107	In115	Sb121	Te125	Au197	Hg202	Pb208	Bi209	SUM
RS034	75000,9	102753,5	2803,43	30932,89	38,85			598088,3		128360,4	16,11	0,65	60571,1	1400,35	26,38	999992,8
RS034	12296,88	983,45	851,4	521,62	2,29			742961,8		151368,7	66,72	0,79	87435,88	3476,47	27,11	999993
RS051	13116,74	4907,6	9683,92	1149,82	5,49			723699,1		160069,9	2,85	2,49	86041,8	2346,34	0,687	1001027
RS051	40312,57	46564,08	27828,28	3217,11	9,12			641220,6		140100,8	4,32	2,28	100198,9	1568,38	0,525	1001027
RS051	107398,8	25629,4	73924,59	5150,77	33,19			530057,4		159742,2	<0,78	3,82	62379,73	35670,59	2,07	999992,6
RS051	11622,18	4858,47	2075,13	1225,18	1,75			682580,3		199259,4	9,35	0,45	96138,78	2221,5	0,204	999992,6
RS051	<2408,73	365,08	136,09	3769,26	14,09			717837,3		140842,8	<1,20	16,74	136343,8	666,68	0,571	999992,4
RS051	10853,34	16618,94	1611,34	897,22	62,93			691524,3		149807,7	<0,72	16,13	128255,6	344,38	0,693	999992,6
RS051	13167,35	2724,47	9811,53	1721,54	68,96			669728,4		152025	<0,93	15,55	146959	3770,08	0,542	999992,4
RS051	37315,32	21775,55	20820,31	3083,88	94,25			655186,9		151312,7	<1,19	14,54	107671,4	2717,33	0,675	999992,9
RS051	<2637,15	1600,03	292,73	1487,85	1232,19			705169,9		148329,3	<1,11	19,14	141567,6	293,15	0,533	999992,4
RS051	75779,16	54888,79	54208,94	10622,9	<2,15			577126,1		123009,5	<1,20	17,49	103050,2	1288,48	0,81	999992,4
RS051	<2314,70	193,73	106,11	442,23	3,15			725843,6		144448,4	2,16	2,36	128822,3	127,87	0,485	999992,4
RS051	42199,43	12497,27	2123,59	74611,21	90,15			626665,8		134461,7	4,91	18,38	101360,3	5959,2	0,86	999992,7
RS051	34695,13	4210,93	998,17	45,97	7,08			482134,4		101049	<0,72	1,74	93017,41	283822,8	9,97	999992,7
RS051	46531,01	2474,88	1678,04	335,75	18,92			418831,2		92134,62	<0,54	1,36	66866,07	371097,4	23,16	999992,4
RS051	29474,53	12473,79	8381,56	34271,29	26,37			673878,5		135658,9	0,63	2,38	104811,2	1012,98	0,709	999992,8
RS051	5645,34	1713,87	187,03	2500,79	155,49			697445,7		160852,2	<1,07	6,61	95620,54	35862,64	2,42	999992,6
RS051	108915,5	32623,73	25431,41	150354,3	3,15			499425,6		126293,3	<1,64	0,71	53775,63	3168,22	1,24	999992,7
RS058	19349,37	1155,93	818,97	8603,69	<1,56			766930,1		175127,8	<1,33	1,43	27295,41	709,84	0,14	999992,7
RS058	41177,89	26664,32	16643,04	1490,65	<1,52			701164,6		188640,9	<0,43	5,04	22297,21	1908,74	0,442	999992,8
RS058	49122,6	8062,76	7380,46	1105,22	<0,84			513918,6		108030,6	2,74	3,69	18577,21	293782,3	5,98	999992,2
RS058	7320,94	1864,93	1854,47	1088,24	<1,46			788531,4		174286,4	1,98	4,99	24020,63	1018,2	0,342	999992,6
RS058	15384,51	3393,62	7435,31	1902,89	2,58			781338,3		166127,1	1,62	1,08	23753,02	651,97	0,441	999992,4
RS058	18328,38	3421,59	2885,24	1889,37	114,52			667469,6		181463,8	13,88	4,05	29484,86	94915,77	1,42	999992,5
RS058	67975,7	6124,53	19130,37	2941,59	12,79			472974,3		129850	0,44	7,78	4777,83	296196,5	0,86	999992,7
RS058	11978,05	2015,79	1904,9	3786,6	<1,41			793443,2		163682,5	<0,70	2,27	22899,38	279,86	0,138	999992,7
RS058	39773,23	4282,95	1102,96	57788,23	4,94			684054,3		186360,1	<0,75	3,47	22775,46	3847,01	0,55	999993,1
RS058	49122,6	8062,76	7380,46	1105,22	<0,84			513918,6		108030,6	2,74	3,69	18577,21	293782,3	5,98	999992,2
RS058	15384,51	3393,62	7435,31	1902,89	2,58			781338,3		166127,1	1,62	1,08	23753,02	651,97	0,441	999992,4
RS060	17449,72	9140,4	6191,27	693,18	48	2,9	0,25	616892,1	0,261	276699,9	10,79	6781,31	12373,31	53698,05	0,946	999982,4
RS060	42968,87	42687,59	28057,94	10313,84	52,58	<2,10	0,42	657523,6	0,231	196289	0,58	38,92	11943,2	10026,83	0,422	999904
RS064	13437,87	10534,9	3756,59	9016,91	11543,24	<24,09	<0,046	784049,6	<0,0122	163603,4	0,74	4,65	3552,89	278,87	0,131	999779,8
RS064	72377,84	46665,67	43797,48	27271,49	4031,5	<36,92	0,098	631417,8	0,034	168137	0,79	4,33	4741,23	859,52	0,109	999304,9
RS064	35730,03	19466,3	22626,11	12848,36	287,56	34,83	0,07	747970,9	0,064	156476,7	<0,44	4,26	3671,13	577,34	0,213	999693,9
RS064	32847,54	32483,68	7602,83	21977,6	39890,02	55,68	<0,091	720306,4	<0,014	140535,6	<0,36	4,47	2917,25	883,28	0,158	999504,5
RS065	28662,57	20143,6	4258,93	35501,16	345,55			710650,6		175517,6	3,05	0,221	20707,09	4189,61	13,01	999993
Average:	35801,98	17388,01	13286,76	19901,56	1972,083	31,13667	0,2095	690789,7	0,1475	190897,5	3,225	189,7389	6533,168	58829,57	3,946333	
StdDev:	21141,67	22294,43	18960,4	41055,69	7490,965	26,58313	0,161083	111662	0,115049	33038,12	5,044129	1113,777	4398,521	126268,9	8,295853	

*Table 12. Major and trace element concentration of **galena** from LA-ICP-MS analysis. Concentration is given in parts per million (ppm).*

Sample	S34	Fe57	Cu63	Zn66	As75	Se78	Mo95	Ag107	In115	Sb121	Te125	Au197	Hg202	Pb208	Bi209	SUM
RS060	136844,7	1336,28	4754,58	15,96	80,16	337,01	<0,046	217,81	0,0502	323,9	<0,115	<0,0024	<0,38	856904	7,07	1000821
RS060	138887,6	7,86	22,16	1,71	72,44	369,08	<0,018	419,22	0,0584	444,7	<0,085	0,0059	<0,20	860388,9	7,49	1000621
RS060	137780,2	3,39	8,46	<0,44	63,99	318,82	0,026	205,26	0,0608	325,12	0,51	<0,0023	<0,27	861747,1	7,93	1000461
RS070	140456	6,52	1,17	1,3	295,67	178,63	0,039	757,09	0,0108	703,87	3,06	<0,0032	0,68	857811,9	3,86	1000220
RS070	142719,8	61,04	5,49	0,67	178,49	174,03	<0,053	727,17	0,008	658,37	2,22	0,02	0,23	855739,1	3,93	1000271
RS064	137849,3	<2,57	5,5	1,27	72,32	534,87	<0,038	2697,48	<0,0055	1021,16	0,53	<0,0030	1,68	858721,7	10,65	1000916
RS071	138123,6	<2,91	0,325	<0,46	96,93	944,2	<0,040	991,85	0,0094	799,85	1,49	0,007	<0,132	859787,4	34,03	1000780
RS071	139773,4	57,17	<0,158	<0,51	98,33	905,71	0,14	1118,53	0,0229	875,54	0,89	<0,0035	<0,136	857924	32,68	1000786
RS075	140599,7	8,59	0,83	3,11	<0,29	187,06	<0,025	1107,96	0,0241	850,64	2,48	0,0366	<0,108	857987,4	44,24	1000792
RS075	143959,1	<3,80	2,42	<0,52	<0,32	493,66	<0,027	1051,07	0,0604	1242,69	12,47	<0,0044	<0,20	854033,2	30,52	1000825
RS075	144649,1	<2,76	3,74	18,58	<0,31	483,99	0,059	1272,88	0,0186	1257,73	15,41	0,0099	0,18	853090,6	32,94	1000825
RS075	140219,8	7,91	7,37	1,45	0,59	538,69	<0,042	1861,44	0,0102	1789,74	25,99	0,0192	<0,160	856285,8	55,05	1000794
Average:	140155,2	186,095	437,4586	5,50625	106,5467	455,4792	0,066	1035,647	0,030345	857,7758	6,505	0,016433	0,6925	857535,1	22,5325	
StdDev:	2510,563	465,3478	1431,84	7,327426	84,53723	256,7519	0,051166	702,2879	0,022294	427,4579	8,623575	0,011573	0,695671	2522,63	17,71079	

*Table 13. Major and trace element concentration of **gudmundite** from LA-ICP-MS analysis. Concentration is given in parts per million (ppm).*

Sample	S34	Fe57	Cu63	Zn66	As75	Se78	Mo95	Ag107	In115	Sb121	Te125	Au197	Hg202	Pb208	Bi209	SUM
RS075	177650,9	317897,7	9,55	9,92	76,99	19,22	0,93	44,43	<0,0140	503816,8	<0,32	0,232	1,43	487,51	0,11	1000016
RS064	197287,9	290886,2	29,24	1282	11845,28	149,58	<0,142	15167,83	<0,015	482407,6	<0,34	0,947	191,93	733,85	0,359	999982,7
RS064	190740,3	314821,3	13,6	78,16	5920,46	83,57	0,088	174,29	<0,0111	487733,5	<0,00	0,0208	19,88	430,35	0,178	1000016
Average:	188559,7	307868,4	17,46333	456,6933	5947,577	84,12333	0,509	5128,85	<MDL	491319,3	<MDL	0,399933	71,08	550,57	0,215667	
StdDev:	9998,468	14787,26	10,39798	715,5505	5884,192	65,18176	0,595384	8694,254		11145,95		0,4854	105,0649	161,2777	0,128702	

*Table 14. Major and trace element concentration of **pyrite** from LA-ICP-MS analysis. Concentration is given in parts per million (ppm).*

Sample	S34	Fe57	Cu63	Zn66	As75	Se78	Mo95	Ag107	In115	Sb121	Te125	Au197	Hg202	Pb208	Bi209	SUM
RS060	492386,6	506555,7	70,23	1,93	974,05	2,64	0,074	14,78	<0,0075	0,975	<0,158	0,0198	<0,49	1,42	<0,0091	1000008
RS060	504739	495199,9	0,66	1,65	56,67	8,26	0,043	<0,021	<0,0080	0,07	<0,194	0,0067	<0,33	10,54	0,0116	1000017
RS060	510664,6	488946,5	1,6	1,01	393,68	S	<0,053	2,7	<0,0062	0,378	<0,176	0,122	<0,27	1,16	<0,0081	1000012
RS060	494858,2	505071,1	<0,169	<0,65	85,79	<1,59	<0,063	0,352	<0,0063	0,392	<0,150	<0,0041	<0,22	0,352	<0,0067	1000016
RS060	509594	489964,1	0,43	1,95	452,55	3,05	<0,046	0,081	<0,0071	0,511	<0,275	0,0163	<0,19	0,156	0,0138	1000017
RS064	509952,1	490032	7,87	23,41	<21,62	<17,45	<0,059	0,24	0,0401	0,185	<0,229	0,0157	<0,21	0,651	<0,0057	1000016
RS064	494387,6	487446,6	37,24	10,04	15820,32	<16,46	<0,091	463,21	<0,0094	94,16	<0,36	0,206	7,08	1749,74	0,078	1000016
RS064	495990,5	503514,6	10,79	9,62	457,55	<16,00	0,84	3,17	0,0198	2,26	<0,148	0,0284	<0,20	27,22	0,0138	1000017
RS070	505245,6	494752,3	1,04	<0,62	<21,94	2,89	5,55	2,72	0,1	0,317	<0,21	0,0252	0,25	4,95	0,0094	1000016
RS070	499158,5	500841,8	0,25	10,77	<27,42	<3,00	0,288	0,118	<0,0090	0,203	<0,00	0,0098	0,35	3,46	<0,0107	1000016
RS070	494198,1	483810,9	15,37	18,57	<23,20	5	0,52	33,96	<0,0142	119,66	1	0,503	8,35	21804,1	0,158	1000016
RS071	512822,5	486482,5	53,19	24,49	623,39	<16,04	<0,081	0,46	<0,0064	9,78	<0,180	0,0075	<0,215	0,749	<0,0099	1000017
RS071	499866,6	486318,2	173,44	5,71	853,4	19,81	1,7	28,69	0,0077	15,53	<0,28	0,227	<0,22	12731,79	0,397	1000016
RS071	493484,9	506013,3	10,28	1,57	458,47	<16,99	0,46	8,49	<0,0068	1,057	<0,193	0,0772	<0,24	38,02	<0,0101	1000017
RS071	488752,4	510535,2	27,27	5,82	683,12	<16,99	<0,032	3,43	<0,0062	0,267	<0,152	0,0061	<0,22	9,01	<0,0095	1000016
RS075	496471,9	502864,3	<0,133	<0,64	656,36	23,27	0,107	<0,024	<0,0063	<0,038	<0,111	<0,0067	0,109	0,133	<0,0073	1000016
RS075	504084,5	495609,3	0,3	<0,72	321,94	<16,11	<0,053	0,12	0,0159	0,31	<0,34	<0,0067	<0,31	<0,103	<0,0072	1000016
RS075	504803	494776	<0,154	7,71	414,02	<13,81	<0,027	15,16	<0,0043	0,393	<0,22	<0,0060	<0,25	0,071	<0,0080	1000016
Average:	500636,7	496040,8	27,33067	8,875	1589,379	9,274286	1,064667	36,10506	0,0367	14,49694	1	0,090764	3,2278	2140,207	0,097371	
StdDev:	7273,792	8274,509	45,74272	8,033146	4103,89	8,657311	1,759978	114,3795	0,037342	35,31726		0,140072	4,12166	5930,393	0,143116	

*Table 15. Major and trace element concentration of **pyrrhotite** from LA-ICP-MS analysis. Concentration is given in parts per million (ppm).*

Sample	S34	Fe57	Cu63	Zn66	As75	Se78	Mo95	Ag107	In115	Sb121	Te125	Au197	Hg202	Pb208	Bi209	SUM
RS075	391727,3	608282,8	0,7	3,53	<0,82	<30,43	<0,172	0,6	0,214	<0,079	<0,48	<0,0152	<0,40	1,45	<0,018	1000017
RS064	378313	617172,6	100,24	4000,74	30,82	<34,62	0,096	142,24	0,032	152,46	<0,39	0,058	3,5	36,51	0,018	999952,3
RS060	406000,2	593489,4	<0,50	<2,14	<14,07	<4,87	<0,147	0,58	0,018	0,202	<0,29	<0,0109	<0,67	2,45	<0,021	999492,9
RS064	394063,9	597784,1	1138,67	4,68	64,47	<35,28	<0,096	1074,01	<0,020	266,12	<0,32	0,199	9,93	5137,74	0,057	999543,9
Average:	392526,1	604182,2	413,2033	1336,317	47,645	<MDL	0,096	304,3575	0,088	139,594	<MDL	0,1285	6,715	1294,538	0,0375	
StdDev:	11351,45	10658,87	630,2408	2307,458	23,79414			517,4284	0,109343	133,4251		0,099702	4,546697	2562,187	0,027577	

*Table 16. Major and trace element concentration of **sphalerite** from LA-ICP-MS analysis. Concentration is given in parts per million (ppm).*

Sample	S34	Fe57	Cu63	Zn66	As75	Se78	Mo95	Ag107	In115	Sb121	Te125	Au197	Hg202	Pb208	Bi209	SUM
RS060	295409,6	53534,97	52,61	647450,6	<11,03	5,88	<0,163	4,35	3,49	2,47	<0,39	0,0249	123,36	2,2	<0,0188	996589,6
RS060	303622,2	56023,92	55,19	636741,9	<12,31	16,99	<0,161	34,27	3,84	8,07	0,38	0,045	140,3	11,14	<0,019	996658,2
RS064	293282,2	50696,41	28,23	651295,6	36,08	<35,34	<0,134	527,38	0,084	32,91	<0,227	0,0655	256,45	210,24	<0,0220	996365,6
RS064	289462,6	49522,48	17,68	656751,2	<12,14	<3,48	<0,149	9,64	0,089	6,48	<0,30	0,123	245,88	2,99	<0,0158	996019,1
RS070	302644,8	38911,42	9,69	655008,3	<17,58	<4,21	0,071	20,01	0,081	2,99	<0,35	0,212	279,85	13,8	0,023	996891,2
RS070	307786,1	42677,5	37,28	645989,4	23,35	8,04	0,32	25,39	0,079	36,26	0,92	0,204	285,84	28,61	0,85	996900,1
RS071	296666,5	35591,08	12,69	664679,3	<38,50	<35,74	<0,150	19,65	0,559	8,03	<0,76	0,228	185,7	6,91	<0,0187	997170,6
RS071	299330,6	41391,58	8,88	654216,1	2044,24	<36,79	<0,099	17,25	0,591	3,09	<0,47	0,301	180,1	5,03	0,036	997197,7
RS071	297510,8	39583,39	22,22	659804,4	<15,87	<38,42	<0,126	37,28	0,621	23,07	0,15	0,208	174,65	14,92	<0,0209	997171,7
RS071	297292,9	37536,86	7,48	661640,2	38,75	<36,01	0,212	407,29	0,606	6,86	<1,08	0,16	186,85	2,55	<0,0195	997120,7
RS071	291947,5	36851,72	7,26	668111,7	<13,83	<37,85	<0,072	7,71	0,624	2,46	<0,34	0,14	176,72	3,26	<0,0203	997109,1
RS075	309725,4	51501,3	17,4	634982,3	<1,03	<37,28	0,075	11,55	3,75	4,25	<0,55	0,025	449,32	4,23	0,036	996699,6
RS075	307612,1	59276,35	23,57	630285,8	1,96	<33,87	<0,128	13,38	0,596	20,76	<0,75	0,131	266,17	3,56	<0,021	997504,3
RS075	299287,1	54483,29	8,75	643530,3	<0,98	<32,73	0,024	13,31	0,76	8,31	<0,63	0,074	289,84	3,28	<0,0195	997625
RS075	296877,3	61153,66	5,93	639155,3	<1,01	<34,00	<0,093	9,43	1,386	2,95	<0,50	0,129	293,04	48,87	<0,0202	997548
RS075	299264,1	58965,27	7,52	639038,9	<1,06	<34,65	<0,116	17,27	1,316	0,58	<0,56	0,133	290,9	0,44	<0,0213	997586,4
RS075	299777,9	57429,48	8,57	640107,3	<0,93	<35,03	<0,164	7,45	1,383	3,91	<0,45	0,16	280,1	1,29	<0,0218	997617,6
Average:	299264,7	48537,1	19,46765	648752,2	428,876	10,30333	0,1404	69,56529	1,167941	10,20294	0,483333	0,139024	241,4747	21,37176	0,23625	
StdDev:	5601,831	8932,061	15,62539	11260,56	903,1329	5,890673	0,1225	151,4808	1,27791	11,04564	0,395264	0,07677	78,71417	50,20406	0,409213	

*Table 17. Major and trace element concentration of **tetrahedrite group** minerals from LA-ICP-MS analysis. Concentration is given in parts per million (ppm).*

Sample	S34	Fe57	Cu63	Zn66	As75	Se78	Mo95	Ag107	In115	Sb121	Te125	Au197	Hg202	Pb208	Bi209	SUM
RS060	341167,2	33747,74	291096,7	44867,85	225924	31,76	0,2	42497,85	0,175	19995,23	<0,40	0,0271	129,77	1,11	0,197	999459,8
RS064	281892,6	57885,88	229184,9	11779,5	<45,79	<35,61	<0,169	188756,7	<0,0197	229937,8	<0,40	0,437	52,27	153,27	0,16	999643,6
RS064	286081,4	52044,48	237957,6	11564,52	12703,41	40,35	<0,159	178622,2	<0,022	220554,6	0,079	0,145	91	6,79	0,188	999666,8
RS064	282224,2	52175,62	236495,2	11473,59	12551,88	<38,04	<0,21	182865,8	0,0171	221837,8	<0,43	0,0116	43,52	10,98	0,175	999678,7
RS064	295748,6	50634,81	237372,2	11502,95	11060,08	33,32	0,039	173995,6	<0,0121	218781,8	<0,51	0,316	67,51	466,07	0,169	999663,4
RS070	294101,1	47838,84	223505,5	12923,41	549,45	6,32	0,129	188193,4	<0,0180	232351,5	<0,61	0,0182	62,72	171,3	0,044	999703,7
RS070	307506	46752,94	216896,1	13082,83	357,96	<8,12	<0,15	187521,8	<0,0138	226898	<1,08	0,075	76,09	605,26	0,079	999697,1
RS071	284000,6	88284,52	243827,9	6823,56	2398,75	85,35	0,17	196666	0,07	177747,2	<0,00	0,016	17,84	10,27	0,55	999862,8
RS071	282301,9	50770,94	209152,6	10534,32	3375,67	56,13	<0,136	219765,5	<0,0165	223824,1	<0,36	0,0166	10,05	5,14	0,674	999797
RS071	287051,7	45812,76	204290,2	33006,09	1389,11	78,77	0,38	204511,9	0,054	223200	<0,83	0,0383	138,78	140,58	0,568	999620,9
RS075	254226	48289,91	147624,7	17490,04	97,37	26,73	<0,095	322688,7	0,022	209293,9	2,02	0,0374	142,87	6,46	0,149	999888,9
RS075	251575,9	48187,34	147879,2	12025,64	173,88	24,27	64,55	326014,3	0,0098	211382,6	1,78	0,0512	162,99	2413,93	0,29	999906,7
RS075	281319,9	104438	132754,3	10208,66	152,8	<20,46	<0,079	283940	<0,011	181461,8	4,8	0,031	146,7	5493,97	0,458	999921,4
RS075	242856,7	49228,67	157581,5	11560,51	39,15	24,39	<0,061	327200,6	0,0142	211233,1	2,68	0,0283	168,09	4,07	0,151	999899,6
RS075	242472,5	44294,3	134881,2	10460,19	23,79	82,13	<0,126	292317,8	0,0153	193636	6,46	0,076	126,95	81596,4	6,97	999904,8
RS075	250450,1	47524,8	150263,6	12010,69	113,05	<27,27	0,133	325247,1	<0,0119	214067,6	2,17	0,0548	201,26	8,86	0,269	999889,6
Average:	279061	54244,47	200047,7	15082,15	18060,69	44,50182	9,371571	227550,3	0,047175	201012,7	2,855571	0,086219	102,4006	5693,404	0,693188	
StdDev:	26054,3	17426,84	48080,46	9788,439	57699,76	26,99278	24,33162	78867,2	0,055991	50878,31	2,114944	0,120082	57,33413	20291,22	1,684251	

Table 18. Microthermometric data for dolomite fluid inclusions in sample CURT.

Fluid inclusion	Ts (°C)	$TmCO_2$ (°C)	Tmhydr (°C)	Salinity (eq. wt. % NaCl)	$ThCO_2$ (°C)	Thtot (°C)
IaA	-37, -58	n.d.	+8.5	3	n.d.	**290 (l)**
IaB	-37, -58	n.d.	+8.5	3	n.d.	**282 (l)**
IbC	-37, -58	n.d.	+7.3	5.5	n.d.	**296 (l)**
IbD	-37, -58	n.d.	+7.3	5.5	n.d.	**284 (l)**
IcE	-37, -58	n.d.	+8.6	3	n.d.	**284 (l)**
IIaA	-38, -58, -100	-56.7	+7.8	4.5	+30 to +31 (g)	**290 (l)**
IIaB	-38, -58, -100	-56.7	+8.1	4	+30 to +31 (g)	**283 (l)**
IIaC	-34, -57, -100	-56.7	+8.1	4	+30 to +31 (g)	**286 (l)**
IIbD	-38, -58	n.d.	+7.3	5.5	n.d.	**284 (l)**
IIbE	-38, -58	n.d.	+7.3	5.5	n.d.	**288 (l)**
IIbF	-39, -58, -100	-56.9	+8.1	4	+30 (l)	**283 (l)**
IIIaA	-39, -59, -100	-56.6	+7.3	5.5	+30 to +31 (g)	**291 (l)**
IIIbB	-39, -61	n.d.	+8.5	3	n.d.	**287 (l)**
IIIbC	**-39, -61**	**n.d.**	**+8.5**	**3**	**n.d.**	**283 (l)**

Table 19. Microprobe analysis of arsenopyrite. Concentration is given in percent (%).

Sample	Assemblage	As	Fe	S	Ag	Cd	Cu	Ni	Pb	Sb	Zn	Total	Tot. Trace	at % As
RS077	Asp-py-po	43,851	33,688	21,306	0,009	0	0,006	0	0,129	0	0,112	99,1011	0,256	0,315847
RS077	Asp-py-po	43,095	33,698	21,893	0,016	0	0	0	0,192	0	0,545	99,439	0,753	0,309001
RS077	Asp-py-po	42,87	34,434	22,104	0,003	0	0	0	0,102	0,115	0,404	100,0319	0,624	0,304645
RS077	Asp-py-po	44,06	34,594	21,466	0,008	0	0	0,004	0,143	0	0,695	100,9699	0,846	0,313294
RS077	Asp-py-po	43,807	34,604	21,51	0,014	0	0,017	0	0,051	0	0,362	100,3649	0,444	0,311798
RS077	Asp-py-po	43,948	34,572	21,228	0,016	0	0	0,005	0,175	0,036	0,189	100,169	0,416	0,314055
RS077	Asp-py-po	44,396	34,263	20,766	0,014	0	0	0,015	0,124	0,093	0,433	100,1039	0,664	0,319647

Table 20. LA-ICP-MS analysis of titanite for geochronology. Concentration is given in parts per million (ppm).

Sample	U	Th	Th/U	206Pb/204Pb	Ratio 207Pb/235U	Ratio 206Pb/238U	ρ	Ratio 207Pb/206Pb	Age (Ma) 207Pb/235U	Age (Ma) 206Pb/238U
RS075	8,1	2,1	0,26	165	9,616 ± 0,243	0,353 ± 0,007	0,90	0,197 ± 0,002	2399 ± 24	1948 ± 33
RS075	3,5	0,8	0,22	341	6,923 ± 0,142	0,34 ± 0,01	0,90	0,147 ± 0,001	2102 ± 18	1899 ± 31
RS075	2,2	0,5	0,22	292	7,45 ± 0,161	0,35 ± 0,01	0,87	0,156 ± 0,002	2167 ± 19	1920 ± 32
RS075	3,9	1,1	0,28	373	6,688 ± 0,138	0,34 ± 0,01	0,90	0,143 ± 0,001	2071 ± 18	1885 ± 30
RS075	3,8	1,0	0,27	386	7,042 ± 0,173	0,34 ± 0,01	0,79	0,151 ± 0,002	2117 ± 22	1875 ± 31
RS075	2,1	0,4	0,18	587	8,418 ± 0,235	0,35 ± 0,01	0,85	0,172 ± 0,003	2277 ± 26	1943 ± 35